ISSN:2538-516X

Journal of

Civil Engineering Researchers

Volume: 6; Number: 1; March 2024

Chief Editorial:
Morteza Jamshidi

Managing Editor:
Kamyar Bagherineghad

J-Researchers

J-Researchers

JOURNAL OF CIVIL ENGINEERING RESEARCHERS

Volume 6, Number 1, March 2024

Contents

Journal of Civil Engineering Researchers

Journal homepage: www.journals-researchers.com

Enhanced Flood Detection Through Precise Water Segmentation Using Advanced Deep Learning Models

Behrokh Bahrami,[a,*] Homayoun Arbabkhah[b]

[a] *Department of Civil and Environmental Engineering, Lamar University, Beaumont, Tx 77710, USA*

[b] *Department of Mechanical Engineering, Amirkabir University of Technology, Tehran, Iran*

ABSTRACT

Floods are natural disasters that can result in significant social, economic, and environmental impacts. Timely and accurate flood detection is crucial for effective disaster management and mitigation. This paper addresses the importance of water segmentation in flood detection and water engineering applications, emphasizing the need for precise delineation of water areas in flood-hit regions. Accurate water segmentation not only aids in assessing the extent of flooding but also plays a vital role in predicting and preventing potential flood events. This study explores the application of advanced deep learning models, namely SegNet, UNet, and FCN32 for automated flood area segmentation. Leveraging a dataset comprising 290 images depicting flood-affected areas, the models are trained to accurately delineate water regions within the images. The experiment results demonstrate the efficacy of these models in effectively segmenting floodwaters. Among the tested models, SegNet emerges as the top performer, achieving an impressive precision rate of 88%. This superior performance underscores the potential of deep learning techniques in enhancing flood detection and response capabilities, paving the way for more efficient and reliable flood prediction systems.

© 2024 Journals-Researchers. All rights reserved.

ARTICLE INFO

Received: February 05,2024
Accepted: March 30,2024

Keywords:
Water segmentation
Deep learning
Flood area detection
UNet
Floodwaters

DOI: 10.61186/JCER.6.1.1
DOR: 20.1001.1.22516530.1399.11.4.1.1

1. Introduction

Floods, which occur when water overflows onto normally dry land, have various causes such as excessive rainwater in saturated ground, overflowing water bodies, rapid snow or ice melting, storm surges, and tsunamis. Climate change exacerbates these events, leading to more intense precipitation and temperature variations. Poor water management practices, including dam discharges and neglected bank maintenance, can also contribute to flooding. Most floods result from extreme rainfall, allowing for some predictability. However, flash floods, developing rapidly within hours, are highly unpredictable and dangerous. Climate change's influence on extreme weather events, such as hurricanes and sea-level rise, poses an increasing threat. Floods cause significant damage globally, exceeding $40 billion annually, with thousands of fatalities. Novel approaches using Artificial Intelligence algorithms for automated image and video analysis from various sources, including surveillance cameras, drones, and social media, are crucial for effective flood monitoring and early warnings [1-4].

* Corresponding author. Tel.: +1-713-542-2970; e-mail: Bbahrami@lamar.edu.

Floods, devastating natural disasters affecting societies globally, have intensified due to climate change, urbanization, and deforestation. Detecting floods early is crucial for minimizing their impact, prompting a shift from traditional methods to advanced technologies like deep learning models. Accurate delineation of water bodies through water segmentation, classifying pixels in images, is essential for precise flood detection. Leveraging deep learning models, particularly for water segmentation, aims to surpass the limitations of traditional techniques in terms of accuracy, speed, and scalability. The growing severity of floods underscores the need for innovative tools to reduce their impact, emphasizing the importance of automated image and video analysis using Artificial Intelligence algorithms for comprehensive flood monitoring and early detection [4-7].

Existing flood detection methods, relying on remote sensing technologies and machine learning algorithms, have shown promise but are hindered by challenges such as false positives, limited scalability, and the inability to capture subtle changes in water dynamics. The introduction of advanced deep learning models offers a potential breakthrough, leveraging the power of neural networks to discern intricate patterns and variations in satellite imagery. Recently, a discernible pattern has arisen, marked by the increasing adoption of deep learning for image analysis. These applications extend across diverse domains, encompassing image analysis such as recognition, classification, and segmentation. Deep neural networks, functioning as comprehensive end-to-end learning models, showcase their ability to autonomously extract intricate features from any high dimensional images. Particularly noteworthy is the application of deep learning algorithms in water detection and segmentation. The adoption of advanced deep learning models is motivated by their capacity to learn hierarchical features and representations from complex data. Convolutional Neural Networks (CNNs), Recurrent Neural Networks (RNNs), and their variants have demonstrated success in image classification and segmentation tasks, making them well-suited for the nuanced demands of flood detection through precise water segmentation.

The main goal of this study is to propel the capabilities of flood detection by employing cutting-edge deep learning models in conjunction with precise water segmentation. Through this approach, we seek to surmount the constraints inherent in existing methods, offering a more precise and timely methodology for the identification and monitoring of flood events. Within this manuscript, we embark on an extensive exploration of water segmentation, leveraging the formidable capabilities of contemporary deep learning models. Our toolkit encompasses well-established models such as SegNet [8], UNet [9], and FCN32 [10], each distinguished by intricate architectures and a profound understanding of visual patterns. These models contribute a wealth of expertise to the domain of water segmentation. We applied this methodology to a publicly available water segmentation dataset, conducting a comprehensive comparative analysis of state-of-the-art deep learning models across 290 images.

Section 2 provides an overview of related studies and previous implementations of deep-learning models in the realm of water segmentation. Moving on to Section 3, we detail our methodology, including information about the dataset and an introduction to three deep-learning models. Finally, in Section 4, we present the experimental results and conduct a statistical analysis of the performance of these deep learning models.

2. Related works

In recent times, there has been a surge in the application of machine learning and deep learning models for tasks within computer vision, notably in object detection and segmentation [11-12]. The prominence of these models in the field of image processing, specifically for flood label detection, has grown considerably. The literature, however, remains relatively sparse on this particular subject.

Yang et al. [13] took on the task of water level monitoring by employing a visual recognition method. A river camera was utilized to measure flood depth resulting from rising water levels. The incorporation of techniques such as the Laplacian method [14] and probabilistic Hough transform [15] allowed for the detection of edges in various objects and the computation of the waterline's straightness. In a separate study, [16] conducted remote calculations of flood levels by measuring the length of a ruler in footage, employing Convolutional Neural Networks (CNNs). Their findings demonstrated the superior performance of CNNs over traditional image processing algorithms, showcasing a standard deviation of 6.69 mm.

In the work [17], CNNs were applied to sift through flooding photos on social media platforms, facilitating label detection. More recently, [18] undertook the estimation of flood depth by identifying submerged vehicles in flooded photos, utilizing the Mask R–CNN framework [19]. The calculated flood depth was then compared with 3D rendered objects using feature maps extracted by Visual Geometry Group Nets [20]. This proposed methodology demonstrated impressive accuracy, with absolute error values reaching as low as 6.49 cm in flood depth calculation. In [21], the authors delved into the study of flood depth using image processing and deep learning, employing traffic stop signs as ubiquitous measurement benchmarks in flood photos. Their approach estimated flood depth in crowdsourced photos with a mean absolute error of 12 inches. Collectively, these studies

contribute to the evolving landscape of flood label detection, showcasing the versatility of approaches ranging from visual recognition and traditional image processing to the application of advanced deep learning models. In [4], the WSOC dataset was introduced. This dataset, an augmentation of existing publicly available datasets, includes diverse water-related labels (e.g., river, sea, waves).

Various state-of-the-art Deep Learning models for semantic segmentation were explored in this study, combining different backbones commonly used for image labeling with semantic segmentation models. Additionally, a new Python package named "FloodImageClassifier" was developed [22]. This package is designed for the classification and detection of objects within collected flood images. "FloodImageClassifier" incorporates various CNN architectures, including YOLOv3, Fast R–CNN (Region-based CNN), Mask R–CNN, SSD MobileNet (Single Shot MultiBox Detector), and EfficientDet, enabling simultaneous object detection and segmentation. The package also includes concepts such as Canny Edge Detection and aspect ratio for floodwater level estimation.

Fig. 1. Some examples with mask image [24]

3. Methods

3.1. Dataset

The flood area segmentation dataset provides a comprehensive collection of 290 images capturing regions affected by flooding, each paired with self-annotated mask images that precisely outline the areas submerged in water [23]. These masks were meticulously generated using Label Studio, a versatile and open-source data labeling software known for its accuracy and efficiency in annotation tasks.

The primary objective of this dataset is to facilitate the development and training of robust segmentation models.

These models aim to precisely delineate the water-affected regions within photographs depicting areas impacted by floods. The annotations within the dataset serve as a valuable resource for enhancing the accuracy and efficacy of segmentation algorithms, enabling the creation of model's adept at recognizing and isolating flood-induced water regions in a given image.

3.2. Deep learning models

In our quest for achieving the accurate and efficient segmentation of floodwater, we harnessed the remarkable capabilities of three distinguished deep learning models. Each of these models boasts unique strengths and intricate architectural features, making them pivotal contributors to the landscape of image analysis and segmentation. The trio of SegNet, UNet, and FCN32 stand out as foundational pillars in this domain, having demonstrated their prowess in handling complex segmentation tasks with precision and effectiveness. These models serve as integral components in our research, offering a diverse set of tools to explore and optimize the segmentation of floodwater, contributing to advancements in the broader field of computer vision and image analysis.

SegNet, a pioneering deep learning architecture designed for semantic image segmentation, boasts a sophisticated structure that has significantly influenced the landscape of computer vision tasks.

Developed by the Visual Geometry Group at the University of Oxford, SegNet's architecture is meticulously crafted to balance computational efficiency with high-performance segmentation capabilities. At its core, SegNet follows an encoder-decoder framework, where the encoder progressively reduces spatial dimensions while capturing essential features from input images. This is achieved through a series of convolutional and pooling layers, with the pooling indices being stored during the encoding process. The critical innovation of SegNet lies in its decoder, which employs upsampling techniques based on the stored pooling indices. This enables precise reconstruction of segmented output, recovering intricate details crucial for accurate segmentation. The encoder-decoder structure is further enriched by incorporating skip connections, allowing the network to capture both local and global context information. SegNet's architecture is characterized by its lightweight design, making it computationally efficient and suitable for real-time applications. Delving into the details, the encoder module typically consists of convolutional layers with batch normalization and rectified linear unit (ReLU) activation functions, facilitating feature extraction. Pooling layers, specifically max-pooling, are strategically placed to reduce spatial dimensions while retaining essential information. The decoder module employs upsampling layers, guided by the stored indices, to reconstruct the segmented output. Skip connections, established between corresponding layers in the encoder and decoder, enhance the network's ability to capture hierarchical features. SegNet's adaptability and effectiveness extend beyond its architecture, making it particularly well-suited for a diverse range of applications.

Its implementation in tasks such as autonomous vehicles, medical image analysis, and, in our specific context, floodwater segmentation, underscores its versatility and the impact of its nuanced design on the advancement of semantic segmentation techniques. UNet, a groundbreaking convolutional neural network (CNN) architecture, has emerged as a cornerstone in the realm of biomedical image segmentation, showcasing exceptional performance in various computer vision tasks. Introduced by Ronneberger et al. in 2015, UNet was specifically designed to address challenges related to object localization and semantic segmentation. The architecture of UNet follows a U-shaped design, featuring a contracting path, a bottleneck, and an expansive path. The contracting path, consisting of multiple convolutional and max-pooling layers, captures hierarchical features while gradually reducing spatial dimensions. The bottleneck, at the center of the U, serves as a bridge between the contracting and expansive paths, preserving critical contextual information. The expansive path, characterized by up-convolutional layers, facilitates precise localization and segmentation by gradually restoring spatial dimensions. Notably, skip connections are incorporated, linking corresponding layers in the contracting and expansive paths. This innovation allows UNet to recover fine-grained details, enhancing its capacity to delineate complex structures in images. UNet's architecture is celebrated for its ability to handle limited annotated data efficiently, making it a favored choice in medical imaging applications, where labeled datasets are often scarce. The adaptability and effectiveness of UNet in diverse segmentation tasks underscore its impact on advancing the field of computer vision.

FCN32, or Fully Convolutional Network with a stride of 32 pixels, represents a pivotal advancement in semantic segmentation by eliminating the need for fully connected layers, enabling efficient end-to-end pixel-wise predictions. Introduced by Shelhamer et al., FCN32 is renowned for its ability to process input images of arbitrary sizes and produce dense pixel-level predictions. The architecture is characterized by a sequence of convolutional layers with large receptive fields, efficiently capturing global context information. Importantly, FCN32 incorporates skip connections, linking convolutional layers with corresponding layers in the decoding path to enhance the localization precision of the model. The decoding process involves up-sampling layers, allowing the network

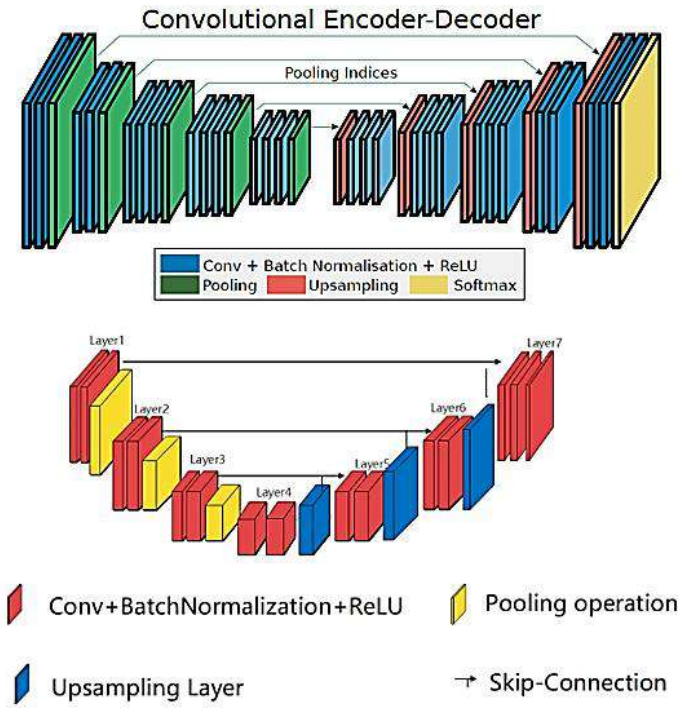

Fig. 2. Top: The Architecture of SegNet. Down: UNet

to produce pixel-wise predictions while preserving spatial information. This approach enables FCN32 to effectively handle varying input sizes and maintain detailed segmentation results. The absence of fully connected layers contributes to computational efficiency and faster inference times, making FCN32 a preferred choice in applications where real-time processing is crucial, such as in our pursuit of floodwater segmentation. The adaptability and accuracy of FCN32 underscore its significance in advancing the field of semantic segmentation and image understanding.

4. Experiments

4.1. Parameter setting

The development of the deep learning model, as detailed in this investigation, was conducted using Keras. All experiments were carried out on a 8-core PC with an i7-6700 processor running at 3.4GHz, 128GB of RAM, and an NVIDIA GeForce RTX 3090. Our approach involved setting the margin at 0.2, implementing random sampling, and executing 1000 training epochs. We employed a publicly accessible dataset consisting of jpeg images for water segmentation. Our preprocessing steps included normalization and standardization of the dimensions for all images. In the course of this study, we allocated 75% of these images for training and validation, reserving the remaining 25% for the testing dataset.

4.2. Metrics

Performance metrics play a crucial role in evaluating the effectiveness of segmentation models. Precision, Sensitivity, also known as True Positive Rate or Recall, and the Dice Coefficient are three crucial metrics in the evaluation of segmentation models. The precision metric provides insights into the model's ability to make accurate positive predictions, minimizing the occurrence of false positives. Sensitivity is formulated as the ratio of true positive predictions to the total number of actual positive instances. It gauges the ability of a segmentation model to accurately capture all relevant regions within the ground truth, emphasizing the minimization of false negatives. On the other hand, the Dice Coefficient measures the similarity between the predicted and true segmentations by evaluating the overlap between the two. A higher Dice Coefficient indicates better agreement between the predicted and actual segmentations, emphasizing a balanced consideration of false positives and false negatives. Sensitivity and Dice Coefficient, together, offer a comprehensive understanding of a segmentation model's performance by highlighting its ability to capture relevant regions while maintaining a precise delineation of the segmented areas. These metrics are particularly valuable in

medical imaging and other fields where the accurate identification of specific regions is crucial.

$$Dice = \frac{2 \times TP}{2 \times TP + FP + FN} \quad (1)$$

$$Recall = \frac{TP}{TP + FN} \quad (2)$$

$$Precision = \frac{TP}{TP + FP} \quad (3)$$

4.3. Results

Tables 1 and 2 provide a comprehensive examination of our analysis, systematically evaluating the performance of different models in water segmentation across a diverse range of metrics. In Table 1, we showcase the results obtained by employing deep learning models with VGG19 [20] as the backbone on the flood area segmentation dataset. On the other hand, Table 2 delves into a detailed exploration of the efficacy of our models utilizing ResNet50 [24]. The VGG-19 is characterized by a configuration comprising 19 layers, including 16 convolutional layers and three fully connected layers. These layers employ 3x3 filters with a stride and padding size of 1 pixel. The choice of compact kernel sizes serves to limit the number of parameters while ensuring comprehensive image coverage. In the VGG-19 model, a 2x2 max pooling operation with a stride of 2 is performed. This model achieved second place in classification and first place in positioning at the 2014 ILSVRC competition, boasting a total of 138 million parameters. ResNet50, belonging to the ResNet (Residual Network) family, stands out as a potent deep-learning model known for its architectural depth and structural innovation. Consisting of a total of 50 layers, the model's architecture introduces groundbreaking residual blocks that redefine the landscape of deep neural networks. These blocks incorporate skip connections, allowing the model to train with exceptional depth while mitigating the vanishing gradient problem. This profound structural innovation empowers ResNet50 to adeptly capture intricate image features, even in the presence of complex and noisy data. Essentially, the architecture's depth accommodates increasingly complex visual data, facilitating the extraction of fine-grained image details.

With 60.8 million parameters, this network excels at recognizing nuanced image variations, making it invaluable for tasks such as medical image detection and classification. The model's distinctive structural resilience and depth position it as a top choice for addressing intricate challenges in image analysis and classification.

Table 1 presents a segmentation comparison of various models with VGG19 as the backbone. The performance metrics, including Dice coefficient, sensitivity, and precision, showcase the effectiveness of each model in accurately delineating water regions in the flood area segmentation dataset. FCN32 demonstrates a Dice coefficient of 0.671±0.0027, sensitivity of 0.652±0.0038, and precision of 0.74±0.028. U-Net exhibits a higher Dice coefficient of 0.75±0.0027, sensitivity of 0.71±0.0019, and precision of 0.821±0.0010. SegNet outperforms both with a Dice coefficient of 0.810±0.0026, sensitivity of 0.77±0.0070, and precision of 0.85±0.054. These results provide a detailed insight into the segmentation capabilities of each model, aiding in the evaluation and selection of the most suitable approach for water segmentation tasks. Table 2 presents a segmentation comparison of various models, employing ResNet50 as the backbone. The table showcases key performance metrics, including Dice coefficient, sensitivity, and precision, offering insights into the models' efficacy in accurately segmenting water regions within the flood area dataset. FCN32 demonstrates a Dice coefficient of 0.690±0.0025, sensitivity of 0.68±0.0024, and precision of 0.77±0.033. U-Net exhibits superior performance with a Dice coefficient of 0.79±0.0038, sensitivity of 0.73±0.0027, and precision of 0.850±0.0034. SegNet continues to excel with a Dice coefficient of 0.84±0.0042, sensitivity of 0.80±0.0062, and precision of 0.88±0.039. These comprehensive metrics aid in the evaluation and comparison of the models, guiding the selection of the most suitable approach for effective water segmentation tasks using ResNet50 as the underlying architecture.

4.4. Statistical analysis

To assess potential statistically significant differences in segmentation performance metrics (Precision, Recall, and Dice) among the models, we can employ statistical techniques like Analysis of Variance (ANOVA), designed for simultaneous comparison of multiple groups. ANOVA allows exploration into whether meaningful disparities exist within the means of different models. The p-values derived from ANOVA serve as indicators to ascertain if significant variations exist among the models for each metric. If the p-values fall below a predetermined significance threshold (e.g., 0.05), it leads to the conclusion that indeed significant differences exist among the models.

The outcomes of the analysis of variance (ANOVA) reveal noteworthy p-values, indicating substantial differences among the models across all three metrics: Precision, Recall, and Dice. Specifically, the p-value for Precision is 3.9e-03, signifying a significant divergence in accuracy among the models. Similarly, the Recall metric yields a p-value of 4.4e-03, reaffirming a significant difference in precision across the models. Additionally, the Dice metric exhibits a small p-value of 5.4e-04, emphasizing a notable variance in recall among the models. In summary, the statistical analysis underscores

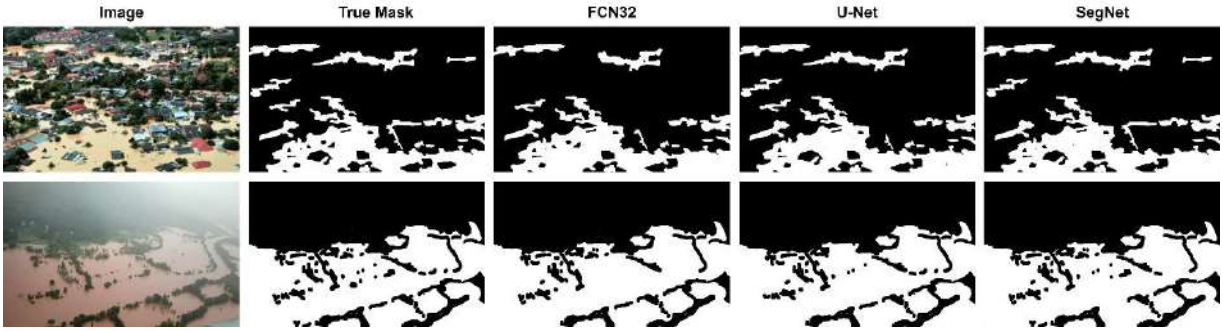

Fig. 3. Segmentation results of FCN, U-Net, and SegNet

Table 1

Segmentation comparison of the different models: VGG19 as backbone

Model	**Dice**	**Sensitivity**	**Precision**
FCN32	0.671±0.0027	0.652±0.0038	0.74±0.028
U-Net	0.75±0.0027	0.71±0.0019	0.821±0.0010
SegNet	0.810±0.0026	0.77±0.0070	0.85±0.054

Table 2

Segmentation comparison of the different models: ResNet50 as backbone

Model	**Dice**	**Sensitivity**	**Precision**
FCN32	0.690±0.0025	0.68±0.0024	0.77±0.033
U-Net	0.79±0.0038	0.73±0.0027	0.850±0.0034
SegNet	0.84±0.0042	0.80±0.0062	0.88±0.039
Model	Dice	Sensitivity	Precision
FCN32	0.671±0.0027	0.652±0.0038	0.74±0.028
U-Net	0.75±0.0027	0.71±0.0019	0.821±0.0010
SegNet	0.810±0.0026	0.77±0.0070	0.85±0.054

significant performance disparities among segmentation models across all metrics, underscoring the influential role of model selection in shaping classification performance.

5. Conclusion

In this study, deep-learning models explicitly designed for floodwater segmentation were thoroughly evaluated. Prominent deep learning architectures were employed, and their performance was meticulously assessed using diverse metrics, including Precision, Recall, and Dice. Valuable insights into the efficacy of these models in addressing the challenge of water segmentation were provided through our comprehensive analysis. SegNet emerged as the top performer, showcasing outstanding and consistent results across all metrics, highlighting its efficiency and effectiveness in accurately segmenting water. With a Dice coefficient of 0.84 and a precision of 0.88, SegNet excelled in minimizing false positives, a critical aspect of this application. Furthermore, a flawless recall score of 0.80 was achieved, demonstrating SegNet's ability to accurately capture the majority of genuine water patches.

References

[1] Taghavian, Hadi, Miroslav Černík, and Lukáš Dvořák. "Advanced (bio) fouling resistant surface modification of PTFE hollow-fiber membranes for water treatment." Scientific Reports 13.1 (2023): 11871. https://doi.org/10.1038/s41598-023-38764-9.

[2] Gheibi, Mohammad, et al. "Design of a decision support system to operate a NO2 gas sensor using machine learning, sensitive analysis and conceptual control process modelling." Chemosensors 11.2 (2023): 126.

[3] Kiyan, Amirhossein, et al. "The operation of urban water treatment plants: A Review of smart dashboard frameworks." Environmental Industry Letters 1.1 (2023).

[4] Zaffaroni, Mirko, and Claudio Rossi. "Water segmentation with deep learning models for flood detection and monitoring." International Journal of Information Systems for Crisis Response and Management (2020): 24-27.

[5] Zadeh, Sara Shomal, Meisam Khorshidi, and Farhad Kooban. "Concrete Surface Crack Detection with Convolutional-based Deep Learning Models." arXiv preprint arXiv:2401.07124 (2024).

[6] Toosi, Golnoosh. "Influence of Vegetation in The Flood Drainage Ditch." Journal of Civil Engineering Researchers 5.4 (2023): 16-21. https://doi.org/10.61186/JCER.5.4.16.

[7] Nguyen, Quynh Nhu, Antonella Frisiello, and Claudio Rossi. "Co-design of a crowdsourcing solution for disaster risk reduction."

Proceedings of the First CoNEXT Workshop on ICT Tools for Emergency Networks and DisastEr Relief. 2017.

[8] Badrinarayanan, Vijay, Alex Kendall, and Roberto Cipolla. "Segnet: A deep convolutional encoder-decoder architecture for image segmentation." IEEE transactions on pattern analysis and machine intelligence 39.12 (2017): 2481-2495.

[9] Ronneberger, Olaf, Philipp Fischer, and Thomas Brox. "U-net: Convolutional networks for biomedical image segmentation." Medical image computing and computer-assisted intervention–MICCAI 2015: 18th international conference, Munich, Germany, October 5-9, 2015, proceedings, part III 18. Springer International Publishing, 2015.

[10] Long, Jonathan, Evan Shelhamer, and Trevor Darrell. "Fully convolutional networks for semantic segmentation." Proceedings of the IEEE conference on computer vision and pattern recognition. 2015.

[11] Kharraji, M., Abbasi, H., Orouskhani, Y., Shomalzadeh, M., Kazemi, F., & Orouskhani, M. (2023). Brain Tumor Segmentation with Advanced nnU-Net: Pediatrics and Adults Tumors. Mostafa and Kazemi, Foad and Orouskhani, Maysam, Brain Tumor Segmentation with Advanced nnU-Net: Pediatrics and Adults Tumors (July 18, 2023).

[12] Voulodimos, Athanasios, et al. "Deep learning for computer vision: A brief review." Computational intelligence and neuroscience 2018 (2018).

[13] Yang, Han-Chung, Chuan-Yi Wang, and Jia-Xue Yang. "Applying image recording and identification for measuring water stages to prevent flood hazards." Natural hazards 74 (2014): 737-754.

[14] Vincent, O. Rebecca, and Olusegun Folorunso. "A descriptive algorithm for sobel image edge detection." Proceedings of informing science & IT education conference (InSITE). Vol. 40. 2009.

[15] Zhu, Zhenhua, Ioannis Brilakis, and Gustavo Parra-Montesinos. "Real-time concrete damage visual assessment for first responders." Construction Research Congress 2009: Building a Sustainable Future. 2009.

[16] Pan, Jinqiu, et al. "Deep learning-based unmanned surveillance systems for observing water levels." Ieee Access 6 (2018): 73561-73571.

[17] Ning, Huan, et al. "Prototyping a social media flooding photo screening system based on deep learning." ISPRS international journal of geo-information 9.2 (2020): 104.

[18] Park, Somin, et al. "Computer vision–based estimation of flood depth in flooded-vehicle images." Journal of Computing in Civil Engineering 35.2 (2021): 04020072.

[19] He, K., Gkioxari, G., Dollár, P., & Girshick, R. Mask r-cnn. In Proceedings of the IEEE international conference on computer vision (2017). (pp. 2961-2969).

[20] Kharazi, Bahareh Alizadeh, and Amir H. Behzadan. "Flood depth mapping in street photos with image processing and deep neural networks." Computers, Environment and Urban Systems 88 (2021): 101628.

[21] Simonyan, Karen, and Andrew Zisserman. "Very deep convolutional networks for large-scale image recognition." arXiv preprint arXiv:1409.1556 (2014).

[22] Pally, R. J., and S. Samadi. "Application of image processing and convolutional neural networks for flood image classification and semantic segmentation." Environmental Modelling & Software 148 (2022): 105285.

[23] https://www.kaggle.com/datasets/faizalkarim/flood-area-segmentation/data

[24] He, Kaiming, et al. "Deep residual learning for image recognition." Proceedings of the IEEE conference on computer vision and pattern recognition. 2016.

Journal of Civil Engineering Researchers

Journal homepage: www.journals-researchers.com

Effect of Geometry and Size of Fiber Reinforced Plastic Deck Profile on Behavior of Bridges

Ali nazemi deylami,[a,*]

[a] *Department of Civil Engineering, Takestan Branch, Islamic Azad University, Qazvin, Iran*

ABSTRACT

Due to the important role that bridges play in rescue operations after an earthquake, it is necessary that these structures have a higher level of protection against seismic attacks. Earthquake identifies the weak points of the structure and causes the most damage there. Bridges are very vulnerable to these attacks due to their low degree of uncertainty. All bridges built before 1971 were designed with the elastic design method (permissible stress). In this method, the effects of plasticity, section cracking, and plastic deformation are not taken into account. The change of seismic locations based on the principles of elastic design is much less. It is because the structure experiences in a real earthquake, one of the consequences of which is the falling of the decks due to the loss of the support surface. The decision to strengthen the bridge was made when there were many bending and shear cracks on the king beams. The bridge was created. The use of FRP profiles can significantly prevent the damage caused by corrosion and is a good alternative to the traditional methods of strengthening the structure. In this study, a design for the deck of a steel bridge with I beams is presented. The shape of reinforcement using FRP fibers with vinyl ester resins has also been investigated, the effect of the geometry of FRP profiles has been investigated. The presented specifications are optimized to obtain a lasting shape and section, especially for the pultrusion process. FRP materials are light, resistant to corrosion and have high tensile strength. These materials come in different forms and range from multi-layer factory sheets to dry sheets that can be twisted on various structural forms before adding resin, is available. The durability and high tensile strength of FRP materials are among the advantages of these materials. The durability and long-term performance of FRP requires more research, which is ongoing and continues.

© 2024 Journals-Researchers. All rights reserved.

ARTICLE INFO

Received: January 12, 2024
Accepted: March 23, 2024

Keywords:
FRP
Glass fibers
Bridge decks
Pultrusion
Materials tests
Optimization

DOI: 10.61186/JCER.6.1.9
DOR: 20.1001.1.22516530.1399.11.4.1.1

1. Introduction

Society has searched continuously for new and better materials for building structures. New materials usually come to the stage due to the necessity to improve structural efficiency and performance. However, new materials in turn provide opportunities to develop new structural forms, and present material scientists and engineers with new challenges. One of the best manifestations of the abovementioned inter-related process is associated with

* Corresponding author. Tel.: +989112435320; e-mail: Nazemideylami@gmail.com.

Fiber Reinforced Polymer (FRP) composite materials in bridge applications to which this research is devoted.

In the past few years, FRP composite bridge deck systems have been experimentally implemented in bridge structures. Worldwide, there are many finished or currently underway FRP deck projects. However, an examination of the published resources shows that proper characterization methods and generally accepted design and analysis procedures of FRP bridge decks have not yet been established. While technical difficulties limit the development of affordable fabrication methods to produce low-cost, large-scale FRP bridge decks, the lack of comprehensive analysis and design codes and guidelines for FRP bridge decks is one of the key reasons that FRP decks have so far been applied only in demonstration projects.

To develop analysis and design guidelines and overcome any potential reluctance to use FRP decks, every potential aspect of deck behavior over its service life should be examined experimentally and analytically. There exist at least two principal characteristics that are of primary importance in FRP bridge deck applications, namely stiffness and strength. The stiffness of an FRP deck is the ability of the deck to resist changes in shape when a load is applied. In FRP deck design, a deflection limit is usually used to consider the deck's stiffness. Deck strength is the deck's ability to resist permanent deflection from applied loads (static, dynamic and environmental loads etc.). The development of analysis and design guidelines is primarily based on the comprehension of the stiffness deflection and strength capacity characteristics of FRP deck systems. Other issues on the use of FRP decks, such as dynamic response, durability, efficiency and structural optimization etc., are also related to the understanding FRP deck stiffness and strength.

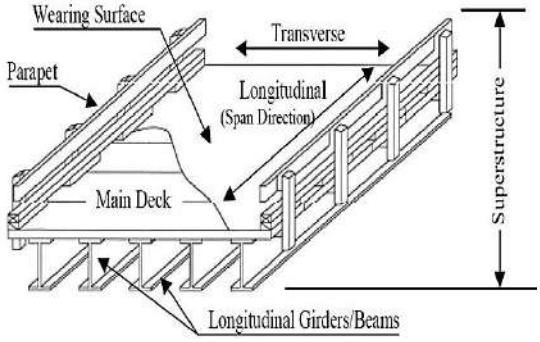

Fig.1 The structure of an engineering bridge [1]

To develop effective FRP deck systems, research pertaining to design and analysis of FRP decks should be fully considered. Analyzing an FRP bridge deck system requires full knowledge of the geometric properties and the material properties. The geometric properties are obtained in the design stage of the deck system. The material and mechanical properties of FRP decks are usually obtained though experimental characterization of the mechanical properties at the coupon, component, and full deck scale levels. In the following section, the development of FRP deck geometric configuration and deck characterization techniques will be reviewed. Also, available analytical models for structural analysis of FRP decks will be presented.

2. Fundamentals of FRP Composite Bridge Decks

A number of terms that are commonly used to describe the upper structure of a bridge are shown in Figure 1. Bridge components more than the bearings are referred to as the superstructure, while the substructure includes all the parts underneath. The main body of the bridge consists of the superstructure, which includes the deck and girders or girders. In this structure, FRP bridge deck is defined as an element made of FRP that transfers shear loads to supports and longitudinal beams.

At present, two major types of FRP deck are currently used in engineering works; Sandwich structure and pultruded structure. Sandwich structures consist of strong, high-stiffness top sheets that can withstand bending loads and have very low density. The core of shear strength is placed between the top sheet and the bottom sheet, which determine the performance of the deck composite. The top sheets are usually made of matte E-glass or a top of polyester or vinyl ester. Core materials include rigid foam or FRP materials in the form of thin-walled cells shown in Figure 2. Cellular materials are the most important materials for structural weight-sensitive applications. Figure 3 shows the sections of the FRP bridge deck.

Pultrusion is an industrial process used to produce continuous parts with a constant cross-section. This process is low cost and with high production volume. This process is similar to the process of metal extrusion, with the difference that instead of pushing the material in the mold, which happens in extrusion, the material is pulled out of the mold, so that the name of this process in English, pultrusion, is also a combination of two words pull (to means pulling) and extrusion. Pultrusion is one of the methods designed to make composites with high mechanical properties that are competitive with traditional and engineering materials. The parts produced by this method have a high volume fraction of fibers; These fibers are mostly placed in the longitudinal direction of the piece. Although with the right weave of fibers, it is possible to have fibers in the transverse direction, but mainly the main properties are in the longitudinal direction. The products obtained from this process have high strength, low weight

and long life, especially in acidic environments. Paltrogen can be used to make any continuous part, provided that it has a constant cross-section and does not have grooves or holes in the direction perpendicular to the tension, such as cans, corners, pipes, rods and similar shapes. The pultrusion process is shown in Figure 4.

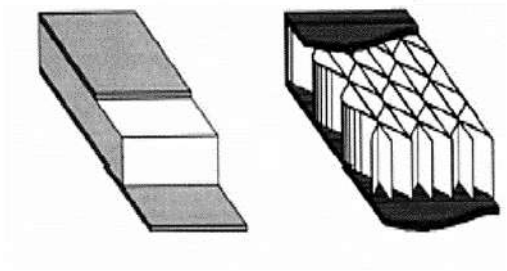

Fig. 2. Examples of types of bridge structures with FRP decks [2].

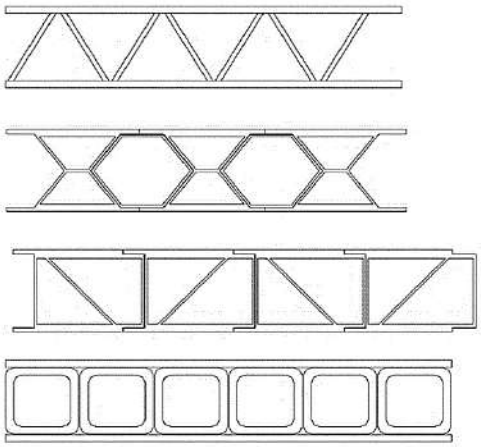

Fig. 3. Types of FRP bridge deck sections [2].

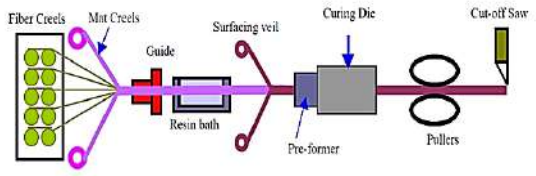

Fig.4. pultrusion process [1]

Table 1 shows the technical comparison between pultruded FRP decks and sandwich sections. As you can see, the sections prepared by the sandwich method are more flexible than the pultruded sections and can create different structures of depth and hardness in the deck. The weight per unit area is usually close to 98 kg/m2, with the exception of the shutter system (Hand/automated lay-up in Table 1), which reduced weight seems to have a higher efficiency in the use of materials. As indicated by the normalized twist, there is currently no consensus on the amount of deck twist and deflection by manufacturers. Due to the technical difficulties of producing larger parts, some pultruded companies have designed designs that use smaller parts of pultruded modules, such as prismatic or box beams and rectangular plates that are connected to form a large deck.

Table. 1. Available features of FRP decking [1]

Deck systems *(Available in the U.S.)*	Depth *(mm)*	[1]Weight *(kg/m²)*	Cost *($/m²)*	[2]Deflection *Reported*	[3]Deflection *Normalized*
Sandwich Construction					
Hardcore Composites (VARTM)	152-710	98-112	570-1184	L/785	L/1120
KSCI (Hand/automated lay-up)	127-610	76	700	L/1300	L/1300
Adhesively Bonded Pultrusions					
DuraSpan	194	90	700-807	L/450	L/340
Superdeck	203	107	807	L/530	L/530
EZSpan	229	98	861-1076	L/950	L/950
Strongwell	120-203	112	700	L/605	L/325

[1] Without wearing surface. [2] Assumes plate action. [3] Normalized to HS20+IM for 2.4 m center-to-center spans.

Fig. 5. Lab testing configuration [1]

3. Experiment-Based Modeling

Zhou's laboratory model (2002) [1] has been used in the verification for modeling in Abaqus software. In this research, the stiffness and strength of bridge decks built with FRP sections have been investigated. The considered sections are multi-cell sections of FRP bridge decks, which include FRP pultruded sections. In this research, two types of loading have been used to analyze FRP sections. A loading according to the ASSHTO bridge code, which is placed on the bridge as a metal piece, and a loading in the form of truck tires, which applies the actual truck load on the bridge. For validation, loading is considered as a truck load (Figure 5).

The model used in this research is used as the primary model and the basis of modeling in the continuation of the current research work. The section of the FRP profile used

is box section. The cross-section of the laboratory is shown in (figure 6).

The test load was applied to each block by means of a hydraulic cylinder mounted on a load frame, by means of designed loaded pieces. To investigate the local failure of the deck under real truck tire loading, real truck contact patches made of silicone rubber were used. First, a real 22.86 cm (9 inch) truck tire was cut into four pieces. Then the two pieces are filled with silicone rubber gel. After about 24 hours of cooling at room temperature, the rubber pieces filled with tires were ready for testing.

The normal stress distribution of a truck tire and the normal stress distribution of a steel patch are shown in (Figure 7).

However, the normal stress distribution obtained from pressure sensor films indicate that failure tests using steel loading patches are not reliable, since there is no contact at all on most of the deck surface and dominated by contact at the edges. The normal stress distribution of the real truck tire is non-uniform as shown in (Figure 8).

Fig. 6. Box cross section profile [1]

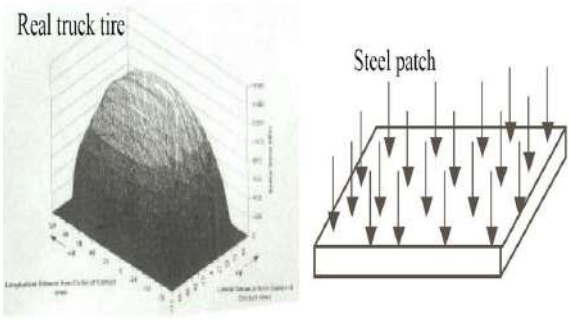

Fig. 7. Normal Stress of a real truck tire and steel Patch [1]

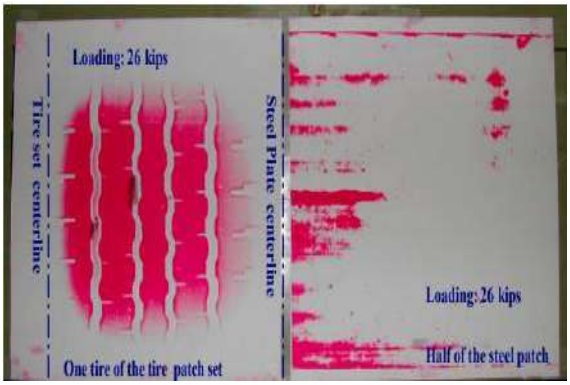

Fig. 8. Normal Stress Distributions of a truck tire and a steel plate using pressure film sensor [1]

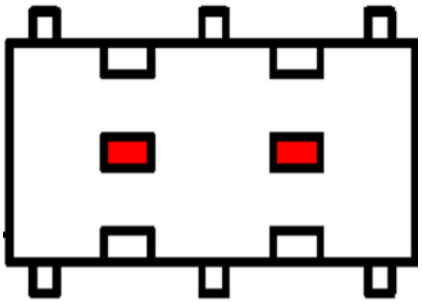

Fig. 9. Normal Stress Distributions of a truck tire [1]

To validate the numerical and laboratory model, loading is used as follows. In this loading, truck tires are loaded in the west and east center of the deck (Figure 9).

The load-displacement diagram is drawn at the points under the load and compared with the laboratory results. (Figure 10).

4. Research method and modeling process in software

The designed cross-section is shown in (Figure 11) [1]. This deck has a length of 4.65 meters and a width of 1.52 meters, which consists of ten box beams (or rectangular tubes) of orthotropic paltrode with dimensions of 15.24 x 15.24 x 0.95 meters. A sheet with a thickness of 0.635 meters at the bottom and a sheet with a thickness of 1.27 meters at the top and 9 steel bolts are placed transversely in the deck. The weight of the deck is about 726 kg with a density of 910.3 kg/m3. To date, no approved specifications and regulations have been proposed for bridges with FRP decks. However, the design and loading ranges in the AASHTO Standard Specification for Highways [AASHTO, 1996] and the AASHTO LRFD Specification, [AASHTO, 1998] for laboratory test models have been used by many FRP deck researchers [1].

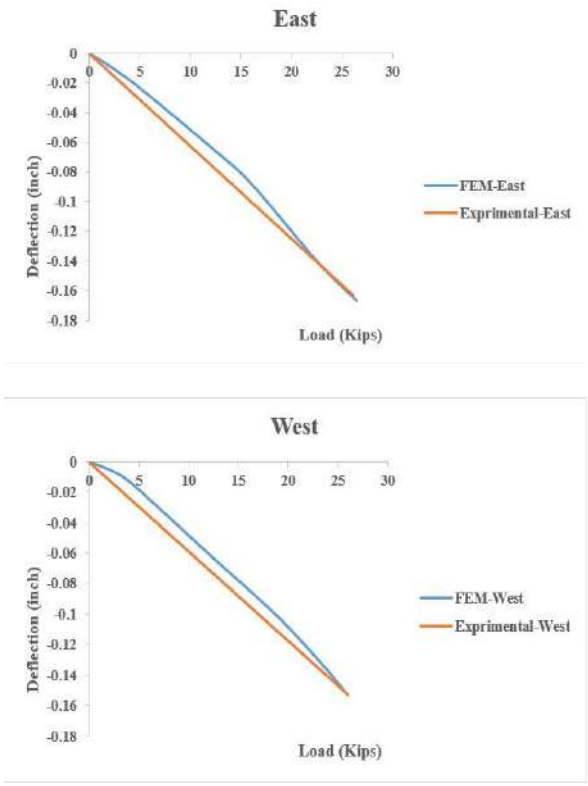

Fig.10. Displacement-load curve as central east and west

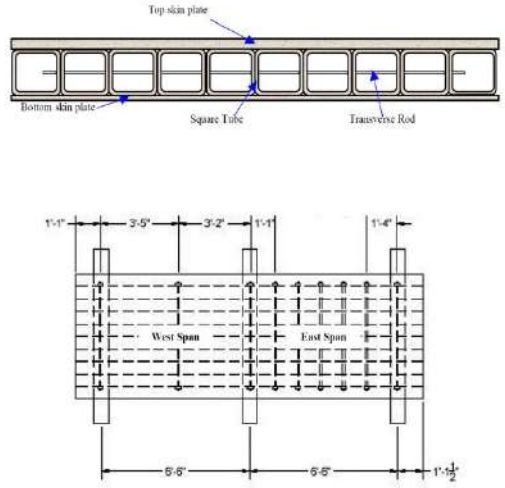

Fig. 11. Cross section of the deck and transverse bars [1]

According to AASHTO [5] Highway Code, when designing the upper members of a bridge, specified loads are used at critical locations to produce the maximum load effect. The load that produces the greatest stress is known as the design load. Bridge designers can extend the design wheel load over a limited level of the deck by calculating the load effects in a reinforced concrete block. This area is defined as the "tire contact area" and the equation used to calculate it is given in the specification.

The parameters investigated in this research include the change of span length and the change of FRP cross-section and the type of loading (traffic and earthquake). The basic model is the study model of Zhou (2002) [1], which has a box section. It is (Figure 12). The second profile examined in this research, the trapezoidal profile was chosen as the second section for examination (Figure 13).

To check and consider the span length of the bridge deck, once the length of the deck has been checked with three I-shaped supports and another time with four I-shaped supports (Figure 14).

To investigate the performance of FRP deck under different loadings, two types of loading have been considered. Traffic loading according to the AASHTO regulations for trucks and the vertical loading component of the Naghan earthquake, which has been applied to the foundations of the bridge.

Abaqus software provides the possibility of separately modeling the components of a model and then assembling and assembling the components to form the model.

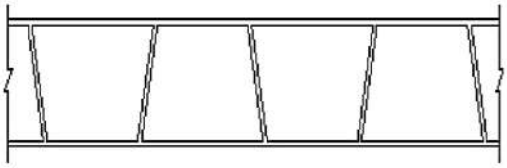

Fig. 13.Trapezoidal cross section [3]

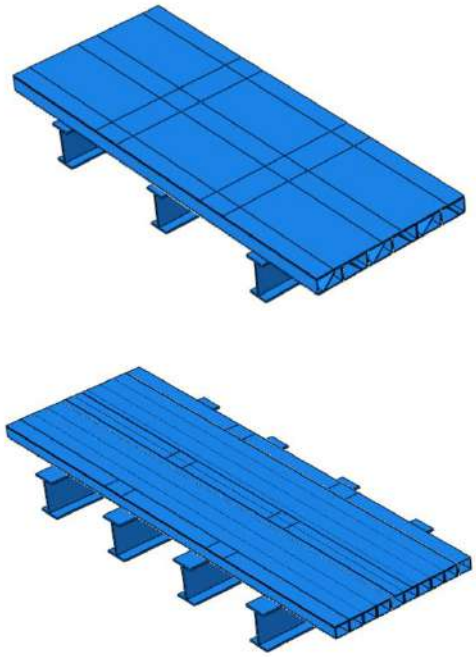

Fig. 14. Deck openings used in research

Behavioral characteristics and materials used in FRP deck modeling are according to the table below. Box and trapezoid sections are considered as below (Table 2).

5. Analysis method and loading steps

To perform the analysis, one of three static methods, explicit dynamic and indirect dynamic methods can be used. In dynamic methods in solving the equations, the effect of inertia is also considered and it may spread to immortal waves in the system, for this reason, if these analytical methods are used, it must be ensured that the loading time is considered long enough that the effects dynamic in the system is negligible. Absorbing boundary conditions can also be used to dampen the waves propagated in the system under dynamic movements. On the other hand, because these methods solve dynamic equations in the system, generally the program execution time to reach the results is much longer than static methods.

Table. 2. Material specification in FRP deck modeling

Property	Value
$E_{xx}\,(psi)$	2.5×10^{6}
$E_{yy}\,(psi)$	0.8×10^{6}
$E_{zz}\,(psi)$	0.8×10^{6}
$G_{xy}\,(psi)$	0.425×10^{6}
$G_{xz}\,(psi)$	0.425×10^{6}
$G_{yz}\,(psi)$	0.364×10^{6}
ν_{xy}	0.33
ν_{xz}	0.33
ν_{yz}	0.10

In the places where two separate elements collide during the nonlinear analysis, the characteristics related to the collision should be defined on two surfaces. Otherwise, the collision is not considered in the solution and in the term two elements collide. To define the feature related to the collision, the collision feature must be defined in the software according to the nature of the collision of the elements. In normal collisions, the collision surface has a tangential and frictional behavior. The use of contact behavior in modeling gives the ability to simulate collision and separation of two surfaces in tension.

The loaded areas of the deck are shown in (Figure 15). Loading mode 2-5 is used to simulate truck axle load. Loading modes 1-4 and 3-6 are used to simulate load axis with the expectation of generating more stresses in the northwest and northeast and southwest and southeast regions for modes 1-4 and 3-6. Mode 2 and Mode 5 will be the loading locations for the failure tests.

The principles of live load loading have been carried out according to the regulations of AAshto [5]. In this research, a 90-ton truck load has been loaded on the bridge. The considered loading mode is the most critical loading mode on the bridge according to the study. According to the width of 10 meters of the crossing and compliance with the distances mentioned in the regulations, the number of crossing lanes for this truck is considered to be 3.

Another mode of loading considered for the current research is earthquake loading, which is chosen as cyclic loading for the current research. Earthquake in the form of acceleration-time entered vertically at the bridge supports. Also, the supports at the place of connection to the bases are considered as holders.

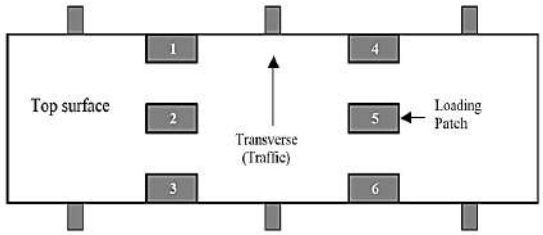

Fig. 15. Deck loaded areas [1]

6. Modeling with Abaqus finite element software

The current research has been carried out with the aim of investigating bridges with FRP decks. The investigated parameters include the type of FRP section, the length of the bridge spans, the type of loading (traffic and earthquake). In Table 3, the investigated models are named.

As can be seen in the table above, the number of models under review is 8 models. To check the performance of the FRP bridge deck under the conditions investigated in this research, the maximum vertical load and displacement diagrams of the deck and the von Mises stress contours of the models have been examined and the results of the models have been compared with each other to obtain the appropriate cross-section and span.

Figure 16 shows the stress versus time diagram for model A-1. This diagram is drawn for the maximum stress developed in FRP sections during loading time. As can be seen in the diagram, the maximum compressive stress is 130 and the tensile stress is 600 MPa.

Figure 17 shows the strain versus time diagram for model A-1. This graph is plotted for the maximum strain developed in FRP sections during loading time. As can be

seen in the diagram, the maximum compressive strain is 5.37 and the tensile strain is 0.58 mm.

In figure 18, the contour of von Mises stress created in the I-shaped supports of model A-1 is drawn. As can be seen in the figure, the highest von Mises stress created is equal to 231 MPa and the lowest von Mises stress is equal to 0.66 MPa.

Table. 3. Introducing the investigated model

Load type	The number of openings	FRP section	MODEL
Traffic	3	BOX	A-1
Traffic	4	BOX	A-2
Earthquake	3	BOX	A-3
Earthquake	4	BOX	A-4
Traffic	3	Trapezius	B-1
Traffic	4	Trapezius	B-2
Earthquake	3	Trapezius	B-3
Earthquake	4	Trapezius	B-4

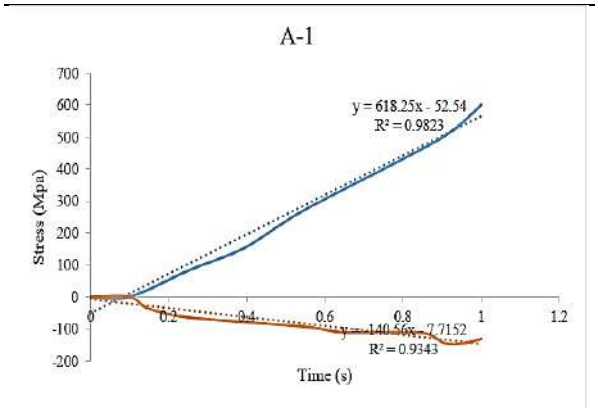

Fig. 16.Stress diagram of model A-1

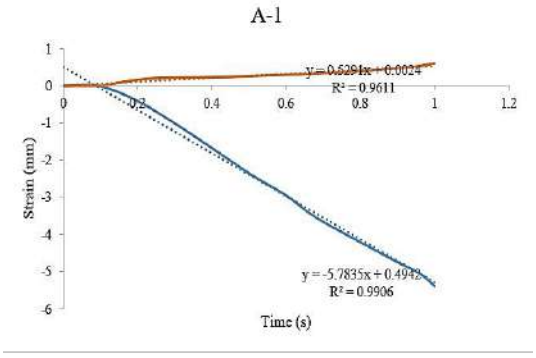

Fig. 17.Strain diagram of model A-1

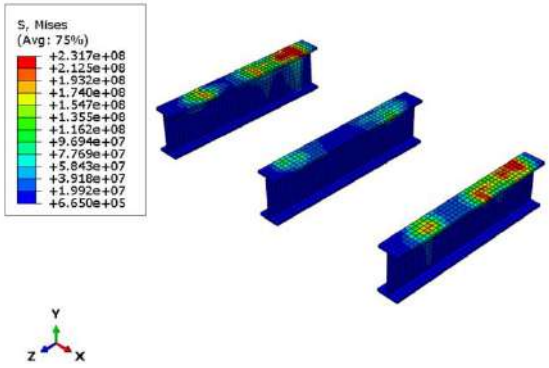

Fig. 18. Von Mises stress contour of model A-1 supports

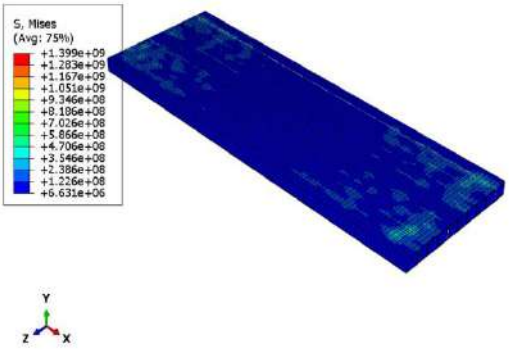

Fig. 19. Von Mises stress contour of FRP sections model A-1

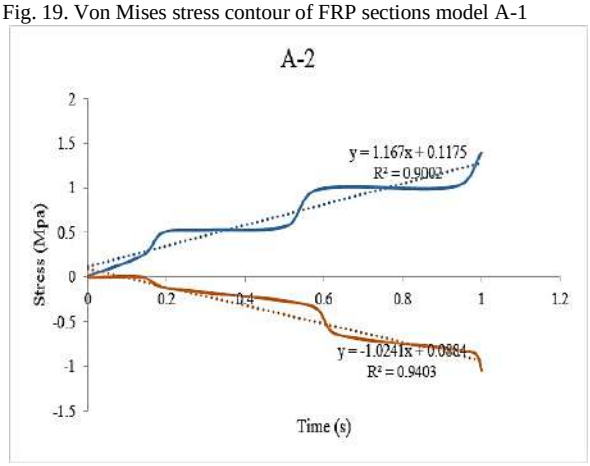

Fig. 20.Stress diagram of model A-2

Figure 19 shows the von Mises stress contour created in the FRP sections of the A-1 deck. As seen in the figure, the highest von Mises stress created in FRP sections is equal to 1399 MPa and the lowest von Mises stress is equal to 6.63 MPa.

Figure 20 shows the stress versus time diagram for model A-2. This diagram is drawn for the maximum stress developed in FRP sections during loading time. As can be seen in the diagram, the maximum compressive stress is 1.05 and the tensile stress is 1.4 MPa.

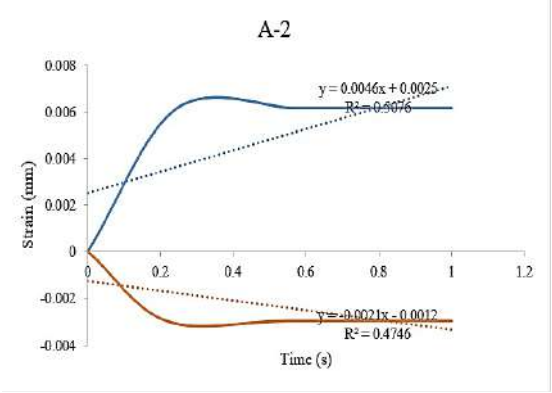

Fig. 21.Strain diagram of model A-2

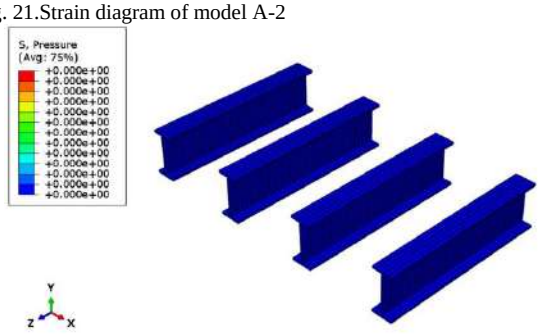

Fig. 22. Von Mises stress contour of model A-2 supports

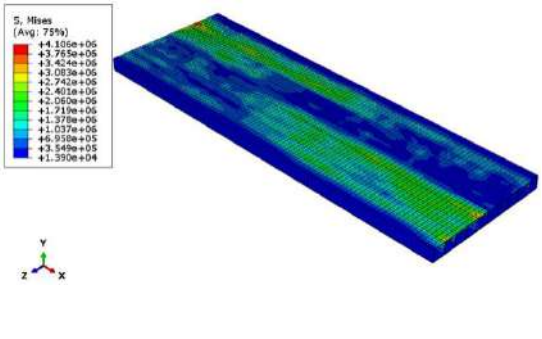

Fig. 23. Von Mises stress contour of FRP sections model A-2

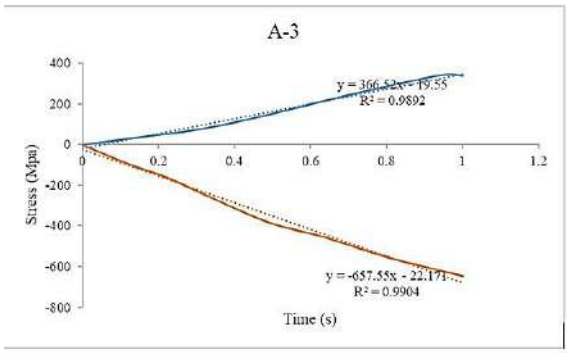

Fig. 24.Stress diagram of model A-3

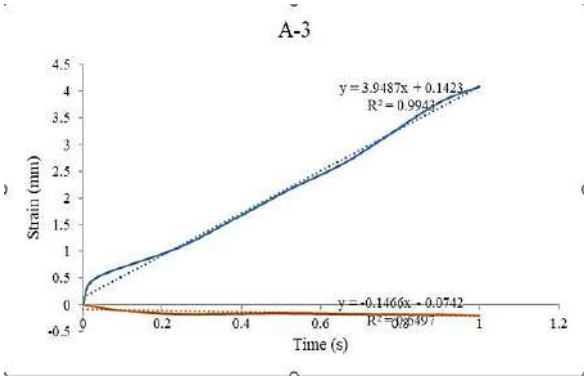

Fig. 25.Strain diagram of model A-3

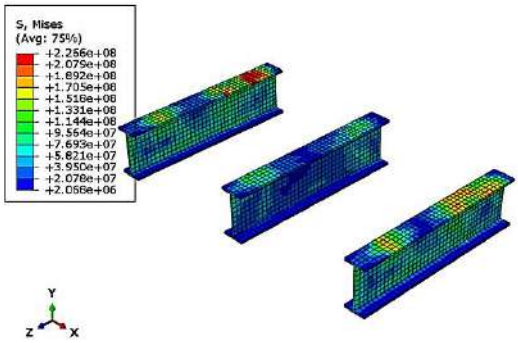

Fig. 26. Von Mises stress contour of model A-3 supports

Figure 21 shows the strain versus time diagram for model A-2. This diagram is drawn for the maximum strain developed in FRP sections during loading time. As can be seen in the diagram, the maximum compressive strain is 0.003 and the tensile strain is 0.006 mm.

In figure 22, the contour of von Mises stress created in the I-shaped supports of model A-2 is drawn. As can be seen in the figure, by reducing the length of the opening and increasing the supports, there is no significant stress due to the traffic load in the supports.

Figure 23 shows the von Mises stress contour created in the FRP sections of the A-2 deck. As seen in the figure, the highest von Mises stress created in FRP sections is equal to 4.1 MPa and the lowest von Mises stress is equal to 0.013 MPa.

Figure 24 shows the stress versus time diagram for model A-3. This diagram is drawn for the maximum stress developed in FRP sections during loading time. As can be seen in the diagram, the maximum compressive stress is equal to 646 and the tensile stress is equal to 343 MPa.

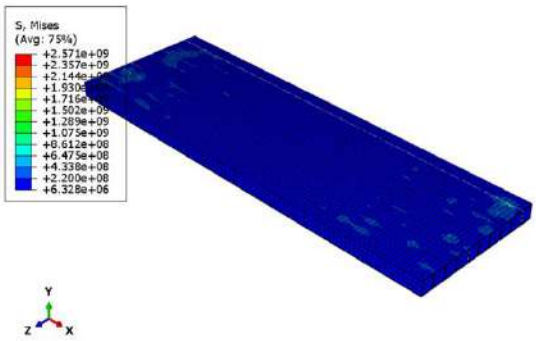

Fig. 27. Von Mises stress contour of FRP sections model A-3

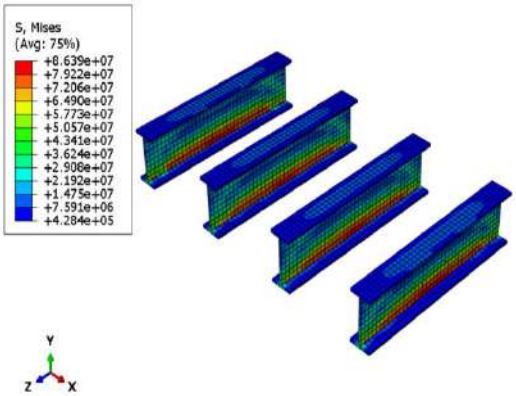

Fig. 30. Von Mises stress contour of model A-4 supports

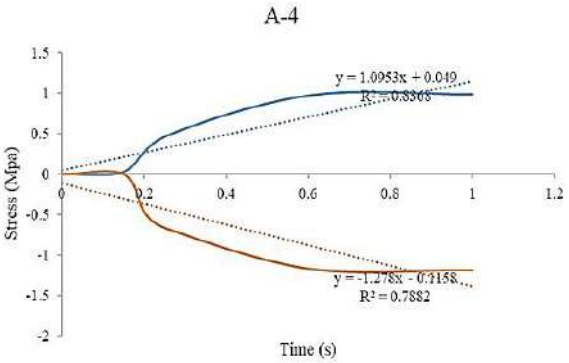

Fig.28.Stress diagram of model A-4

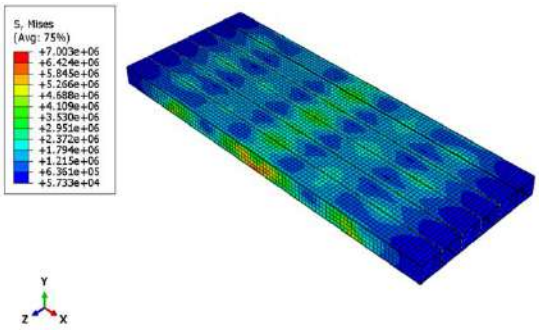

Fig. 31. Von Mises stress contour of FRP sections model A-4

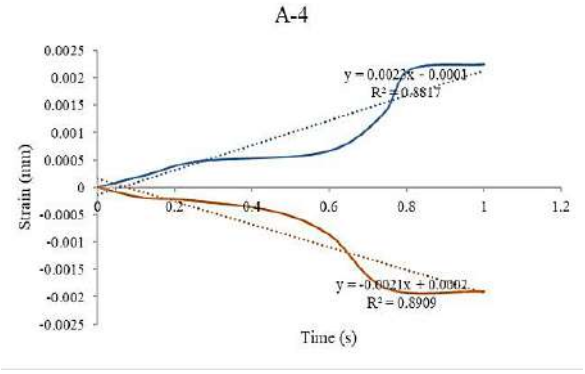

Fig. 29.Strain diagram of model A-4

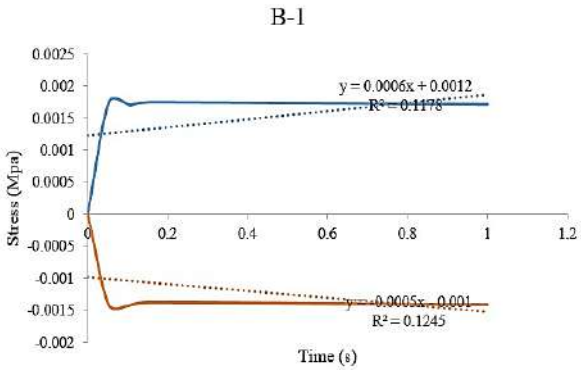

Fig. 32.Stress diagram of model B-1

Figure 25shows the strain versus time diagram for model A-3. This diagram is drawn for the maximum strain developed in FRP sections during loading time. As can be seen in the diagram, the maximum compressive strain is 0.21 and the tensile strain is 4.09 mm.

In Figure 26, the contour of the von Mises stress created in the I supports of the A-3 model is drawn. As can be seen in the figure, the highest von Mises stress created is equal to 226 MPa and the lowest von Mises stress is equal to 2.06 MPa.

Figure 27 shows the von Mises stress contour created in the FRP sections of the A-3 deck. As seen in the figure, the highest von Mises stress created in FRP sections is equal to 2571 MPa and the lowest von Mises stress is equal to 6.32 MPa.

Figure 28 shows the graph of stress versus time for model A-4. This diagram is drawn for the maximum stress developed in FRP sections during loading time. As can be seen in the diagram, the maximum compressive stress is 1.18 and the tensile stress is 0.98 MPa.

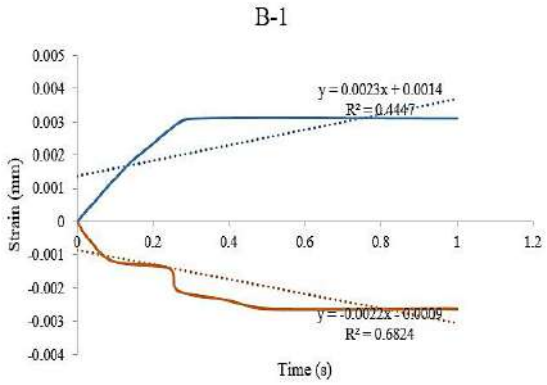

Fig. 33.Strain diagram of model B-1

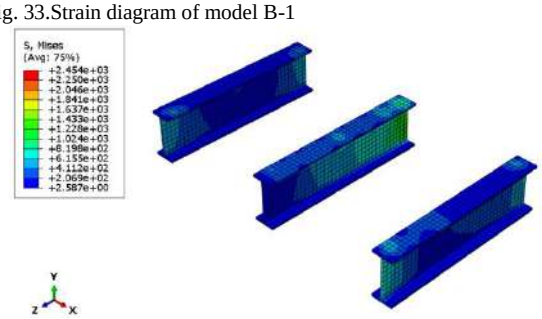

Fig. 34. Von Mises stress contour of model B-1 supports

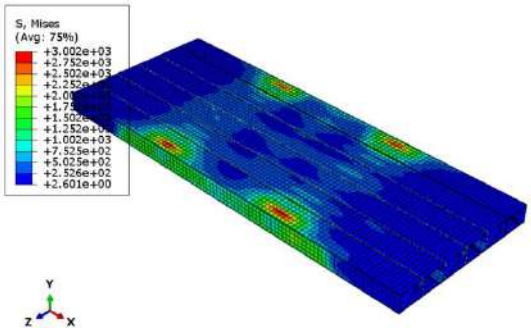

Fig. 35. Von Mises stress contour of FRP sections model B-1

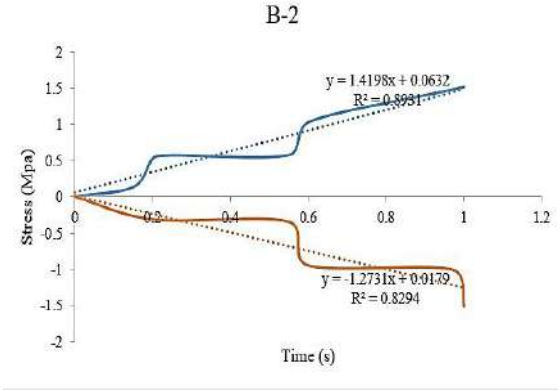

Fig. 36.Stress diagram of model B-2

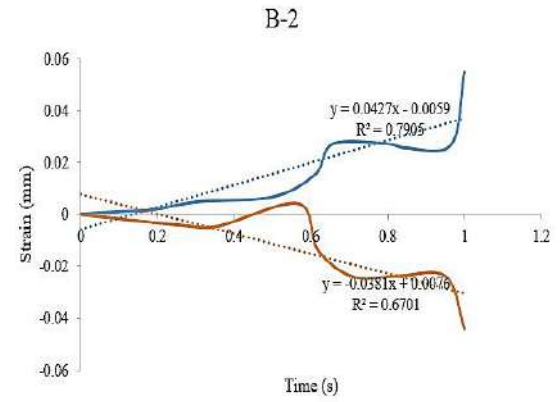

Fig. 37.Strain diagram of model B-2

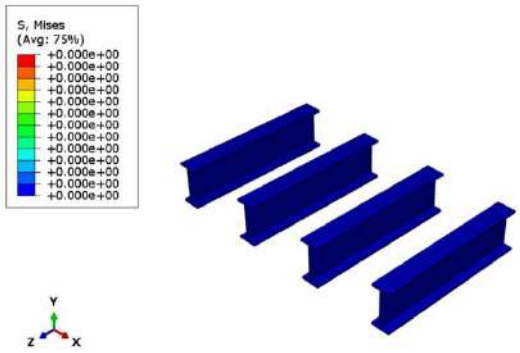

Fig.38. Von Mises stress contour of model B-2 supports

Figure 29 shows the strain versus time diagram for model A-4. This diagram is drawn for the maximum strain developed in FRP sections during loading time. As can be seen in the diagram, the maximum compressive strain is 0.0018 and the tensile strain is 0.0022 mm.

In Figure 30, the contour of the von Mises stress created in the I supports of the A-4 model is drawn. As seen in the figure, the highest von Mises stress created is equal to 86 MPa and the lowest von Mises stress is equal to 1.48 MPa.

Figure 31 shows the von Mises stress contour created in the FRP sections of the A-4 deck. As seen in the figure, the highest von Mises stress created in FRP sections is equal to 7 MPa and the lowest von Mises stress is equal to 0.05 MPa.

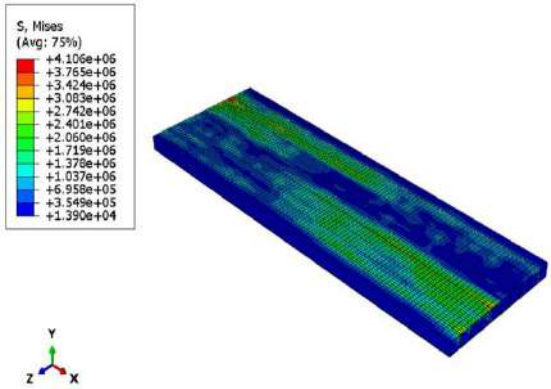

Fig.39. Von Mises stress contour of FRP sections model B-2

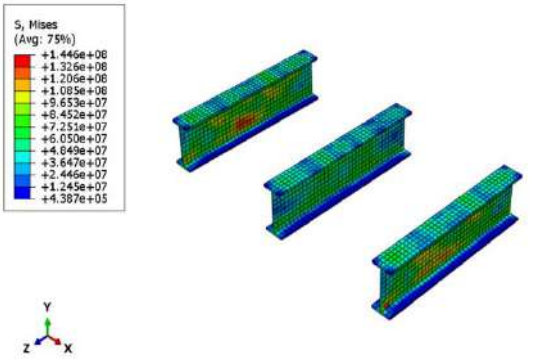

Fig.42. Von Mises stress contour of model B-3 supports

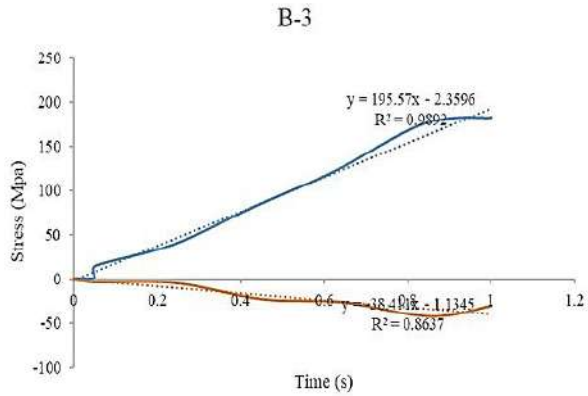

Fig. 40.Stress diagram of model B-3

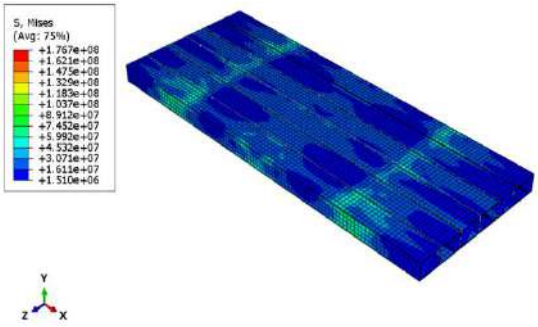

Fig.43. Von Mises stress contour of FRP sections model B-3

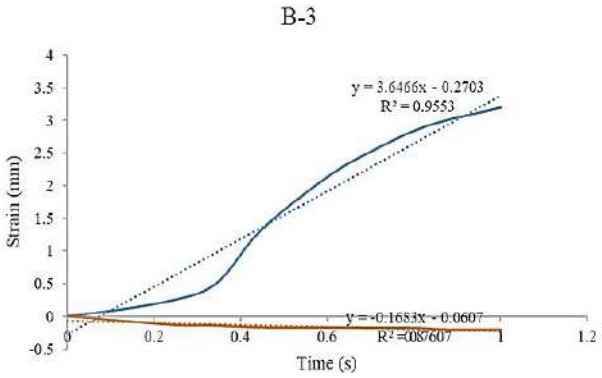

Fig. 41.Strain diagram of model B-3

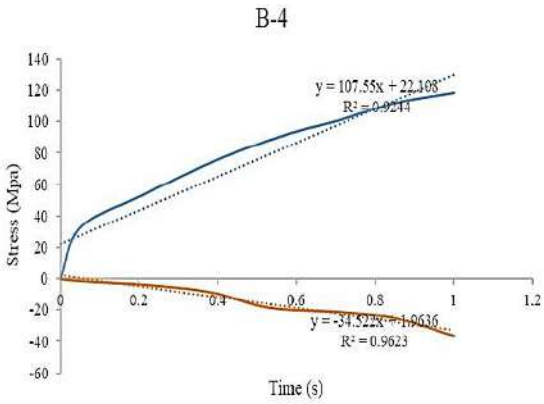

Fig. 44.Stress diagram of model B-4

Figure 32 shows the stress versus time diagram for model B-1. This diagram is drawn for the maximum stress developed in FRP sections during loading time. As can be seen in the diagram, the maximum compressive stress is equal to 0.0014 and the tensile stress is equal to 0.0017 MPa.

Figure 33 shows the strain versus time diagram for model B-1. This diagram is drawn for the maximum strain developed in FRP sections during loading time. As can be seen in the diagram, the maximum compressive strain is equal to 0.0026 and the tensile strain is equal to 0.003 mm.

Figure 34 shows the contour of the von Mises stress created in the I-shaped supports of model B-1. As seen in the figure, the highest von Mises stress created is equal to 2.45 k Pa and the lowest von Mises stress is equal to 0.66 Pascal.

Figure 35 shows the contour of the von Mises stress created in the FRP sections of the model B-1 deck. As can be seen in the figure, the highest von Mises stress created in FRP sections is equal to 3 kilopascals and the lowest von Mises stress is equal to 2.6 Pa.

Figure 36 shows the stress versus time diagram for model B-2. This diagram is drawn for the maximum stress developed in FRP sections during loading time. As can be seen in the diagram, the maximum compressive stress is equal to 1.5 and the tensile stress is equal to 1.51 MPa.

Figure 37 shows the strain versus time diagram for model B-2. This diagram is drawn for the maximum strain developed in FRP sections during loading time. As can be seen in the diagram, the maximum compressive strain is 0.043 and the tensile strain is 0.054 mm.

In Figure 38, the contour of the von Mises stress created in the I-shaped supports of the B-2 model is drawn. As it can be seen in the figure, by reducing the length of the opening and increasing the supports, there is no significant stress due to the traffic load in the supports.

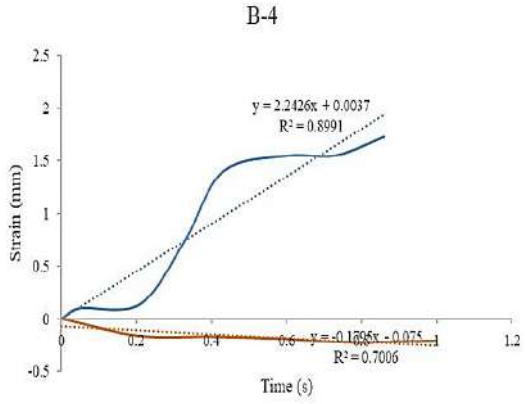

Fig. 45.Strain diagram of model B-4

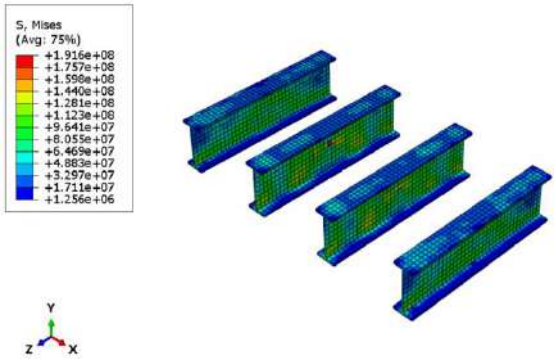

Fig.46. Von Mises stress contour of model B-4 supports

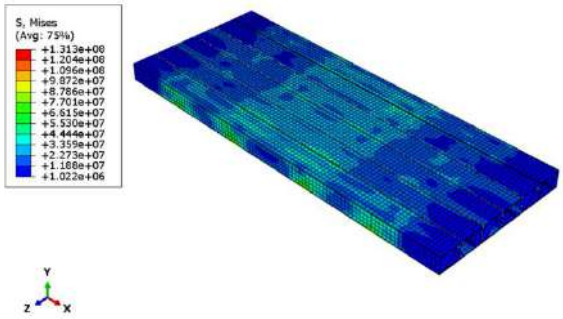

Fig.47. Von Mises stress contour of FRP sections model B-4

Figure 39 shows the von Mises stress contour created in the FRP sections of the model B-2 deck. As can be seen in the figure, the highest von Mises stress created in FRP sections is equal to 4.2 MPa and the lowest von Mises stress is equal to 0.014 MPa.

Figure 40 shows the graph of stress versus time for model B-3. This diagram is drawn for the maximum stress developed in FRP sections during loading time. As can be seen in the diagram, the maximum compressive stress is 42 MPa and the tensile stress is 182 MPa.

Figure 41 shows the strain versus time diagram for model B-3. This diagram is drawn for the maximum strain developed in FRP sections during loading time. As can be seen in the diagram, the maximum compressive strain is 0.207 and the tensile strain is 3.2 mm.

In Figure 42, the contour of the von Mises stress created in the I-shaped supports of the B-3 model is drawn. As seen in the figure, the highest von Mises stress created is equal to 144 MPa and the lowest von Mises stress is equal to 0.43 MPa.

Figure 43 shows the von Mises stress contour created in the FRP sections of the B-3 deck. As seen in the figure, the highest von Mises stress created in FRP sections is equal to 176 MPa and the lowest von Mises stress is equal to 1.51 MPa.

Figure 44 shows the stress versus time diagram for model B-4. This diagram is drawn for the maximum stress developed in FRP sections during loading time. As can be seen in the diagram, the maximum compressive stress is equal to 36 and the tensile stress is equal to 118.25 MPa.

Figure 45 shows the strain versus time diagram for model B-4. This diagram is drawn for the maximum strain developed in FRP sections during loading time. As can be seen in the diagram, the maximum compressive strain is 19 and the tensile strain is 23.9 mm.

In Figure 46, the contour of the von Mises stress created in the I-shaped supports of the B-4 model is drawn. As seen in the figure, the highest von Mises stress created is equal to 191.6 MPa and the lowest von Mises stress is equal to 1.25 MPa.

Figure 47 shows the von Mises stress contour created in the FRP sections of the B-4 deck. As can be seen in the

figure, the highest von Mises stress created in FRP sections is equal to 131.3 MPa and the lowest von Mises stress is equal to 1 MPa.

7. Conclusion

As can be seen in models 2 and 4 where the length of the deck spans is reduced, the amount of stress created in the FRP sections of the deck is greatly reduced. Also, in models 2 and 4, where the length of the deck openings has been reduced, the amount of strain created in the FRP sections of the deck has been greatly reduced. Therefore, it can be concluded that by reducing the length of the deck span in bridges with FRP box sections, the amount of stress and strain of the deck is reduced.

The compared stresses in trapezoidal FRP sections under traffic and earthquake loading show that in models 3 and 4, where the loading is in the form of an earthquake, the amount of stress created in the FRP sections of the deck has increased greatly. As in models 3 and 4, where the loading is in the form of an earthquake, the amount of strain created in the FRP sections of the deck has increased greatly. Therefore, it can be concluded that in bridges with trapezoidal FRP sections, the amount of deck stress and strain depends on the type of loading rather than the length of the span and the type of loading. By comparing the stress of trapezoidal and boxy FRP sections under traffic loading, it can be seen that in the model with boxy section and longer opening length, the amount of stress created in the FRP sections of the deck is higher than the rest of the models. Also, the strain of trapezoidal and boxy FRP sections under traffic loading has been compared. As can be seen, in the model with a boxy cross-section and longer opening length, the amount of strain created in the FRP sections of the deck is higher than the rest of the models. Therefore, it can be concluded that the stress and strain created in box sections is more than trapezoidal sections.

Comparing the stress of trapezoidal and boxy FRP sections under earthquake loading shows that in the boxy model with 3 openings, the amount of stress created in the FRP sections of the deck is much less than the rest of the models. Also, comparing the strain of trapezoidal and boxy FRP sections under earthquake loading, as can be seen in the boxy model with 3 openings, the amount of strain created in the FRP sections of the deck is much less than the rest of the models.

Acknowledgments

I would like to thank my dear supervisor Prof. Dr. Asghar Vatani Oskouei and my wife for helping me in this study.

References

[1] Zhou, Aixi. Stiffness and strength of fiber reinforced polymer composite bridge deck systems. Diss. Virginia Polytechnic Institute and State University, 2002.
[2] Liu, Zihong. Testing and analysis of a fiber-reinforced polymer (FRP) bridge deck. Diss. Virginia Tech, 2007.
[3] Camata, Guido, and P. Benson Shing. Evaluation of GFRP Deck Panel for the O'Fallon Park Bridge. No. CDOT-DTD-R-2004-2,. Colorado Department of Transportation, Research Branch, 2004.
[4] Davalos, Julio F., et al. "Modeling and characterization of fiber-reinforced plastic honeycomb sandwich panels for highway bridge applications." Composite structures 52.3-4 (2001): 441-452.
[5] American Association of State Highway and Transportation Officials (AASHTO), “Specifications for Highway Bridges”, Washington, 17th Edition, 2010
[6] Japan Road Association. "Reference for Seismic Retrofit of Existing Highway Bridges." Maruzen, Tokyo, Japan (1998).
[7] Karbhari, Vistasp M. "Materials considerations in FRP rehabilitation of concrete structures." Journal of materials in civil engineering 13.2 (2001): 90-97.

Journal of Civil Engineering Researchers

Journal homepage: www.journals-researchers.com

Evaluation of Geopolymer Concrete Based on Fly Ash Containing Steel Fibers and Rubber Crumbs Using Cement as a Partial Substitute for Fly Ash

Shahin Charkhtab Moghaddam,[a] Rahmat Madandoust,[b,*] Morteza Jamshidi,[a] Iman M. Nikbin,[c]

[a] *Department of Civil Engineering, Chalous Branch, Islamic Azad University,Chalous, Iran*

[b] *Department of Civil Engineering, University of Guilan, Rasht, Iran*

[c] *Department of Civil Engineering, Rasht Branch, Islamic Azad University, Rasht, Iran*

ABSTRACT

In this study, geopolymer concrete made from fly ash was utilized, with different proportions of cement (0%, 10%, and 20%) replacing fly ash to examine the influence of cement presence in geopolymer concrete. To increase tensile strength and impact resistance, 0.5 and 1 percent steel fibers were used. Adding 0.5 percent fibers improved compressive strength by 9 percent, and for 1 percent fibers, it was 26 percent. The tensile strength also significantly increased with the addition of fibers. Adding 0.5% fibers, on average, increased the tensile strength by 25%, with the increase being 34% for 1% fibers. It was also noted that substituting cement for fly ash had little effect on compressive strength, but replacing 10% cement could be considered as the optimal substitution level in terms of tensile strength in the samples.

The test results for impact resistance indicated a significant effect of steel fibers on the number of impacts until the first crack appeared and the complete rupture of the samples. Adding fibers increased the resistance to complete rupture by 12 to 22 percent with 0.5 percent fibers, and between 49 to 64 percent for 1 percent fibers. Replacing 10 percent rubber crumbs improved the impact energy of concrete, increasing the energy until the first crack by 10 percent on average and the energy until complete rupture by 15 percent.

© 2024 Journals-Researchers. All rights reserved.

ARTICLE INFO

Received: February 09,2024
Accepted: March 27,2024

Keywords:
Mechanical properties
Geopolymer concrete
Ash
Steel fibers
Rubber crumbs

DOI: 10.61186/JCER.6.1.22
DOR: 20.1001.1.22516530.1399.11.4.1.1

1. Introduction

The concrete industry is facing various challenges due to the increasing use of Portland cement, primarily because of limited cement resources. On one side, reducing production and carbon dioxide emissions, on the other hand the increasing construction activities and high demand for cement have led researchers to seek suitable alternatives for cement in concrete. Researchers have introduced fly ash, metakaolin, iron slag and other pozzolans as suitable substitutes for cement [1-3]. Substituting these pozzolans for cement not only

* Corresponding author. Tel.: +989113314970; e-mail: Rmadandoust@guilan.ac.ir.

effectively reduces environmental pollution but also enhances the mechanical properties of concrete and decreases the widespread need for cement [4]. Using rubber crumbs as a partial substitute for aggregates in geopolymer concrete can reduce the environmental effects caused by the accumulation of waste rubber tires. However adding rubber crumbs to concrete reduces its resistance properties due to the lower hardness of rubber crumbs compared to natural aggregates and their weak bonding with cement paste [5]. This can be compensated for by adding steel fibers which not only offset a considerable portion but also overall enhance the geopolymer concrete's resistance [6]. Therefore, in this study geopolymer concrete based on fly ash has been used. Additionally the effects of adding rubber crumbs and steel fibers as well as cement as a partial substitute for fly ash on the mechanical properties of concrete have been evaluated.

1.1. Case studies on the mechanical properties of geopolymer concrete based on fly ash and the impact of steel fibers, rubber crumbs, and cement in it

In recent years, there has been a significant amount of research focused on geopolymer concrete, aiming to enhance its quality, strength, and longevity through the addition of various materials like different types of fibers and other additives below are some of these studies:

In 2018, Guo conducted a study on the mechanical properties of geopolymer concrete reinforced with steel fibers [7]. The results of this research indicate that adding steel fibers up to 0.4% increases the compressive strength of geopolymer concrete. However further additions of steel fibers decrease the compressive strength. Moreover, the flexural strength of concrete decreases with the addition of 0.1% fibers but then increases by 20% with the addition of up to 0.5% fibers.

In another study, Islam investigated the effect of adding 0.5% steel fibers to fly ash-based geopolymer concrete on its mechanical properties [8]. The results suggest that adding fibers leads to a slight increase in compressive strength and a significant increase in tensile strength. However, the increase in tensile and impact resistance due to the addition of fibers is much greater. For example the increase in compressive strength is 33-35% higher than the increase in tensile strength. Additionally it was observed that adding 0.5% fibers had no significant effect on the elastic modulus of geopolymer concrete.

Vijai [6] examined geopolymer concrete composed of 90% fly ash and 10% cement. The impact of adding 0.25%, 0.5%, and 1% steel fibers on the concrete strength was measured. The results indicate that adding fibers increases the compressive, tensile and flexural strength by 73%, 128%, and 17%, respectively.

In a study conducted by Park in 2016 [5] it was determined that adding rubber powder up to 20% significantly reduces the compressive strength of fly ash-based geopolymer concrete. Researchers suggested an optimal use of rubber powder to minimize the reduction in concrete strength, typically between 10% to 15%.

Hongen [9, 10] investigated the addition of cement to fly ash-based geopolymer concrete and its impact on compressive strength. Adding cement enables the concrete to perform well at ambient temperatures due to cement hydration. Hydration leads to increased compressive and tensile strength as well as providing energy for polymerization. In this research, adding 5% cement resulted in increased compressive strength. Many studies have reported a reduction in compressive strength when rubber powder is added to geopolymer concrete attributed to poor adhesion between rubber crumbs and other materials and the low inherent strength of rubber crumbs. Reductions in strength of up to 33% have been reported.

1.2. Objectives and Necessity of the Project

Geopolymer is a novel material in the construction industry with desirable performance and efficiency. It is made using natural pozzolans and industrial waste containing aluminum silicate making it environmentally friendly. It can serve as a substitute material to reduce pollution caused by the production of Portland cement used in concrete. On the other hand the mechanical properties and durability of this concrete have prompted further research into the factors influencing these two characteristics. Given the importance of sustainable development and recycling of waste rubber, using rubber crumbs in concrete can reduce environmental impacts resulting from the accumulation of waste rubber. However, adding rubber crumbs to concrete reduces its resistance properties due to the lower hardness of rubber crumbs and their weak bonding with other concrete components. Therefore steel fibers have been used to increase the concrete's resistance and compensate for the decrease in resistance due to rubber crumbs. Past research has shown that adding rubber crumbs reduces the concrete's resistance but reinforcing the concrete with steel fibers not only prevents the reduction but also increases its resistance. The combined effect of steel fibers and rubber crumbs in normal concrete has been investigated in many studies, and the current study aims to examine the parameters affecting fly ash-based geopolymer concrete containing rubber crumbs and steel fibers. Some studies have considered fly ash-based geopolymer concrete to have a similar structure to normal concrete[16, 17] but the addition of steel fibers and rubber crumbs due to their different bonding with fly ash compared to cement, can have different effects.

Table1
Concrete mixture proportion.

Number	Mix Id	(Kg/m^3) Cement	Fly ash	Crum rubber	Coarse aggregate	Fine aggregate	Steel fiber
1	G100%SF0%	0	408	19.67	1347	491.83	0
2	G100%SF0.5%	0	408	19.20	1347	479.95	39
3	G100%SF1%	0	408	18.72	1347	468.08	78
4	G90%SF0%	40.8	367.2	20.23	1347	505.83	0
5	G90%SF0.5%	40.8	367.2	19.76	1347	493.95	39
6	G90%SF1%	40.8	367.2	19.28	1347	482.08	78
7	G80%SF0%	81.6	326.4	20.79	1347	519.83	0
8	G80%SF0.5%	81.6	326.4	20.32	1347	507.95	39
9	G80%SF1%	81.6	326.4	19.84	1347	496.08	78
10	G100%SF0%CR0%	0	408	0	1347	576.63	0

The necessity of assessing the strength of geopolymer concrete through different tests is heightened by above factors. Tests such as compressive and tensile strength and modulus of elasticity are conducted to determine the concrete's resistance and ultrasonic wave velocity tests are used to assess the quality of concrete and the effect of steel fibers and rubber crumbs in concrete. Additionally, impact tests are conducted to assess the dynamic impact resistance and the effect of rubber crumbs and steel fibers and the substitution of cement instead of fly ash are analyzed and investigated.

2. Laboratory Experimental Design

2.1. Consumables

Portland Type II cement produced by Deilaman Cement plant with a specific weight of 33.3 kilograms per cubic meter and a specific surface area of 3200 square centimeters per gram was used in this study. Fly ash in powdered form with a density of 2.45 grams per cubic centimeter was utilized. The fine aggregate used was washed natural sand with a fineness modulus of 2.95 and a specific weight of 2.75 grams per cubic centimeter and the coarse aggregate was crushed stone with a maximum size of 19 millimeters and a specific weight of 2.65 grams per cubic centimeter in accordance with ASTM-C33 requirements. Steel fibers with hooked ends 0.5 centimeters in length, a diameter of 0.8 millimeters, and an aspect ratio of 62.5 and a density of 7.87 grams per cubic centimeter produced by Daroocham Factory were used. The rubber crumbs used in this research have a specific weight of 0.95 grams per cubic centimeter. The curing process in this research was carried out at 60 degrees Celsius in accordance with geopolymer concrete standards.

2.2. Mixing Design

For this project, 10 mixing designs were selected. Given that geopolymer concrete is the material of choice, no water content was used in their formulation. Design 1 to 9 incorporate 10% by volume of fine rubber crumps, and the geopolymer concrete samples are grouped into three main categories.

The first group contains 100% fly ash with varying volumes of steel fibers (0%, 0.5%, and 1%). The second group contains 90% fly ash with 10% cement and varying volumes of steel fibers (0%, 0.5%, and 1%). The third group contains 80% fly ash and 20% cement with varying volumes of steel fibers (0%, 0.5%, and 1%).

Mixing design number 10 consists of 100% geopolymer concrete without fibers and rubber crumbs. To achieve consistent workability in each mixing design and to achieve a slump of approximately 20 ± 100 millimeters, a superplasticizer of 6.2 kilograms per cubic meter and an alkali solution of 163.2 kilograms per cubic meter were added to each mixing design. The mixing design for the samples is provided in "Table 1".

2.3. Conducted Experiments

In this study, the compressive strength test was conducted based on the BS EN 12390 standard [18], using cubic specimens with dimensions of 100 millimeters. Additionally, the splitting tensile strength test was performed according to ASTM C496 [19] regulations. The specimens for this test were cylindrical with a diameter of 15 millimeters and a height of 30 centimeters. The ultrasonic pulse velocity test [20] was carried out following ASTM C597 standards using a DUNDIT MODEL PC1012 with an accuracy of ±0.1 microseconds for a transducer

frequency of 55 KHz and ±2% for time-of-flight measurement. The parameter measured by the ultrasonic testing device was the transit time in microseconds, from which the wave velocity through the samples was determined considering their dimensions. The concrete resistance against dynamic (impact) loads was assessed based on the ACI 544-2R committee report [21] using the drop weight hammer test. In the current investigation, the weight-drop testing device with repeated impact loads was applied to disc specimens with a diameter of 15 centimeters and a height of 63.5 centimeters. The number of repetitive impacts (a weight of 4.54 kilograms dropped from a height of 457 millimeters) on a steel anvil placed at the center of the sample's surface was recorded to reach a specific level of cracking (first visible crack and complete spalling).

3. Results and Discussion

3.1. Compressive and Tensile Strength Test Results

In this section, the results of the conducted evaluations and the influence of parameters on compressive and tensile strength test results, including the presence of rubber crumbs, substitution of cement for fly ash, and the impact of steel fibers, are presented.

As illustrated in "Figure 1," the compressive strength values increase with the addition of steel fibers. In the current study, the reason for the increased compressive strength in specimens containing steel fibers can be explained as follows: since concrete containing rubber crumbs has lower and softer resistance compared to ordinary concrete, the fibers present in the concrete act before the complete failure of the sample due to cracks created in the concrete. These fibers enhance the resistance of the specimen. Under axial loads, cracks occur in the microstructure of the concrete. The most significant effect of fibers is preventing crack propagation in geopolymer concrete. Therefore, the ability of fibers to transfer stress prevents the development and propagation of microcracks caused by internal stresses in the concrete.

Considering the shape and quantity of fibers, they bear some of the stresses occurring within the fly ash matrix and transfer the rest to the stable portions of the fly ash matrix [6, 22]. Similarly, Seymouz et al. stated in their research that, in general, the compressive strength of concrete mixtures increases with the addition of fibers. This increase is due to the constraints imposed by the fibers in the concrete. Under compressive force, concrete tends to expand due to the Poisson effect, while fibers counteract this effect, resulting in an increase in compressive strength [23]. According to Figure 2, the increase in compressive strength with the addition of 0.5% steel fibers in mixtures containing 80%, 90%, and 100% fly ash is 9%, 4%, and 2%, respectively, and the increase in compressive strength with the addition of 1% steel fibers is 21%, 8%, and 26%, respectively.

Substituting cement as part of the fly ash, as previously mentioned, can increase hydration and may enhance compressive strength. According to Figure 2, replacing 10% of cement has either maintained or decreased compressive strength in the samples, and replacing 20% of cement instead of fly ash has decreased compressive strength in all samples. This can be attributed to two related factors. First, based on previous research [9], the optimal replacement percentage for substituting cement instead of fly ash in geopolymer concrete has been stated as 5%, and higher amounts have led to a decrease in compressive strength. The second factor is the curing temperature, which becomes significant with the addition of cement. As mentioned earlier, geopolymer concrete curing is conducted at a temperature of 60 degrees Celsius, while adding cement may alter the curing temperature and the required time for curing to increase compressive strength.

Adding steel fibers to geopolymer concrete (containing fly ash and rubber particles) increased the tensile strength. In Figure 3, it can be observed that with an increase in the volume percentage of fibers from 0 to 1%, the tensile strength of the mixtures in the first to third groups increased from 2.3, 3.92, and 3.26 MPa to 3.4, 4.9, and 3.86 MPa, respectively. The ability of fibers to prevent crack propagation can be considered a factor in this increase. The mechanism of increasing tensile strength is due to the presence of fibers, which involve stress transfer through surface shear between the matrix and fibers or through interlocking of fibers and matrix (if the fiber surface undergoes deformation). This stress sharing between the matrix and fibers continues until the matrix cracks, after which all stresses are transferred to the fibers. Thomas and Ramaswamy also attributed the increase in tensile strength of concrete containing steel fibers to the bridging effect of fibers in the cement matrix. Substituting 10% of cement resulted in an increase in tensile strength in all samples, and then, with further substitution up to 20%, the tensile strength decreased. In other words, the optimal percentage of cement substitution considering tensile strength is stated as 10%.

3.1.1. The relationship between compressive strength and tensile strength

In Table 2, the relationship between compressive strength and tensile strength is presented by various researchers. Relationship number 1 is derived for conventional concrete, Relationship number 2 represents the correlation between strengths in low-calcium geopolymer concrete cured at ambient temperature and Relationship number 3 is suitable for geopolymer concrete

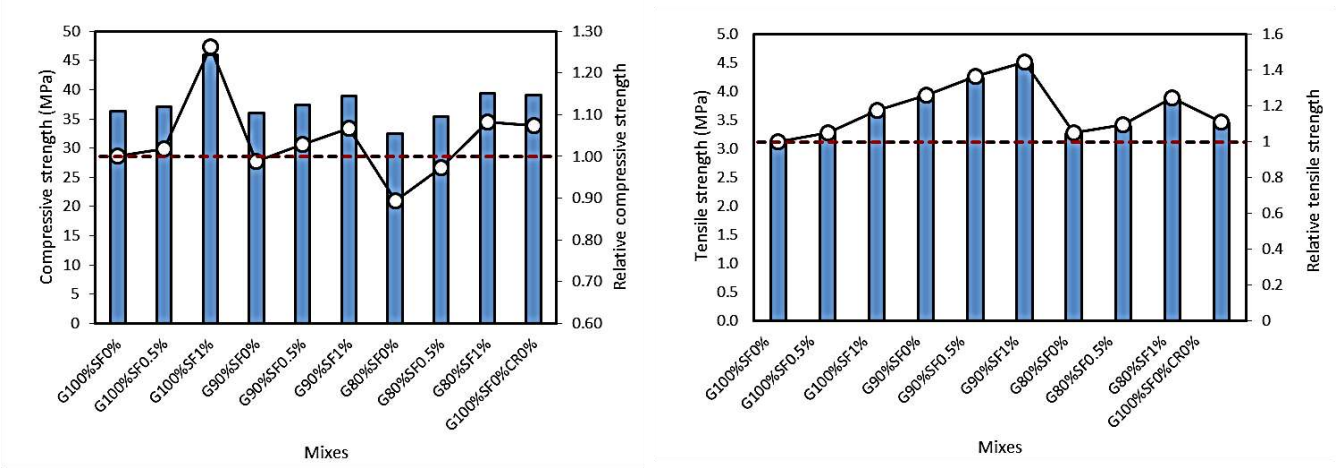

Figure 1: Variations in the values of compressive and tensile strengths of the specimens

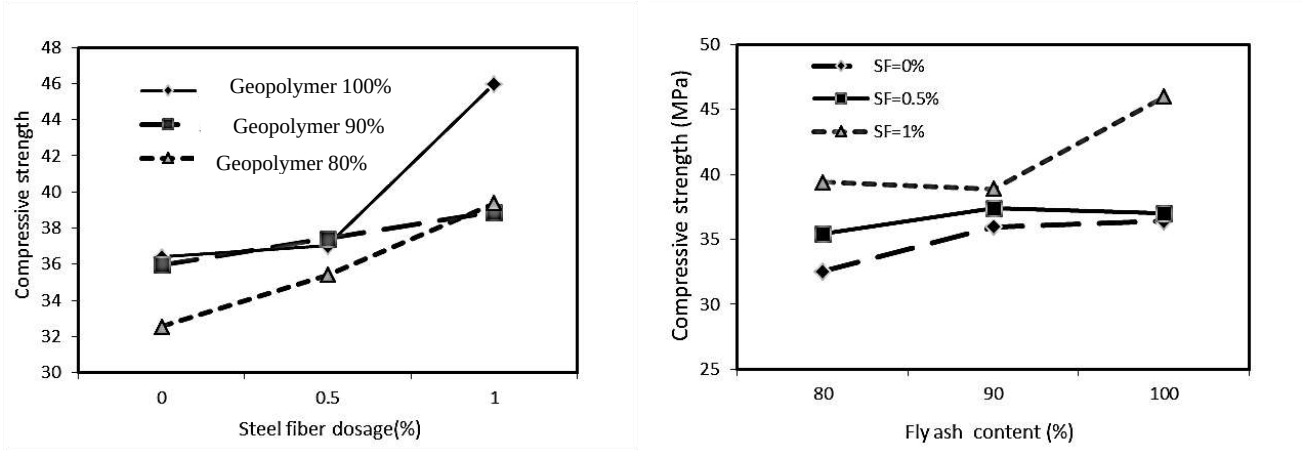

Figure 2: The effect of steel fibers and cement substitution instead of fly ash on the compressive strength of the specimens

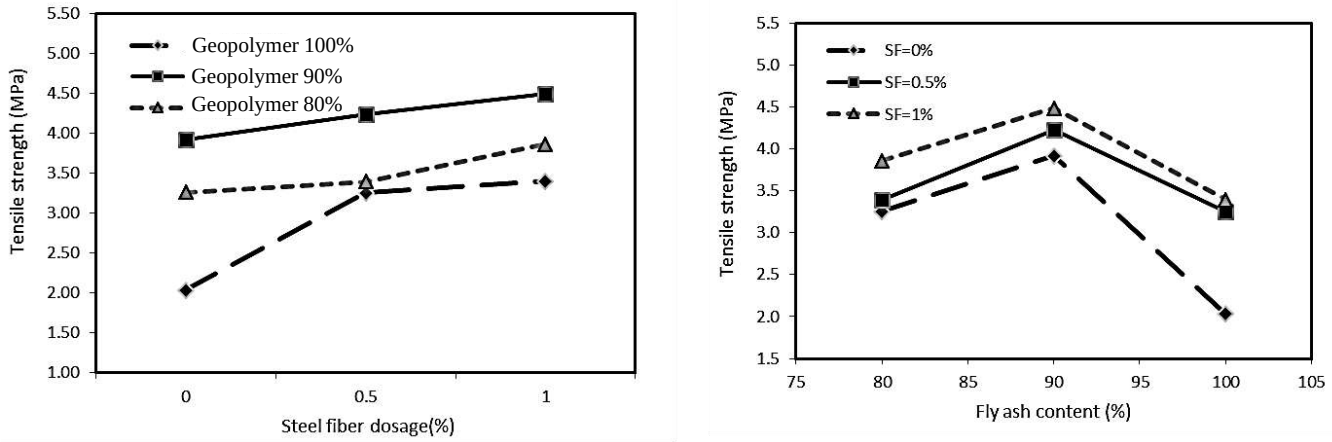

Figure 3: The effect of steel fibers and cement substitution instead of fly ash on the tensile strength of the specimens

cured in a furnace at 60 degrees Celsius. Relationship number 4 is derived in this study. As shown in Figure 5 Relationship number 1 which is used for conventional concrete, is very close to the relationship obtained in this study, with only a 7% difference between them. Relationship 1 predicts lower tensile strength values.

Relationship number 2, due to curing at ambient temperature has a significant difference from the relationship obtained with an average error percentage of 48% indicating that this standard cannot be used for geopolymer concrete cured at 60 degrees Celsius. Relationship number 3 presented here also has good agreement with the current study with an average error of 8%, and the predicted tensile strengths by this standard are higher than the obtained results.

Table 2
Predicted Equations between Tensile Strength and Compressive Strength

Number Eq	Equations	Reference
1	$f_t = 0.59\sqrt{f_c}$	ACI363R-92[26]
2	$f_t = 0.93(f_c)^{0.5}$	Nath [27]
3	$f_t = 0.69(f_c)^{0.5}$	Diaz[28]
4	$f_t = 0.7225(f_c)^{0.4632}$	This study

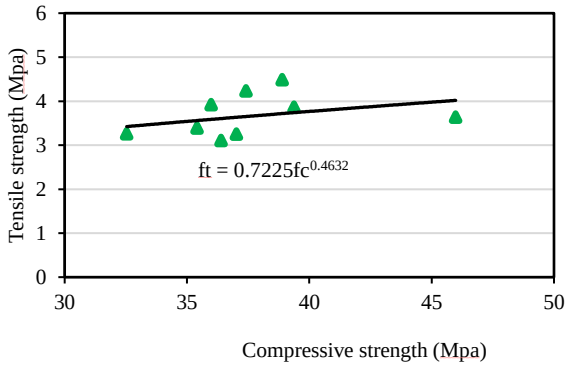

Figure 4: Relationship between Compressive Strength and Tensile Strength in Different specimens

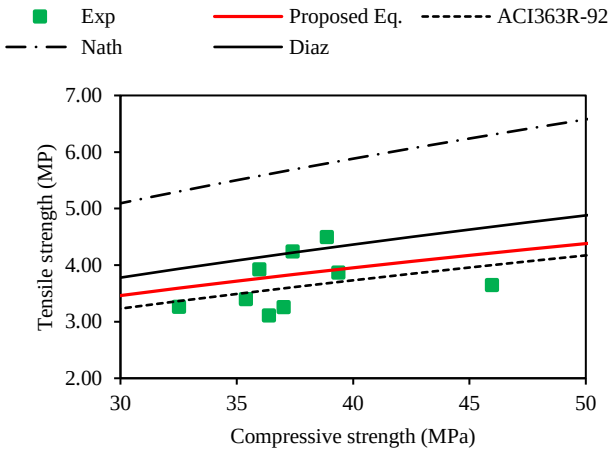

Figure 5: Relationship between Compressive Strength and Tensile Strength by the Current Study and Others

3.2. Results of the elastic modulus tests

Overall, it has been reported that geopolymer concretes processed at high temperatures have lower elastic moduli compared to normal concrete. According to the study by Olivia et al. [29], geopolymer concrete based on fly ash processed by heat with compressive strength of about 55 MPa showed an elastic modulus 14.9 to 28.8% lower than that of normal concrete at equivalent compressive strength. Hardjito et al. [30] reported that the elastic modulus of geopolymer concrete based on fly ash processed by heat is about 10% lower than that of OPC (ordinary Portland cement) concrete with similar compressive strength. Yost et al. [31] found that the elastic modulus of geopolymer concrete based on fly ash is 11 to 16% lower than the theoretical values predicted using ACI 318.

Regarding the effect of steel fibers on the modulus of elasticity of concrete, results are highly contradictory. Some researchers believe that concrete containing steel fibers has a higher elastic modulus compared to plain concrete [32], while others have suggested that there is very little difference between the elastic moduli of concrete containing steel fibers and plain concrete, and some have reported the opposite behavior [33, 34]. For example, Neves [35] observed that the presence of fibers slightly reduces the elastic modulus of concrete and explained that fibers oriented parallel to the loading direction act like voids, and additionally, the addition of fibers creates extra voids in the mix. Research on the effect of fibers on the elastic modulus of geopolymer concrete is very limited, and in a study conducted by Li Y on the effect of rubber particles and steel fibers on concrete, the influence of fibers on the modulus of elasticity of rubber-containing concrete was insignificant, similar to this investigation, and they explained that steel fibers act as good bridges between cracks, distributing and dispersing the load effectively, thus preventing crack propagation, resulting in increased compressive strength and modulus of elasticity [36].

In "Figure 6," the elastic modulus of the samples is plotted. The increase in the elastic modulus due to the addition of 0.5% fibers in samples containing 80, 90, and 100% fly ash was 6.9%, 6.4%, and 5%, respectively, and by adding 1% fibers, it was 10%, 15%, and 11% compared to the fiber-free sample in the same group. The effect of substituting cement for fly ash has also been such that the modulus increased with 10% cement replacement and decreased with further substitution.

3.2.1. Relationship between elastic modulus and compressive strength

Figure 7 illustrates the variations of elastic modulus with changes in compressive strength. The elastic modulus increases with increasing compressive strength. The prediction of elastic modulus of the samples was made

based on the compressive strength obtained in the present study and using the equations provided in Table 3. The predicted values are presented in Figure 7. Equation number 1 is for normal concrete, while equations number 2 and 3 are for geopolymer concrete. As evident from Figure 7 although equation number 1 is provided for normal concrete, it showed good alignment with the present research with an average error of 5%. Equation number 2 specific to geopolymer concrete with fly ash, exhibited an average error of 10%, and equation number 3 for geopolymer concrete with low-calcium fly ash cured at room temperature, showed a discrepancy of approximately 16% compared to laboratory results. This emphasizes the importance of curing temperature, and in this study, conducted at a curing temperature of 60 degrees Celsius, the use of codes prescribing curing at room temperature may not be appropriate.

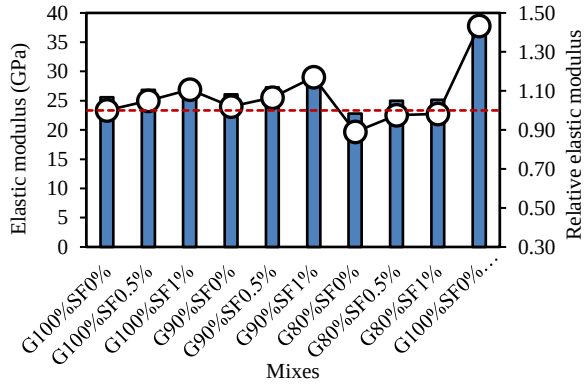

Figure 6: Variations in the values of elastic modulus for the specimens

Table 3
Relationship between elastic modulus and compressive strength of specimens

Number Eq	Equations	Reference
1	$E_c = 3320\sqrt{f_c'} + 6900$	ACI 363[37]
2	$E_c = 0.037 \times \rho^{1.5} \times \sqrt{f_c}$	Diaz-Loya et al.(GC)[41]
3	$E_{cj.a} = 3510\sqrt{f_c}$	Pradip and Sarker(GC)[27]
4	$\boldsymbol{E_c = 3116.9(f_c)^{0.5881}}$	This study

3.3. Results of Ultrasonic Pulse Velocity (UPV) Test:

3.3.1. Results of UPV Test:

The UPV is influenced by various physical and mechanical properties of the samples. Therefore, multiple parameters such as operational conditions, concrete porosity, aggregate type, Interfacial Transition Zone (ITZ) characteristics, sodium hydroxide concentration, additives

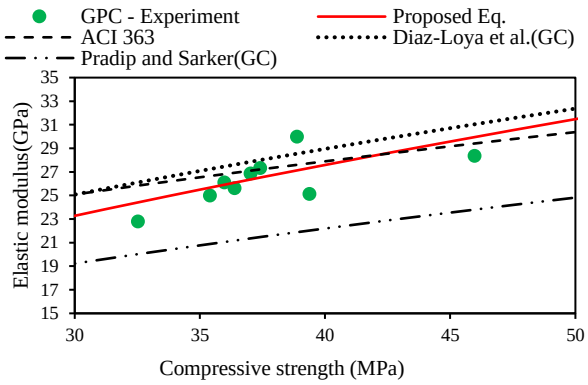

Figure 7: Comparison of the relationship between elastic modulus and compressive strength in the current study and other researches, along with the calculation of prediction error

(like steel fibers, rubber crumbs, etc.), aggregate ratio, size, geopolymer material type (e.g., fly ash, slag, metakaolin, etc.), test ambient temperature, concrete age, etc. play a significant role in this test. This method serves to estimate concrete quality by employing regression analysis between compressive strength and UPV. The UPV passing through the samples is observable in Figure 8.

The findings indicate that the addition of fibers leads to an increase in ultrasonic wave velocity. However, this increase is relatively small, typically less than 12.5%. Similar minimal impacts of fibers on UPV have been reported elsewhere with researchers attributing negligible variations to uniformity in the concrete matrix across all mixtures [44]. This rise may be due to the fact that UPV in steel is typically 1.2 to 1.9 times higher than in geopolymer concrete [45].

According to Chart 6 all designs fall within the good range [46]. As long as UPV values are within this category, it indicates that the concrete in question lacks cracks or voids that could compromise its structural integrity [47]. Conversely substituting cement for fly ash had little effect on wave velocity. In geopolymer concrete, operating in dry environment of an oven leads to the formation of fine cracks, voids and micro-fractures which diminish the material's integrity resulting in lower ultrasonic wave transmission rates. However, fly ash exhibits a lower reduction in speed due to its effective pore-filling properties. These cracks are typically fine and mainly affect ultrasonic wave velocity with minimal impact on sample compressive strength [48].

In design 10, 100% fly ash geopolymer concrete without fibers and rubber crumbs was used with results indicating an increase in ultrasonic wave velocity in samples without rubber crumbs. This phenomenon can be attributed to the nature of rubber crumbs and their cavities which reduce wave velocity. Specifically, the UPV in the sample containing rubber crumbs (design 1) decreased by 12%

compared to the sample without rubber crumbs (design 10).

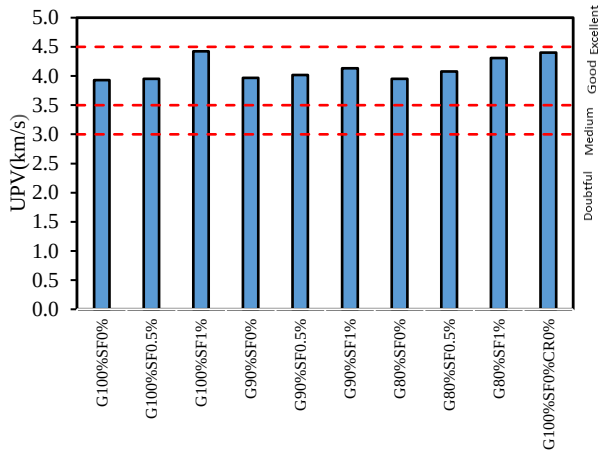

Figure 8: Variation in UPV Values of Samples

3.4. Results of Impact Resistance Tests

The impact test results for the mixing designs are presented in Figure 10. In a study, adding 10% rubber crumbs to geopolymer concrete increased the impact energy for the initiation of the first crack and ultimate failure by less than 20% [49]. In all groups, as the percentage of steel fibers increased to 0.5% and 1%, the number of impacts increased both for the initial crack and final fracture. This implies that the energy absorption capacity in geopolymer concrete increases with the addition of fibers. In another study by Aziza Islam et al. [8], it was found that adding 0.5% steel fibers increased the impact resistance for the initiation of the first crack by 1.1 to 1.3 times. They attributed this improvement to the fibers preventing the growth of microcracks and reducing the propagation of small cracks before they connect and form a larger, more effective crack. However, the greatest effect of fibers is observed in preventing complete fracture, which delays the complete failure of specimens. In the study [8], adding steel fibers increased the energy required for complete failure by 3.1 to 3.6 times. The improvement in performance due to the addition of steel fibers to geopolymer concrete against impact tests has also been observed in other studies [50-52]. As it is evident, the effects of steel fibers on impact resistance are much greater than those of rubber crumbs, which is why the replacement percentage of rubber crumbs remains constant (10%), and the effects of steel fibers on impact resistance have been observed. In normal concrete [53], adding 0.5% fibers increased the impact energy to initiate the first crack by approximately 30% and complete fracture by about 40%. The increase for 1% fibers was 120% and 150%, respectively, indicating that the effect of steel fibers on increasing impact energy in geopolymer concrete is greater than in ordinary concrete. In the present study, adding 0.5% steel fibers to specimens containing 80%, 90%, and 100% fly ash increased the impact energy for initiating the first crack by 5%, 6%, and 5.6%, respectively, and adding 1% fibers increased this value to 13%, 12%, and 19%, respectively. Furthermore, adding 0.5% steel fibers increased the impact energy for complete fracture by 16%, 12%, and 22%, and adding 1% fibers increased this value to 64%, 49%, and 50%, respectively. As the results show, adding fibers has a greater effect on complete fracture than on the initiation of the first crack. The flexibility index, obtained by dividing the absorbed energy until complete fracture by the energy required to initiate the first crack, indicates that adding steel fibers has increased the flexibility index of geopolymer concrete, with a much higher increase observed for adding 1% fibers than for adding 0.5% fibers. The absorbed energy, which is equal to the difference between the energy required for the first crack and the energy required for complete fracture, is shown in Figure 11. It is evident that adding steel fibers increases the absorbed energy, with a greater increase observed for concretes with 20% cement replacement. The percentage of absorbed energy also indicates the significant effect of steel fibers after the initiation of the first crack until complete fracture. On the other hand, based on the obtained results, it can be concluded that replacing cement with fly ash in geopolymer concrete has no significant effect on the impact resistance of the specimens.

3.4.1. The Impact of Rubber Crumbs on Impact Resistance

This section examines the effect of rubber crumbs on impact resistance. For this purpose, 100% geopolymer concrete containing various amounts of steel fibers was used in two conditions: without rubber crumbs and with 10% rubber crumbs. The energy required to initiate the first crack, the energy required for complete failure of the specimens, and the energy absorbed by the concrete are shown in Figure 12. It is evident from the results that adding 10% rubber crumbs increases the amount of impact energy until the initiation of the first crack, with the increase being 5.7% for specimens without steel fibers, 5.6% for those with 0.5% fibers, and 11.1% for those with 1% fibers. The energy required for final failure has also increased, with increases of 1.9%, 12.2%, and 17.8%, respectively. The amount of energy absorbed by the concrete due to the addition of fibers has also increased by 36.4%, 53.1%, and 41.7%, respectively, with the values increasing from 224 to 305, from 651 to 997, and from 1221 to 1730 joules. It is evident that the improvement in impact energy with the help of rubber crumbs is slightly higher in concrete with higher percentages of steel fibers. The increase in absorbed energy due to the addition of

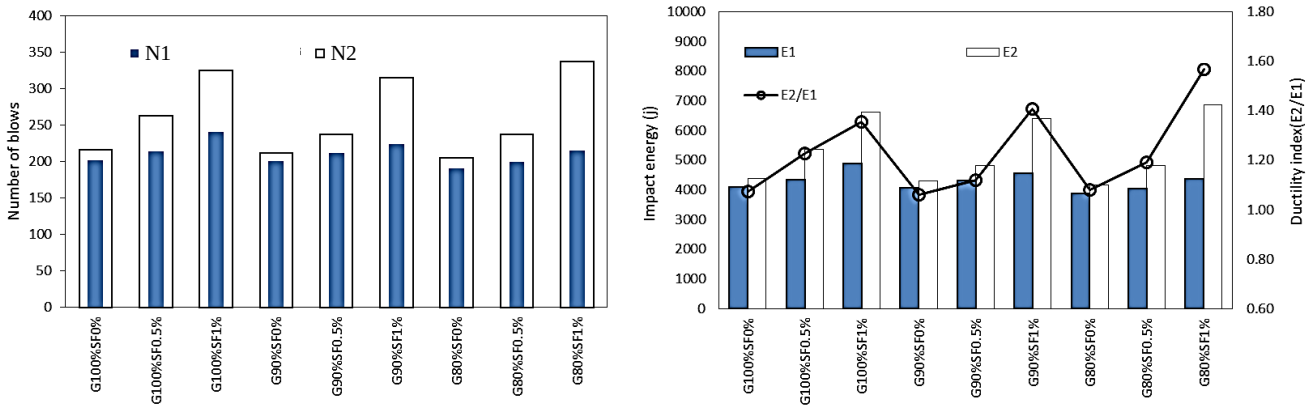

Figure 10: Number of impacts and impact energy until the initiation of the first crack and final fracture of specimens

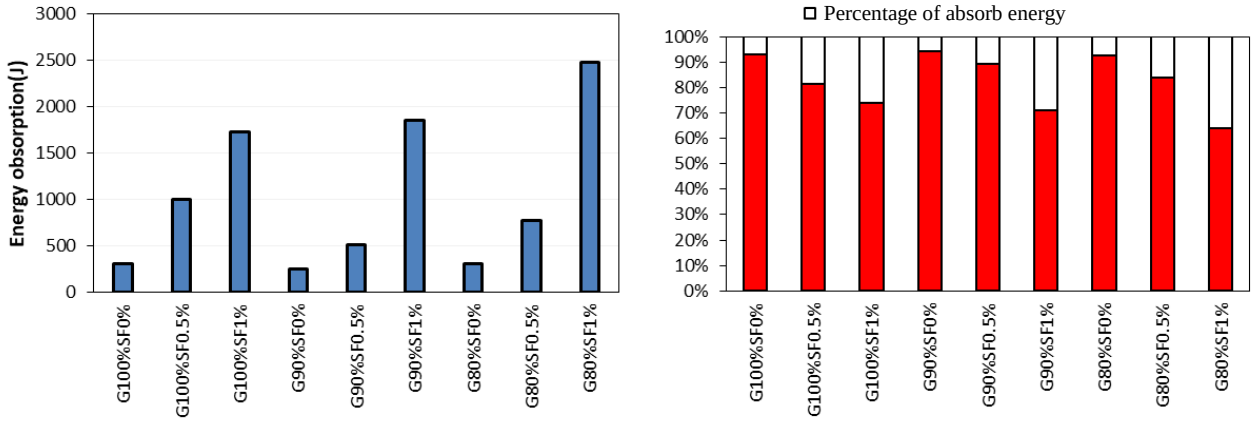

Figure 11: Variations in the amount and percentage of absorbed energy with different fiber contents for various fly ash and cement compositions

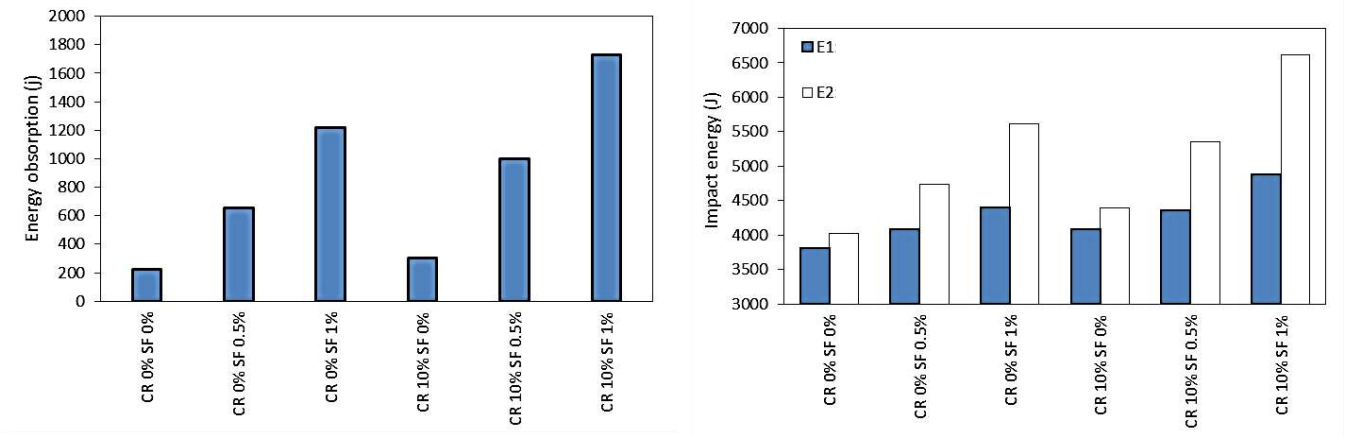

Figure 12: Comparison of the impact energy and the amount of energy absorbed for the sample without rubber crumb and containing 10% rubber crumb

rubber crumbs can also be justified by the decrease in ultrasonic wave velocity resulting from the addition of rubber crumbs. In this study, adding 10% rubber crumbs has resulted in a 12% reduction in ultrasonic wave velocity, indicating that rubber crumbs, due to their material properties and inherent porosity, have been able to attenuate some of the ultrasonic wave energy. This phenomenon holds true for impact energy as well, as adding rubber crumbs has increased the energy absorbed during impact testing.

3.5. Results of SEM, XRD, and XRF

The outcomes from scanning electron microscopy (SEM) can significantly aid in identifying the structure and behavior of concrete. In Figure 13 on the left side the steel fibers used in design 3 are evident. Steel fibers with their bridging properties between cracks and cohesive effect on concrete have a significant impact on enhancing geopolymer concrete [54]. Panda and Padhi [55] conducted an SEM analysis in their study on the characteristics of rubber-containing concrete to examine the bond properties of rubberized concrete. They stated that rubber crumps act as a barrier against crack propagation and reduce the initiation of primary cracks [56]. According to their findings rubber crumps appear as voids within the geopolymer paste forming a weak bond with it. Researchers in SEM experiments on rubber-containing concrete have indicated the presence of gaps (voids) between the geopolymer paste and rubber particles [57, 58]. They attributed the existence of these gaps to the weak bond between the geopolymer paste and rubber particles. On the right side of Figure 13 the microstructure presents in design 9 geopolymer concrete is evident. There are numerous voids in the concrete, which can be attributed to the presence of rubber crumps. Many researchers in SEM experiments on rubber-containing concrete have pointed out the presence of voids between the cement or pozzolan paste and rubber crumps [57, 58]. They attributed the existence of these voids to the weak bond between the rubber crumps and other concrete constituents. In a study [59, 60] that examined the effect of geopolymer concrete microstructures based on fly ash after adding Portland cement to it, it was acknowledged that the addition of cement leads to a denser and more compact concrete due to the improved microstructure resulting from the proximity of hydrated products along with the alumina silicate polymer structure.

The chemical analysis and physical characteristics of geopolymer concrete based on fly ash according to ASTM C618 [61] standard is provided in the table below. As evident from the XRF results in Table 4, with the addition of 10% cement to the fly ash-based geopolymer concrete, the levels of SiO2 and Al2O3, which are the main constituents of geopolymer concrete, have decreased by 13.6% and 36.8%, respectively, while the levels of CaO and Fe2O3 have increased significantly. LOI indicates the weight loss due to combustion at 1000°C, providing a good estimate of the carbon content as a meaningful constituent, which is 27% higher in Design 6 compared to Design 1.

The XRD results for Designs 1 and 6 are illustrated in Figure 14. For this experiment, sections of the central parts of the specimens were separated and ground into uniform powders for testing. According to researchers' findings, the peak intensities are displayed between 15° to 40°, indicating variations in atomic arrangements and structures. By studying the angles at which the XRD peaks are formed and their relative intensities, the materials and their phases can be identified. It is evident that the major difference in the results of the two designs lies in the peak intensity, which is higher in Design 6. The primary reason for this increase is the presence of calcium.

4. Conclusion

This study investigated the mechanical properties of fly ash-based geopolymer concrete containing steel fibers and crumb rubber. The variations included 0.5% and 1% steel fibers and the substitution of cement with fly ash by 10% and 20%. The following conclusions were drawn from the conducted experiments:

1- Compression and tensile strength tests revealed that adding steel fibers to geopolymer concrete increases both strengths. Specifically, the addition of 0.5% steel fibers increased compressive strength by 4% to 60%, while for 1% steel fibers it ranged from 14.5% to 67%.

2- Regarding tensile strength, adding 1% steel fibers improved it by 14.5% to 70%. Additionally, it was observed that replacing cement with fly ash did not significantly affect compressive strength but adding 10% cement could be considered the optimal replacement amount in terms of tensile strength with further replacement resulting in reduced tensile strength.

3- Elastic modulus testing indicated that adding steel fibers increased the modulus of elasticity and replacing 10% of cement with fly ash also increased it.

4- Ultrasonic wave testing results demonstrated good quality for all samples. The increase in fibers led to an increase in the speed of wave transmission through the concrete. The substitution of cement with fly ash had little effect on wave speed.

5- Impact resistance test results showed a significant impact of steel fibers on the number of impacts until the first crack initiation and complete failure of the specimens. Adding fibers increased the resistance to complete failure by 12% to 22% for 0.5% fibers and 49% to 64% for 1% fibers. Moreover, replacing cement with fly ash had minimal effect on concrete resistance to impact. Substituting 10% crumb rubber improved the impact energy of the concrete increasing the energy until the first crack initiation by 10%, energy until complete failure by 15%, and absorbed energy by 43% on average.

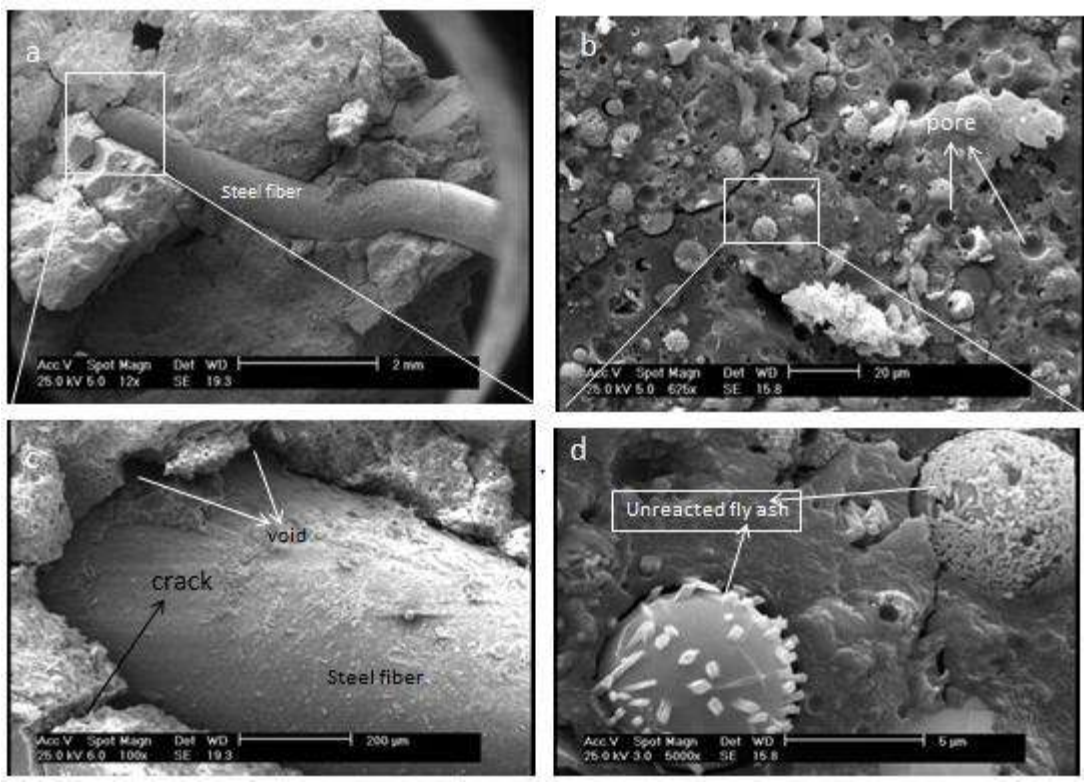

Figure 13: SEM microstructure for geopolymer concrete containing rubber crumps and steel fibers: (a, c): mix 3; (b, d): mix 9

Table 4
XRF Test Values for Samples of mixes 1 and 6

Chemical composition of materials in the composition of concrete								Mix Id
LOI	Fe_2O_3	NA_2O	K_2O	MgO	CaO	AL_2O_3	SiO_2	
7.97	0.03	1.13	0.0	2.62	0.04	17.1	71.1	Mix 1
10.18	3.13	1.89	2.4	1.45	7.9	10.8	61.4	Mix 6

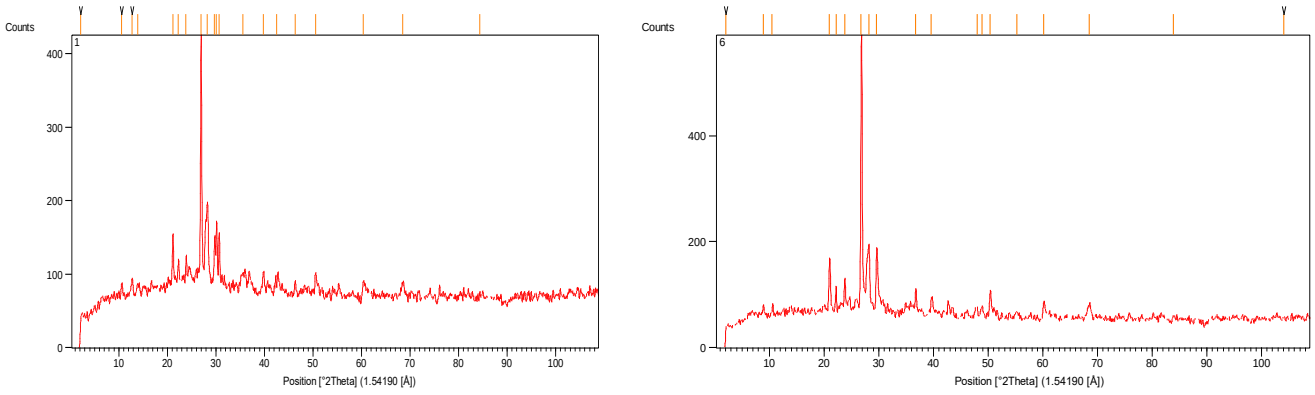

Figure 14: XRD for Samples of mixes 1 and 6

References

[1] Nuaklong, Peem, Vanchai Sata, and Prinya Chindaprasirt. "Influence of recycled aggregate on fly ash geopolymer concrete properties." Journal of Cleaner Production 112 (2016): 2300-2307.

[2] Singh, B., et al. "Geopolymer concrete: A review of some recent developments." Construction and building materials 85 (2015): 78-90.

[3] Zhuang, Xiao Yu, et al. "Fly ash-based geopolymer: clean production, properties and applications." Journal of Cleaner Production 125 (2016): 253-267.

[4] Ryu, Gum Sung, et al. "The mechanical properties of fly ash-based geopolymer concrete with alkaline activators." Construction and building materials 47 (2013): 409-418.

[5] Park, Yeonho, et al. "Compressive strength of fly ash-based geopolymer concrete with crumb rubber partially replacing sand." Construction and Building Materials 118 (2016): 43-51.

[6] Vijai, K., R. Kumutha, and B. G. Vishnuram. "Effect of inclusion of steel fibres on the properties of geopolymer concrete composites." (2012): 381-389.

[7] Guo, Xiaolu, and Xuejiao Pan. "Mechanical properties and mechanisms of fiber reinforced fly ash–steel slag based geopolymer mortar." Construction and Building Materials 179 (2018): 633-641.

[8] Islam, Azizul, et al. "Influence of steel fibers on the mechanical properties and impact resistance of lightweight geopolymer concrete." Construction and Building Materials 152 (2017): 964-977.

[9] Hongen, Zhang, et al. "Influence of Cement on Properties of Fly-Ash-Based Concrete." ACI Materials Journal 114.5 (2017).

[10] Vijay, K., R. Kumutha, and B. G. Vishnuram. "Influence of curing types on strength of Geopolymer concrete." International Conference on Advances in Materials and Techniques in civil Engineering (ICAMAT 2010). 2010.

[11] Azmi, Ahmad Azrem, et al. "Effect of crumb rubber on compressive strength of fly ash based geopolymer concrete." MATEC web of conferences. Vol. 78. EDP Sciences, 2016.

[12] Mehdipour, Sadegh, et al. "Mechanical properties, durability and environmental evaluation of rubberized concrete incorporating steel fiber and metakaolin at elevated temperatures." Journal of Cleaner Production 254 (2020): 120126.

[13] Dezhampanah, Soudabeh, et al. "Environmental performance and durability of concrete incorporating waste tire rubber and steel fiber subjected to acid attack." Journal of cleaner production 268 (2020): 122216.

[14] Eldin, Neil N., and Ahmed B. Senouci. "Observations on rubberized concrete behavior." Cement, Concrete, and Aggregates 15.1 (1993): 74-84.

[15] Taylor, Scott. "Mechanical properties of crumb rubber geopolymer concrete." The UNSW Canberra at ADFA Journal of Undergraduate Engineering Research 11.2 (2018).

[16] Devika, C. P., and R. Deepthi. "Study of flexural behavior of hybrid fibre reinforced geopolymer concrete beam." Int. J. Sci. Res 4.7 (2015): 130-135.

[17] Ma, Chau-Khun, Abdullah Zawawi Awang, and Wahid Omar. "Structural and material performance of geopolymer concrete: A review." Construction and Building Materials 186 (2018): 90-102.

[18] EN, British Standard. "Testing hardened concrete. Method of determination of compressive strength of concrete cubes." BS EN 12390 (2000).

[19] ASTM, C.-. Standard Test Method for Splitting Tensile Strength of Cylindrical Concrete Specimens.

[20] Galan, Andrej. "Estimate of concrete strength by ultrasonic pulse velocity and damping constant." Journal Proceedings. Vol. 64. No. 10. 1967.

[21] 544-2R-89, A., 'Measurement of properties of fiber reinforced concrete'. Reported by ACI Committee, 1999. 544

[22] Topcu, Ilker Bekir, and Mehmet Canbaz. "Effect of different fibers on the mechanical properties of concrete containing fly ash." Construction and Building Materials 21.7 (2007): 1486-1491.

[23] Simões, T., et al. "Influence of fibres on the mechanical behaviour of fibre reinforced concrete matrixes." Construction and Building Materials 137 (2017): 548-556.

[24] Gul, Misba, Alsana Bashir, and Javed A. Naqash. "Study of modulus of elasticity of steel fiber reinforced concrete." Int. J. Eng. Adv. Technol 3.4 (2014): 304-309.

[25] Thomas, Job, and Ananth Ramaswamy. "Mechanical properties of steel fiber-reinforced concrete." Journal of materials in civil engineering 19.5 (2007): 385-392.

[26] 363, A.C. State-of-the-art Report on High-strength Concrete (ACI 363R-84). 1984. American Concrete Institute.

[27] Nath, Pradip, and Prabir Kumar Sarker. "Flexural strength and elastic modulus of ambient-cured blended low-calcium fly ash geopolymer concrete." Construction and Building Materials 130 (2017): 22-31.

[28] Diaz-Loya, E. Ivan, Erez N. Allouche, and Saiprasad Vaidya. "Mechanical properties of fly-ash-based geopolymer concrete." ACI materials journal 108.3 (2011): 300.

[29] Olivia, Monita, and Hamid Nikraz. "Properties of fly ash geopolymer concrete designed by Taguchi method." Materials & Design (1980-2015) 36 (2012): 191-198.

[30] Hardjito, Djwantoro, and B. Vijaya Rangan. "Development and properties of low-calcium fly ash-based geopolymer concrete." (2005).

[31] Yost, Joseph Robert, et al. "Structural behavior of alkali activated fly ash concrete. Part 1: mixture design, material properties and sample fabrication." Materials and structures 46 (2013): 435-447.

[32] Madandoust, Rahmat, et al. "Assessment of factors influencing mechanical properties of steel fiber reinforced self-compacting concrete." Materials & Design 83 (2015): 284-294.

[33] Ibrahim, I. S., and MB Che Bakar. "Effects on mechanical properties of industrialised steel fibres addition to normal weight concrete." Procedia engineering 14 (2011): 2616-2626.

[34] Sunagar, Prashant. "Properties of Geopolymer Concrete with Fly Ash and GGBS as Source Material: Effect of Mixture Composition." SPAST Abstracts 1.01 (2021).

[35] Neves, Rui D., and J. C. O. Fernandes de Almeida. "Compressive behaviour of steel fibre reinforced concrete." Structural concrete 6.1 (2005): 1-8.

[36] Li, Yue, and Yaqiang Li. "Experimental study on performance of rubber particle and steel fiber composite toughening concrete." Construction and Building Materials 146 (2017): 267-275.

[37] 363, A.C., State of the art of high strength concrete. American Concrete Institute, (1993).

[38] AS3600-09. "Concrete structures, Standards Association of Australia." (2009).

[39] Carrasquillo, Ramon L., Arthur H. Nilson, and Floyd O. Slate. "Properties of high strength concrete subjectto short-term loads." Journal Proceedings. Vol. 78. No. 3. 1981.

[40] Hardjito, Djwantoro. Studies of fly ash-based geopolymer concrete. Diss. Curtin University, 2005.

[41] Sumajouw, D. M. J., et al. "Fly ash-based geopolymer concrete: study of slender reinforced columns." Journal of materials science 42 (2007): 3124-3130.

[42] Lee, N. K., and Haeng-Ki Lee. "Setting and mechanical properties of alkali-activated fly ash/slag concrete manufactured at room temperature." Construction and Building Materials 47 (2013): 1201-1209.

[43] Qian, Xiaoqian, and Zongjin Li. "The relationships between stress and strain for high-performance concrete with metakaolin." Cement and concrete Research 31.11 (2001): 1607-1611.
[44] Sahmaran, Mustafa, Alperen Yurtseven, and I. Ozgur Yaman. "Workability of hybrid fiber reinforced self-compacting concrete." Building and Environment 40.12 (2005): 1672-1677.
[45] Reufi, Erjola, Jozefita Marku, and Thomas Bier. "Ultrasonic pulse velocity investigation of Polypropylene and steel fiber reinforced concrete." International Journal of Civil and Environmental Engineering 10.3 (2016): 332-335.
[46] Whitehurst, Eldridge Augustus. "Soniscope tests concrete structures." Journal Proceedings. Vol. 47. No. 2. 1951.
[47] Kwan, Wai Hoe, et al. "Influence of the amount of recycled coarse aggregate in concrete design and durability properties." Construction and building materials 26.1 (2012): 565-573.
[48] Ren, Weibo, Jinyu Xu, and Erlei Bai. "Strength and ultrasonic characteristics of alkali-activated fly ash-slag geopolymer concrete after exposure to elevated temperatures." Journal of Materials in Civil Engineering 28.2 (2016): 04015124.
[49] Aly, Aly Muhammed, et al. "Performance of geopolymer concrete containing recycled rubber." Construction and Building Materials 207 (2019): 136-144.
[50] Shaikh, Faiz Uddin Ahmed. "Review of mechanical properties of short fibre reinforced geopolymer composites." Construction and building materials 43 (2013): 37-49.
[51] Nia, A. Alavi, et al. "An experimental and numerical study on how steel and polypropylene fibers affect the impact resistance in fiber-reinforced concrete." International Journal of Impact Engineering 46 (2012): 62-73.
[52] Mo, Kim Hung, et al. "Impact resistance of hybrid fibre-reinforced oil palm shell concrete." Construction and Building Materials 50 (2014): 499-507.
[53] Wang, H. T., and L. C. Wang. "Experimental study on static and dynamic mechanical properties of steel fiber reinforced lightweight aggregate concrete." Construction and Building Materials 38 (2013): 1146-1151.
[54] Al-Mashhadani, Mukhallad M., et al. "Mechanical and microstructural characterization of fiber reinforced fly ash based geopolymer composites." Construction and building materials 167 (2018): 505-513.
[55] Padhi, S., and K. C. Panda. "Fresh and hardened properties of rubberized concrete using fine rubber and silpozz." Advances in concrete construction 4.1 (2016): 049.
[56] Hall, Matthew R., Khalid B. Najim, and Christina J. Hopfe. "Transient thermal behaviour of crumb rubber-modified concrete and implications for thermal response and energy efficiency in buildings." Applied thermal engineering 33 (2012): 77-85.
[57] Guo, Shuaicheng, et al. "Evaluation of properties and performance of rubber-modified concrete for recycling of waste scrap tire." Journal of Cleaner Production 148 (2017): 681-689.
[58] Segre, Nádia, and Inés Joekes. "Use of tire rubber particles as addition to cement paste." Cement and concrete research 30.9 (2000): 1421-1425.
[59] Mehta, Ankur, and Rafat Siddique. "Properties of low-calcium fly ash based geopolymer concrete incorporating OPC as partial replacement of fly ash." Construction and building materials 150 (2017): 792-807.
[60] Their, Jumah Musdif, and Mustafa Özakça. "Developing geopolymer concrete by using cold-bonded fly ash aggregate, nano-silica, and steel fiber." Construction and Building Materials 180 (2018): 12-22.
[61] C618, A. Standard specification for coal fly ash and raw or calcined natural pozzolan for use in concrete. in American Society of Testing and Materials. 2008. West Conshohocken Pennsylvania, USA.

Journal of Civil Engineering Researchers

Journal homepage: www.journals-researchers.com

Nanotechnology in Construction: Innovations, Applications, and Impacts

Meqdad Feizbahr,[a,*] Pantea Pourzanjani[b]

[a] *Department of Architecture, Scientific-Applied Training Center of Mahestan, Tonekabon, Iran*

[b] *Department of Engineering, Kamalolmolk University of Nowshahr, Iran*

ABSTRACT

Nanotechnology has emerged as a transformative force in the construction industry, revolutionizing traditional building materials and methods. This paper delves into the multifaceted applications of nanotechnology in construction, focusing on its impact on building coatings, materials, colors, insulation, and sensors. By incorporating nanoparticles like carbon nanotubes and titanium dioxide, construction materials gain enhanced mechanical properties and durability. Nano-coatings applied to surfaces such as glass, wood, and concrete offer benefits like water repellence, UV resistance, and antibacterial properties, contributing to energy efficiency and cost savings. Furthermore, advancements in self-healing concrete, fire-resistant glass, and smart surfaces demonstrate the potential of nanotechnology to address longstanding challenges in construction. The paper also explores the use of nanotechnology in paints, insulation, and sensors, highlighting innovations such as self-cleaning paints, antistatic coatings, and nano-acoustic insulators. Overall, the integration of nanotechnology into the construction sector promises improved product quality, energy efficiency, and longevity, heralding a new era of sustainable and resilient built environments.

© 2024 Journals-Researchers. All rights reserved.

ARTICLE INFO

Received: December 19, 2023
Accepted: February 17, 2024

Keywords:
Nanotechnology
Nanomaterial in architecture Self-cleaning
Nano-Coating

DOI: 10.61186/JCER.6.1.35
DOR: 20.1001.1.22516530.1399.11.4.1.1

1. Introduction

Nanotechnology significantly influences building construction, with steel, glass, and concrete industries playing effective roles (Figure 1) [1]. The incorporation of nanoparticles, notably carbon nanotubes (CNT) and titanium dioxide (TiO2), enhances the mechanical properties of main structures in construction [2]. Moreover, nano coatings applied to both interior and exterior building facades hold particular importance in the carpentry sector [3]. The nano-coatings applied to the building offer various benefits, including water repellence, minimized dirt absorption, and UV ray resistance on surfaces such as cement, brick, Pottery roof Tiles, stone, tile, marble, wood, ceramic, glass, steel, and concrete. Furthermore, advancements in construction materials, such as reinforced concrete, self-repairing and self-cleaning glass, fire-resistant coatings, and energy-controlling glass, contribute to reducing energy consumption [4-6]. Additionally, employing antibacterial colors derived from nanotechnology prevents bacterial penetration in structures like office buildings, residential complexes, and hospitals,

* Corresponding author. Tel.: +989373230737; e-mail: meqdad.feizbahr@gmail.com.

extending their lifespan and maintaining a bacteria-free environment [1, 7].

These innovations exemplify the significant impact of nanotechnology in the construction industry. Experts predict that, like historical advancements like steam engines and information technology, nanotechnology will revolutionize various sectors. By reducing materials to nano dimensions and combining them with nano polymers, novel materials with unprecedented hardness and durability can be synthesized, such as clay and ceramic-based compounds [8-11].

The advantages of using nanotechnology in the construction industry can be considered as [1, 13]:

- Improved product quality
- Energy efficiency
- Cost savings
- Enhanced product durability

2. Nanotechnology in building coatings

This technology is applied to both internal and external surfaces of buildings, including glass, plastic, wood, steel, stone, brick, tile, ceramic, cement, and concrete surfaces. These "smart surfaces" are typically either super-hydrophilic or super-hydrophobic, allowing for surface reactions. It's important to note that these coatings are antibacterial and safe for human health [14, 15].

Self-cleaning surfaces employ photocatalytic coatings with TiO2 nanoparticles, activated by sunlight, to break down dirt and oxidize VOCs into harmless byproducts. These surfaces, applied through nanocoating films or integrated into substrates like concrete, are exemplified by architectural landmarks such as the Jubilee Church in Rome, Marunouchi Building in Tokyo, and 40 Bond Street Apartment in London, showcasing advanced self-cleaning facade systems (Figure 2) [16].

2.1. Stone and wood nano-coating

These antibacterial nano-coatings provide resistance to water, air, organic, and inorganic materials, making them essential in the construction industry. They maintain the original appearance of the surface while preventing adhesion and repelling water, grease, and other contaminants [17]. Moreover, nano-coating for permeable stone surfaces, which have absorbent properties, serves various purposes. These coatings typically consist of diamond, silver, glass, and ceramic particles, with water and alcohol as the carrier phase. They can withstand temperatures up to 300 degrees Celsius [18]. Benefits include [19, 20]:

- Covering porous surfaces while maintaining breathability
- Protecting surfaces against environmental factors
- Easy cleaning of stains, including fats and oils with water
- Prevention of mold, algae, and similar formations

Protection against dirt accumulation.

3. Applications of nanotechnology in the construction industry

3.1. Wooden surfaces

Stone and wood nano-coating are used not only on regular wooden surfaces but also on polished and painted wooden surfaces. They are applied to polished wooden surfaces within three months of polishing, while multipurpose nano-coating is suitable for painted wooden surfaces [21, 22].

3.2. Fiber Cement

Buildings constructed with fiber cement can accumulate stains and dirt over time. The cement used in the facade absorbs dirt and sunlight, making it difficult to remove stains. Applying stone and wood nano-coatings to the facade can prevent the penetration of dirt and bacteria, preserving the original appearance [23].

3.3. Bricks and Ceramics

The presence of large trees near buildings can cause green stains to develop on the facade over time.

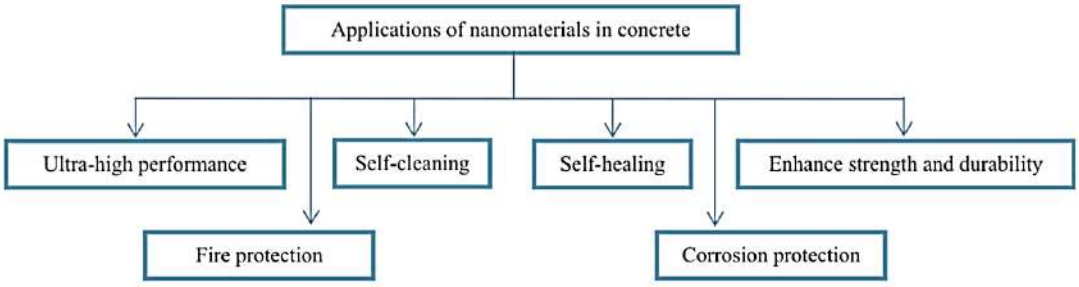

Figure 1. Applications of nanomaterials in concrete [12]

Jubilee Church in Rome

Marunouchi Building in Tokyo

40 Bond Street Apartment in London

Figure 2. self-cleaning facade systems in buildings

High-pressure cleaning may temporarily remove these stains but can lead to increased adhesion and faster dirt absorption [24]. Stone and wood nano-coatings can prevent such staining and adhesion. For pricing inquiries regarding bricks, you can refer to Sivan Land [25].

3.4. Sandstones and Aerated Concrete

Sandstones and aerated concrete, commonly used in studios and porches, are prone to absorbing dirt and grease, leading to a rapid deterioration in appearance [26]. Traditional pressure cleaning methods may prove ineffective. Stone and wood nano-coatings allow the surface to breathe while preventing material penetration, preserving the original color and structure [27].

3.5. Stone Tiles and Slabs

Applying stone and wood nano-coatings protects buildings, gardens, and sculptures from environmental damage, maintaining their color over time [28].

3.6. Glass

Nano glass coatings, widely used in automobile construction, offer various benefits in the construction industry, including [29]:

3.6.1. Self-cleaning glasses

These coatings create a hydrophilic film on the glass surface, promoting self-cleaning properties under sunlight. TiO2 nanoparticles in the coatings possess hydrophilic and antiseptic properties, breaking down organic pollutants [30].

3.6.2. Energy-controlling glasses

These glasses regulate ultraviolet and infrared waves while controlling visible light transmission, offering energy-saving benefits [31].

3.6.3. Fireproof glass

Utilizing nanoparticles, fire-resistant glasses prevent breakage by forming a protective coating under heat. Fire-resistant glasses have been created by using nanoparticles, which form a sponge-like coating due to heat and prevent the glass from breaking [32].

3.6.4. Smart glasses

These glasses can adjust light absorption, providing simultaneous light and heat control [30].

3.6.5. Anti-reflective glasses

Ideal for applications requiring low light reflection, such as fashion shows and exhibitions, these glasses are widely used in the construction industry [33].

3.7. Concrete

Many research studies are being conducted in the field of applying advanced technologies to concrete buildings to enhance our understanding of this subject at a fundamental scientific level. Technologies such as atomic force microscopy (AFM), scanning electron microscopy (SEM), and focused ion beam (FIB) microscopes, designed for nanoscale studies, are being utilized. For daily concrete prices, please refer to Sivan Land [25].

3.7.1. Self-healing Concrete

Controlling and preventing cracks is a fundamental challenge in structural engineering. Self-healing concrete technology enables immediate repair processes to commence once damage occurs [34].

3.7.2. Nanosilicas (SiO2)

Utilizing silica nanoparticles allows for an increase in particle density within concrete, thereby enhancing the density of micro and nanostructures constituting concrete. Consequently, mechanical properties are improved [35].

Additionally, incorporating silica nanoparticles into cement-based materials regulates chemical decomposition caused by calcium silicate hydrate (H-C-S) due to calcium settling in water. Moreover, it prevents water penetration into the concrete, thereby enhancing its durability [36].

3.7.3. Carbon Nanotubes (CNT)

Extensive research is being conducted on the applications of carbon nanotubes, uncovering remarkable properties. For instance, despite having one-sixth the density of steel, carbon nanotubes exhibit five times the Young's modulus and eight times the strength of steel. Incorporating half to one weight percent of these pipes into the concrete matrix significantly enhances sample properties. Carbon nanotubes are utilized in both single-walled and multi-walled forms [37, 38].

3.7.4. Single-wall Carbon Nanotube:

Nano-clay Particles: Various types of nanoparticles in different adhesives (binder mortars) and their impact on key concrete erosion-related characteristics are being investigated [39]. These characteristics include preventing the transfer of chlorine ions, resistance to carbon dioxide, water vapor diffusion, water absorption, and penetration depth. A solvent consisting of low molecular weight epoxy resin and Nano-Clay has shown promising results in this regard [40].

Iron Oxide Nanoparticles or Hematite (Fe2O3): The addition of iron oxide nanoparticles to the concrete matrix not only enhances concrete strength but also facilitates monitoring of concrete stress levels through shear electrical resistance measurements [41].

Titanium Dioxide Nanoparticles (TiO2): Titanium dioxide nanoparticles serve as a reflective coating to enhance concrete properties on building facades. Through robust photocatalytic reactions, these particles can decompose organic pollutants, volatile organic compounds (VOCs), and bacterial membranes. Consequently, they are added to paints, cements, and glasses to impart antiseptic properties. TiO2-containing concrete exhibits a white color and distinctive luster, maintaining effective binding properties. Ordinary concrete buildings lack such features [42].

3.8. Steel

Steel is one of the most important metals in the construction industry. Research has shown that adding copper nanoparticles to steel reduces the surface roughness of the steel. Consequently, it decreases the number of stress-inducing factors and, eventually, cracks caused by fatigue in structures such as bridges and towers, where intermittent loading is prevalent [43].

3.9. Sensors

Sensors based on nanoscale technology can offer a wide range of automation capabilities in concrete structures. These sensors can be utilized for various purposes, including controlling the quality and durability of concrete. They enable measurements such as density, concrete degradation rate, and key parameters affecting concrete durability, such as temperature, humidity, chlorine concentration, pH, carbon dioxide levels, tensile strength, rebar corrosion, and vibration [44, 45].

3.10. Cement

As widely recognized, cement plays a pivotal role in various construction processes, offering myriad applications. Nanotechnology holds the promise of significantly enhancing the physical and chemical properties of cement [46].

3.11. Concrete

Utilizing lightweight concrete in construction renders buildings both lighter and more resistant to earthquakes. Additionally, it proves cost-effective in the construction industry. The reduction in mass results in smaller dimensions for columns, beams, and roof thickness, thereby conserving construction materials. Moreover, due to its minuscule pores, lightweight concrete provides at least 10 times better heat and sound insulation compared to regular concrete. For inquiries regarding construction material prices, Sivan Land is a reliable reference.

3.12. Heat-Generating Smart Nano Concrete

Heat-generating intelligent nano-concrete can provide real-time, accurate temperature information to a central control system. Upon detecting freezing temperatures, the system promptly adjusts the environmental temperature [47].

4. Nanotechnology in colors

4.1. Self-cleaning paints

These paints can be formulated by incorporating various types of self-cleaning nanoparticles into the paint resin. They offer high transparency and suitability for both interior and exterior surfaces of buildings. These paints are highly valued for enhancing durability, reducing costs, and minimizing equipment maintenance time [48].

4.2. Antibacterial paints

Utilizing nanotechnology and antibacterial coatings creates inherent antibacterial properties on surfaces that remain effective even after washing or exposure to detergents. These coatings inhibit bacterial and microbial growth, protecting against fungi and mold in public spaces and similar environments [49].

4.3. Antistatic paints.

Antistatic coatings, capable of conducting electricity and dissipating static charge, are essential in areas where flammable materials are present. Offering robust chemical and physical properties, antistatic paint enhances quality and durability [50].

4.4. Scratch-resistant paints.

These paints offer excellent scratch resistance, making them suitable for application on exterior and interior surfaces, doors, windows, and flooring [51].

5. Nanotechnology in Insulation

5.1. Sound insulation.

Nano acoustic insulators reduce the speed of sound waves and are thinner than conventional insulators, making them more suitable for use in the construction industry [52].

5.2. Thermal insulation

Insulators with higher thermal resistance allow less heat transfer, resulting in greater energy savings. Thus, the effectiveness of insulators lies in their thermal resistance rather than their thickness [53].

5.3. Moisture insulation

Resistance to moisture penetration significantly impacts the durability of building materials. Clay nanoplates and cellulose fibers serve as effective moisture-resistant coatings without any adverse side effects [54].

6. Conclusion

In conclusion, nanotechnology represents a paradigm shift in the construction industry, offering innovative solutions to age-old challenges. The applications of nanomaterials and coatings have demonstrated remarkable improvements in product quality, energy efficiency, and durability across various construction materials and surfaces. By leveraging nanotechnology, buildings can achieve superior performance, resilience, and sustainability while reducing maintenance costs and environmental impact. The development of self-healing concrete, fire-resistant glass, and smart coatings underscores the potential of nanotechnology to revolutionize construction practices and mitigate risks associated with climate change and resource depletion. Moving forward, continued research and investment in nanotechnology will be crucial to unlocking its full potential and realizing the vision of smart, adaptive, and environmentally responsible built environments. As the construction industry embraces nanotechnology, it stands poised to usher in a new era of innovation, efficiency, and resilience in building design and construction.

References

[1] Aldoasri, Mohammad A, et al. "Protecting of Marble Stone Facades of Historic Buildings Using Multifunctional Tio2 Nanocoatings." Sustainability 9.11 (2017): 2002. Print.
[2] Alvansazyazdi, Mohammadfarid, et al. "Evaluating the Influence of Hydrophobic Nano-Silica on Cement Mixtures for Corrosion-Resistant Concrete in Green Building and Sustainable Urban Development." Sustainability 15.21 (2023): 15311. Print.
[3] Betz, Peter, and Angelika Bartelt. "Scratch Resistant Clear Coats: Development of New Testing Methods for Improved Coatings." Progress in organic coatings 22.1-4 (1993): 27-37. Print.
[4] Some Properties of Fiber-Cement Composites with Selected Fibers. Proceedings of the Conferencia Brasileira de Materiais e Tecnologias Não Convencionais: Habitações e Infra-Estrutura de Interesse Social Brasil-NOCMAT. 2004. Print.
[5] Casini, Marco. Smart Buildings: Advanced Materials and Nanotechnology to Improve Energy-Efficiency and Environmental Performance. Woodhead Publishing, 2016. Print.
[6] Deschamps, Carina, Neil Simpson, and Michael Dornbusch. "Antistatic Properties of Clearcoats by the Use of Special Additives." Journal of Coatings Technology and Research 17.3 (2020): 693-710. Print.
[7] Divya, C, and P Harish. "Experimental Investigation on Nanosilica and the Behaviour of Ordinary Portland Cement and Blended Cement and Its Effects on Properties." International Research Journal of Engineering and Technology, e-ISSN (2018): 2395-0056. Print.
[8] El-Samny, Maged Fouad. "Nanoarchitecture." University Of Alexandria, Egypt (2008). Print.
[9] Elkarmoty, Mohamed, Stefano Bonduà, and Roberto Bruno. "A 3d Optimization Algorithm for Sustainable Cutting of Slabs from Ornamental Stone Blocks." Resources Policy 65 (2020): 101533. Print.
[10] Falikman, VR. "Nanocoatings in Modern Construction." Nanotekhnologii v Stroitel'stve 13.1 (2021): 5-11. Print.
[11] Farahmand, Sara, et al. "Experimental and Theoretical Investigation About the Effect of Nano-Coating on Heating Load." International Journal of Industrial Chemistry 11 (2020): 147-59. Print.

[12] Feizbahr, Mahdi, et al. "Review on Various Types and Failures of Fibre Reinforcement Polymer." Middle-East Journal of Scientific Research 13.10 (2013): 1312-18. Print.
[13] Feizbahr, Mahdi, et al. "Improving the Performance of Conventional Concrete Using Multi-Walled Carbon Nanotubes." Express Nano Letters 1.1 (2020): 1-9. Print.
[14] Feizbahr, Meqdad, and Pantea Pourzanjani. "The Impact of Advanced Concrete Technologies on Modern Construction and Aesthetics." Journal of Review in Science and Engineering 2024 (2024): 1-9. Print.
[15] Ferdosi, Sima Besharat. "Thermal Effect on the Post-Buckling and Mechanical Response of Single-Walled Carbon Nanotubes: A Numerical Investigation." Mechanical Engineering 9 (2022): 1-6. Print.
[16] Foudi, H, et al. "Synthesis and Characterization of Zno Nanoparticles for Antibacterial Paints." Chemical Papers 77.3 (2023): 1489-96. Print.
[17] Frigione, Mariaenrica, and Mariateresa Lettieri. "Novel Attribute of Organic–Inorganic Hybrid Coatings for Protection and Preservation of Materials (Stone and Wood) Belonging to Cultural Heritage." Coatings 8.9 (2018): 319. Print.
[18] Hanus, Monica J, and Andrew T Harris. "Nanotechnology Innovations for the Construction Industry." Progress in materials science 58.7 (2013): 1056-102. Print.
[19] Hosseini, Payam, et al. "Effects of Nano-Clay Particles on the Short-Term Properties of Self-Compacting Concrete." European Journal of Environmental and Civil Engineering 21.2 (2017): 127-47. Print.
[20] Hu, Xiaochun, Xiaojun Zhu, and Zhiqiang Sun. "Fireproof Performance of the Intumescent Fire Retardant Coatings with Layered Double Hydroxides Additives." Construction and Building Materials 256 (2020): 119445. Print.
[21] Huo, Yanlin, et al. "Mass Ggbfs Concrete Mixed with Recycled Aggregates as Alkali-Active Substances: Workability, Temperature History and Strength." Materials 16.16 (2023): 5632. Print.
[22] Huseien, Ghasan Fahim, Kwok Wei Shah, and Abdul Rahman Mohd Sam. "Sustainability of Nanomaterials Based Self-Healing Concrete: An All-Inclusive Insight." Journal of Building Engineering 23 (2019): 155-71. Print.
[23] Jayasuriya, D, et al. "Mid-Ir Supercontinuum Generation in Birefringent, Low Loss, Ultra-High Numerical Aperture Ge-as-Se-Te Chalcogenide Step-Index Fiber." Optical Materials Express 9.6 (2019): 2617-29. Print.
[24] Nanotechnology and the Building Industry. Proceedings of the International Conference on Nanotechnology: Fundamentals and Applications Ottawa, Ontario, Canada. 2010. Print.
[25] Khandve, Pravin. "Nanotechnology for Building Material." International Journal of Basic and Applied Research 4 (2014): 146-51. Print.
[26] Khorramabadi, Reza, and Sima Besharat Ferdosi. "Post-Buckling and Vibration Analysis of Double-Curved Sandwich Panels with Sma Embedded Faces." Composites Part C: Open Access 12 (2023): 100419. Print.
[27] Krystek, Małgorzata, and Marcin Górski. "Nanomaterials in Structural Engineering." New uses of micro and nanomaterials (2018). Print.
[28] Kwalramani, Manish A, and ZI Syed. "Application of Nanomaterials to Enhance Microstructure and Mechanical Properties of Concrete." International Journal of Integrated Engineering 10.2 (2018). Print.
[29] Non-Autoclaved Aerated Concrete on the Basis of Composite Binder Using Technogenic Raw Materials. Materials Science Forum. 2019. Trans Tech Publ. Print.
[30] Maghsodi, Z, et al. "Spatial Prediction of Soil Units Using Geographic Information Systems in Sivan Lands of Ilam Province." Iranian Journal of Soil Research 33.2 (2019): 253-67. Print.
[31] Mansour, Rowan Mohamed, N EL-Sayad, and Lamis Saad El-Din El-Gizawi. "Applying Nano Coatings on Buildings to Improve Thermal Performance & Energy Efficiency: A Simulation of a Health Care Building in Egypt." ISVS EJ 10 (2023): 384-96. Print.
[32] Massoudinejad, Mohamadreza, et al. "Use of Municipal, Agricultural, Industrial, Construction and Demolition Waste in Thermal and Sound Building Insulation Materials: A Review Article." Journal of Environmental Health Science and Engineering 17 (2019): 1227-42. Print.
[33] Meoni, Andrea, et al. "A Multichannel Strain Measurement Technique for Nanomodified Smart Cement-Based Sensors in Reinforced Concrete Structures." Sensors 21.16 (2021): 5633. Print.
[34] Meqdad, Feizbahr, and Pourzanjani Pantea. "The Evolution of Architectural Styles: From Modernism to Postmodernism." Journal of Review in Science and Engineering 2023 (2023): 1-12. Print.
[35] Nazari, Marzieh, Mohammad Javad Mahdavinejad, and Mohammadreza Bemanian. "Protection of High-Tech Buildings Facades and Envelopes with One Sided Nano-Coatings." advanced materials research 829 (2014): 857-61. Print.
[36] Nguyen, Tam Duy, et al. "Electrochromic Smart Glass Coating on Functional Nano-Frameworks for Effective Building Energy Conservation." Materials Today Energy 18 (2020): 100496. Print.
[37] Ogunsona, Emmanuel O, et al. "Engineered Nanomaterials for Antimicrobial Applications: A Review." Applied Materials Today 18 (2020): 100473. Print.
[38] Onyelowe, Kennedy C, et al. "Multi-Objective Prediction of the Mechanical Properties and Environmental Impact Appraisals of Self-Healing Concrete for Sustainable Structures." Sustainability 14.15 (2022): 9573. Print.
[39] Papadaki, Dimitra, George Kiriakidis, and Theocharis Tsoutsos. "Applications of Nanotechnology in Construction Industry." Fundamentals of Nanoparticles. Elsevier, 2018. 343-70. Print.
[40] Persano, Francesca, et al. "Recent Advances in the Design of Inorganic and Nano-Clay Particles for the Treatment of Brain Disorders." Journal of Materials Chemistry B 9.12 (2021): 2756-84. Print.
[41] Creating Semi-Quanta Multi-Layer Synthetic Cnt Images Using Cyclegan. 2023 IEEE Applied Imagery Pattern Recognition Workshop (AIPR). 2023. IEEE. Print.
[42] Sao, Priyanshu, Dipak Nath, and VJ Priyadharshini. Introduction to Nanoscience and Nanotechnology. AG Publishing House (AGPH Books), 2010. Print.
[43] Seifan, Mostafa, et al. "Bio-Reinforced Self-Healing Concrete Using Magnetic Iron Oxide Nanoparticles." Applied microbiology and biotechnology 102 (2018): 2167-78. Print.
[44] Selim, Ali Q, Lotfi Sellaoui, and Mohamed Mobarak. "Statistical Physics Modeling of Phosphate Adsorption onto Chemically Modified Carbonaceous Clay." Journal of Molecular Liquids 279 (2019): 94-107. Print.
[45] Sev, Ayşin, and Meltem Ezel. "Nanotechnology Innovations for the Sustainable Buildings of the Future." World Academy of Science, Engineering and Technology International Journal of Civil, Environmental, Structural, Construction and Architectural Engineering 8.8 (2014): 886-96. Print.
[46] Shen, Weiguo, et al. "Preparation of Titanium Dioxide Nano Particle Modified Photocatalytic Self-Cleaning Concrete." Journal of cleaner production 87 (2015): 762-65. Print.
[47] Sobolev, Konstantin, and Surendra P Shah. Nanotechnology of Concrete: Recent Developments and Future Perspectives. ACI Farmington Hills, MI, USA, 2008. Print.
[48] Solanki, Nishal Ashvin, Pooria Pasbakhsh, and Ali Rashidi. "Improving the Thermal, Termite Resistance and Anti-Wetting Properties of Tropical Timber Using a Polymethyl

Acrylate/Halloysite Coating." Clay Nanoparticles. Elsevier, 2020. 257-73. Print.

[49] Taheri, Shima. "A Review on Five Key Sensors for Monitoring of Concrete Structures." Construction and Building Materials 204 (2019): 492-509. Print.

[50] Teja, DS, K Jayachandra, and B Balakrishna Bharath. "An Experimental Study on Effect of Nano Silica and Behavior of Opc and Blended Cement." Print.

[51] Vardanjani, Mehdi Jafari, and Mehdi Karevan. "Design, Fabrication, and Characterization of Thermal and Optical Properties of Nano-Composite Self-Cleaning Smart Window." Optical and Quantum Electronics 53 (2021): 1-25. Print.

[52] Vunain, Ephraim, et al. "Nanoceramics: Fundamentals and Advanced Perspectives." Sol-gel based nanoceramic materials: preparation, properties and applications (2017): 1-20. Print.

[53] Wan, Huiwen, et al. "Study on the Structure and Properties of Autoclaved Aerated Concrete Produced with the Stone-Sawing Mud." Construction and Building Materials 184 (2018): 20-26. Print.

[54] Yilmaz, Semih, and Nilhan Vural. "Potential Use of Nanotechnology in Conservation Applications of Historical Buildings." Print.

[55] Zhang, Bao-Sen, et al. "Cu Nanoparticles Effect on the Tribological Properties of Hydrosilicate Powders as Lubricant Additive for Steel–Steel Contacts." Tribology International 44.7-8 (2011): 878-86. Print.

[56] Zhou, Linglin, et al. "A Facile Approach to Fabricate Self-Cleaning Paint." Applied Clay Science 132 (2016): 290-95. Print.

Journal of Civil Engineering Researchers

Journal homepage: www.journals-researchers.com

A Comparative Study of Numerical Methods for Predicting Crack Propagation in Reinforced Concrete Hollow Core Slabs

Alireza Sheikhnasiri, [a,*]

[a] *Department of Civil Engineering, Arman Institution of Engineering and Technology, Tehran, Iran*

ABSTRACT

Hollow core slabs are commonly used in prefabricated building construction and are calculated and constructed using gravity loads. The dead loads of the structure are reduced by using this slab system. Different criteria, such as the initiation and propagation of cracks in the hollow core slab, are used to analyze these slabs. Fracture mechanics is the basis for studying crack propagation. The present study was conducted to analyze the propagation of cracks in hollow core slabs under common loading conditions using the finite element method and numerical modeling to analyze cracks in reinforced concrete members. This research is theoretically conducted using finite element software. This research takes into account the potential varieties of cracks in concrete slabs. Slabs should consider all three types of cracks, which are shear, flexural, and flexural-shear cracks obtained from the reference test. Two Contour integral and XFEM methods are used to analyze cracks in Abaqus software. To validate and control the modeling process, the laboratory results of the research of Ibrahim N. Najma, Raid A. Daudb, and Adel A. Al-Azzawi. December 2, 2019, has been used. The outcomes of this study showed that the probability of the formation of a flexural-shear crack in the slab is higher than in other crack forms.

© 2024 Journals-Researchers. All rights reserved.

ARTICLE INFO

Received: January 16,2024
Accepted: March 23,2024

Keywords:
CDP Numerical Method
Crack growth
Reinforced concrete slab
Hollow core slab
XFEM method
Contour integral method

DOI: 10.61186/JCER.6.1.42
DOR: 20.1001.1.22516530.1399.11.4.1.1

1. Introduction

Slabs are one of the important components of structures that carry the important task of carrying loads on the structure [1]. There are various methods for predicting the behavior of normal and solid slabs, the most important of which are the theories based on fracture lines. In the case of hollow core slabs, despite their increasing use, it can be said that due to the geometric diversity and characteristics of the holes or internal cavities of these slabs, there are many areas for research, especially in the field of predicting the occurrence and propagation of cracks. Its impact on the general behavior of the members is doubled, especially since the various theories and relationships presented by researchers in the field of crack analysis are also very diverse, and considering the relative youth of this branch of science, evaluating their effectiveness in hollow core slabs needs to be investigated.

N. Najma et al. (2019) conducted a study on the Behavior of reinforced concrete segmental hollow core

* Corresponding author. Tel.: +989904417166; e-mail: Alireza.sa30@gmail.com.

slabs under monotonic and repeated loadings. The investigation includes testing of twelve specimens that are solid and hollow core slab models. The test program was carried out to study the effects of load type, core diameters, core shape, number of cores, and steel fiber existence. The test results showed that core shape and core number have remarkably influenced cracking pattern, ultimate load, and failure mode. Also, when considering repeated loading protocol, the ultimate load capacity, load at yielding, and ductility are reduced [2].

Salehi. et al, (2016), investigated the numerical study of the behavior of one-way prestressed hollow core slabs. Due to the earthquake-proneness of different regions of the world, Reducing the weight of buildings is one of the methods that have been considered to reduce earthquake forces. The use of prefabricated hollow slabs is one of the ways to reduce the dead load of the building. In this study, 4 types of hollow prefabricated slabs with different thicknesses were modeled under specific dead load in ABAQUS finite element software. With additional nonlinear static analysis, the capacity of slabs and their nonlinear behavior have been evaluated. The results show that with the increase in the thickness of the slab, the final shear strength of the slab increases. The results also show that the ultimate strength has decreased in the hollow slab with polygonal (non-circular) holes [3].

Shafizadeh. et al, (2014), investigated the introduction of a finite element modeling method for pre-stressed slabs with holes in the core by ABAQUS software and investigated the changes in friction coefficient. In recent studies, prefabricated prestressed hollow core slabs (HC) have generally covered the market of many countries for use in buildings with performance in the floor and ceiling area with an advanced method in the factory and with a low cost in installation. Today, hollow core slabs (HC) have strengthened their position. Prestressing increases the usability of hollow core slabs compared to reinforced concrete slabs, thus increasing the cracking moment and other functions of the slab. Therefore, in this research, a finite element modeling method has been introduced to simulate these slabs in ABAQUS software [4].

Aikaterini S. et al, (2015), In an article that studied Nonlinear finite element analysis of reinforced concrete slab-column joints under static and quasi-dynamic loads was performed to investigate their failure modes in terms of ultimate load and crack patterns. Three-dimensional finite element analysis (FEA) was performed with appropriate modeling of element size and mesh and constitutive modeling of concrete. The material parameters of the damaged plasticity model in ABAQUS were calibrated based on the results of the internal slab-column connection test. The predictive ability of the calibrated model was demonstrated by simulating different slab-column joints without shear reinforcement. Internal samples of slab-column under static loading, internal samples under static and reverse cyclic loading, and edge samples under static and horizontal loading were investigated. Comparison between experimental and numerical results shows that the calibrated model correctly predicts the shear response of punched slabs. [5]

R. J. C. Silva et al. (2021), investigated the punching shear strength of 21 hollow slabs. In the articles under this title, to compare the ultimate load of 10 hollow slabs with different sizes of holes, numerical modeling was done with the help of ANSYS software. Loads and failure modes were investigated and it was found that in the case of shearing in the area of the ribs of the hollow slab, samples with less solid parts have lower load-bearing properties than samples with more solid parts. Hollow slabs with areas that have a larger volume are punched like flat slabs and show similar behavior. The evidence showed that the samples with a solid area of 15% of the slab opening have a suitable capacity [6].

Al-Awazi and Al-Assadi (2017) in an article titled " Nonlinear behavior of one-way reinforced concrete hollow block slabs " investigated 11 slab samples, 8 of which were hollow and the other samples were flat slabs with simple supports. Two types of loading and geometric sections (23.3% and 29.1% volume reduction) were considered for the slabs. The proposed finite element model showed a good fit with the results. The difference in the bearing capacity obtained with the laboratory sample was only 10%, which is a small and appropriate difference. 29.1% reduction in cross-sectional area under two loading patterns showed an increase in capacity equal to 8.6% and 5.7% compared to flat slab. Despite the appearance of cracks in the hollow core slabs with a lower load than the reference slabs, the crack development in the hollow core slabs during loading is slower than that in the solid slab, which is a result of the presence of reinforcement in the upper web of the slab [7].

Al-Awazi and Al-Asadi (2016) in an article entitled Numerical analysis of reinforced concrete hollow-core slabs, in this study, three hollow slabs were investigated and compared with flat slabs. The purpose of this research was to investigate the effect of reducing the weight and size of the holes on the final capacity of the hollow slab. Parameters such as the ratio of the opening cut to the effective depth, the size and shape of the holes, the type of loading, and the effect of the upper rebars of the slab were taken into consideration. The results showed that reducing the weight of the slab with the help of holes has reduced the final bearing capacity of the slab. Increasing the cross-sectional area of the ribs in the section of the hollow block slab shows better results than increasing the number of ribs in the same percentage reduction of the cross-sectional area [8].

Somasekhar Anjaly et al. (2015) conducted a study on the effect of openings in hollow slabs and it was found that the openings that are located in the cavity area of the hollow slab with a width less than 10% of the width of the strips do not have much effect on the final load capacity of the hollow slab and the openings created by the two middle strips are surrounded and can be widened up to 40% of the width of the strips. Also, the openings that are surrounded by the column strip and the middle strip can have a width equal to 20% of the cases [9].

Sheikhnasiri Alireza conducted a Comparative study of numerical methods used in the prediction of post-crack behavior of waffle slabs. the waffle slab sample was modeled with two types of distributed and concentrated loading conditions and two types of simple and fixed support conditions. The models were modeled by two methods of concrete damage plasticity and smeared cracked concrete by Abaqus software. Various parameters of these samples, including the load-displacement diagram, the load coincident with the formation of cracks, the displacement in the middle of the slab opening, and the pattern of the formation and propagation of cracks, etc., were discussed and investigated. The outcomes of this study showed; a relatively good correspondence between the two methods of Concrete damage plasticity and the concrete smeared crack model, but due to the definition of failure in the Concrete damage plasticity method, more accurate results can be obtained. [10]

2. Methodology

This research is theoretically conducted using finite element software. This research takes into account the potential varieties of cracks in concrete slabs. Slabs should consider all three types of cracks, which are shear, flexural, and flexural-shear cracks obtained from the reference test. Two Contour integral and XFEM methods are used to analyze cracks in Abaqus software. To validate and control the modeling process, the laboratory results of the research of Ibrahim N. Najma, Raid A. Daudb, and Adel A. Al-Azzawi. December 2, 2019, has been used. According to the results, the most destructive type of crack in the slab and also the best method of crack analysis can be extracted from the software.

2.1. Validation

To conduct the research, 7 samples of hollow slabs have been defined. The shape and location of cracks are defined based on the reference article. First, a sample without cracks is analyzed and compared with the laboratory sample. 6 other samples were analyzed in two groups with flexural, shearing, and flexural-shearing cracks using Contour integral and XFEM methods and then compared. Table (1) shows the mentioned models by type of crack analysis. Concrete with a compressive strength of 42.7 MPa and a modulus of elasticity of 29926 MPa has been used. Concrete was modeled by the concrete damage plasticity method. Rebars with a yield strength of 524 MPa ultimate strength of 650 MPa and modulus of elasticity of 200000 MPa were used.

2.2. Modeling

Abaqus finite element analysis software was used to model and analyze samples. Fig. 1. To Fig. 4. show examples of hollow slab cracks modeled in Abaqus software. The location of the considered cracks in the model made by Abaqus was considered based on the location of the cracks in the laboratory sample.

Table 1: Type of crack analysis

Type of crack analysis	No crack	Flexural crack	Shear crack	Flexural-shearing
None	Model 1	-	-	-
Contour integral	-	Model 2	Model 3	Model 4
XFEM	-	Model 5	Model 6	Model 7

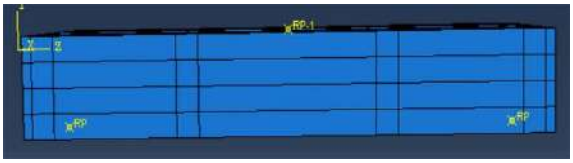

Fig. 1. Schematic view of the hollow core slab with no crack

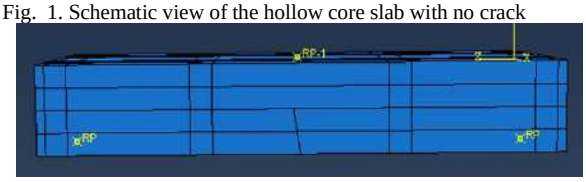

Fig. 2. Schematic view of the hollow core slab with flexural crack

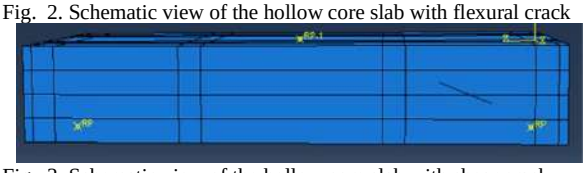

Fig. 3. Schematic view of the hollow core slab with shear crack

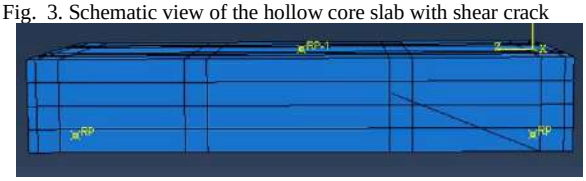

Fig. 4. Schematic view of the hollow core slab with shear crack

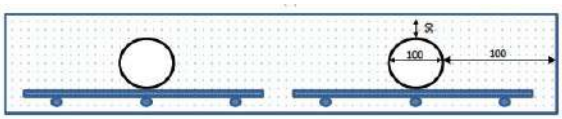

Fig. 5. Schematic view of rebars front section

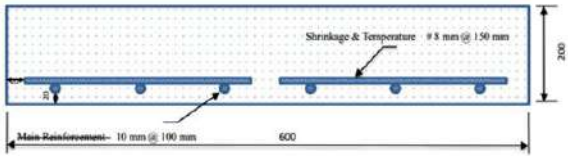

Fig. 6. Schematic view of rebars side section

The waffle slab was modeled with dimensions of 200 x 600 x 1200 mm. Two holes with a diameter of 100 mm and a distance of 100 mm from the short side and 50 mm from the upper and lower parts were considered. The reinforcement detailing on the bottom of slab #6mmØ and spacing of 100 mm for main rebars, and #8mmØ at 150mm for shrinkage. Fig. 5. And Fig.6. Shows rebar details.

The conditions of loading and support are such that the support on both sides of the beam is hinged and the beam is subjected to a monotonic load of 250 KN by a jack. Fig. 7. Shows load and boundary conditions for the slab model. Two analysis methods, Contour integral and XFEM, were considered for the samples.

First, model number 1 was analyzed under the mentioned specifications and its results were compared with the laboratory results for validation. Fig. 8. Shows the load- displacement of model 1, and Fig. 9. Is a comparison of numerical and experimental results.

By superimposing the two force-displacement diagrams obtained from Abaqus and the laboratory model, the difference between the experimental and numerical force was equal to 10 kilonewtons or 5%, and the displacement difference was equal to 0.4 mm or 2%.

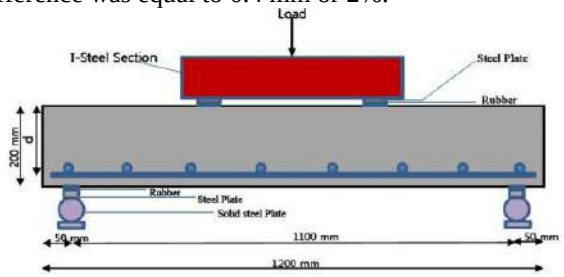

Fig. 7. Load and boundary conditions for the slab model

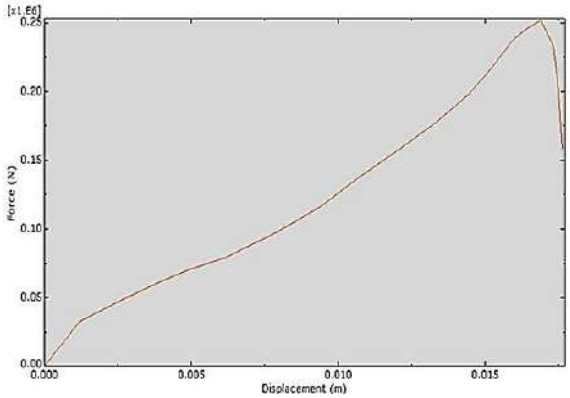

Fig. 8. Load- displacement of Abaqus model

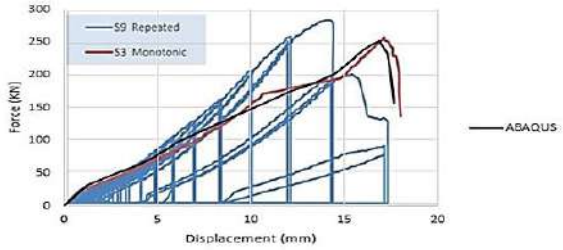

Fig. 9. Load- displacement of Abaqus model and experimental results

3. Results and discussion

The results of the load-displacement diagram of all 3 cracking models as mentioned are shown in Fig.10. and Fig.11. for the Contour integral and XFEM method.

For model 1, in both analytical methods, according to the diagram, at the maximum displacement of 17.8 mm, the applied force is equal to 250,000 newtons. For model 2 or sample with flexural crack and contour integral method, according to the diagram, in the maximum displacement of 6.7 mm, the applied force is equal to 100,000 newtons. In model number 3, at the maximum displacement of 9.5 mm, the applied force is equal to 140,000 newtons. For model 4, in the maximum displacement of 5.1 mm, the applied force is equal to 58,000 newtons. According to the diagram in Fig. 11. for model 5, at the maximum displacement of 8.1 mm, the applied force is equal to 130,000 newtons. For model 6, the maximum displacement is 11.5 mm, and the force is equal to 160,000 newtons. And for model 7, it is equal to 6.5 mm in force equal to 81000 newtons. It is also possible to see the amount of energy absorbed by the slab according to the first crack until the moment of failure of the slab are shown in Fig. 12. and Fig. 13.

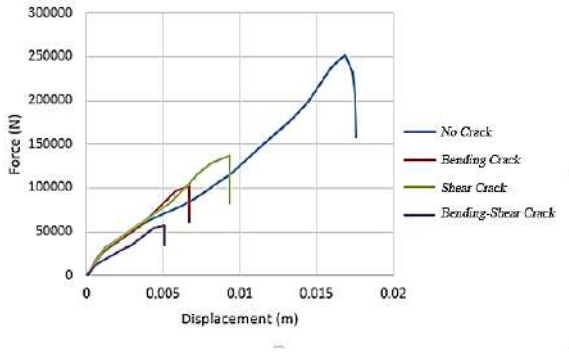

Fig. 10. Load- displacement of models 1, 2, 3, and 4 in the contour integral method

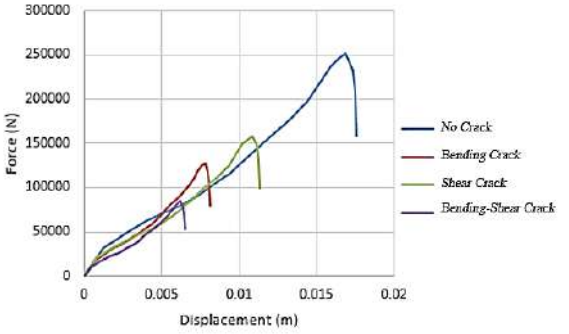

Fig. 11. Load- displacement of models 1, 5, 6, and 7 in the XFEM method

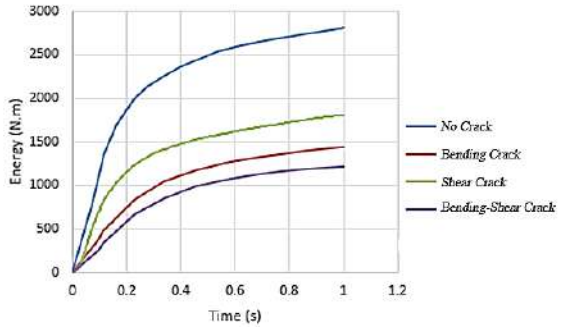

Fig. 12. Absorbed energy of models 1, 2, 3, and 4 in the contour integral method

Table 2: The maximum energy input to the structure, displacement, capacity, and strain of studied model.

Model Number	Strain	Displacement mm	Load Capacity N	Maximum Energy N.m
1	0.049	17.8	250000	2800
2	0.016	6.7	100000	1500
3	0.029	9.5	140000	1800
4	0.012	5.1	58000	1200
5	0.02	8.1	130000	1600
6	0.027	11.5	160000	2000
7	0.02	6.5	81000	1400

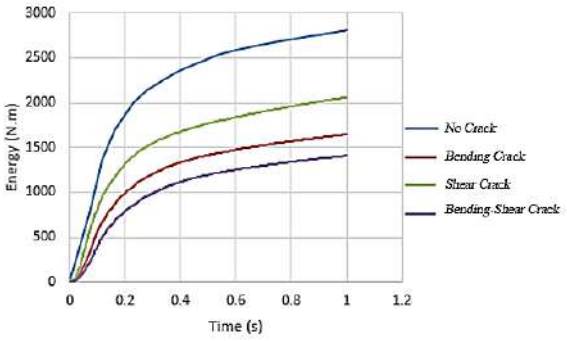

Fig. 13. Absorbed energy of models 1, 5, 6, and 7 in the XFEM method

Table 2 shows the maximum energy input to the structure, displacement, capacity, and strain of each model.

4. Conclusions

The following points were concluded based on the values obtained from the model.

- In the crack analysis by the Contour integral method, at the initiation of the first flexural, shear, and flexural-shear crack until the moment of slab failure, the bearing capacity is 60%, 44%, and 77% respectively, and for displacement 62%, 46%, and 71% and also for the absorbed energy is reduced by 46%, 36%, and 57%.
- In the crack analysis by the XFEM method, the creation of the first flexural, shear, and flexural-shear crack until the moment of failure of the slab, the bearing capacity is 48%, 32%, and 67% respectively, and for displacement 54%, 35% and 63%, and also for absorbed energy 42%, 28%, and 50% decrease.
- Modeling the crack initiation and propagation criteria in the Contour integral method requires the design of element meshes considering the possibility of crack growth. If modeling crack propagation and opening is also considered, the work will be much more complicated. In this way, the path of crack expansion should be predicted in advance and the surface of the elements should be placed on this path. In this method, a singularity is defined at the tip of the crack, which requires using a special type of element. In the new method known as XFEM or Extended Finite Element Method, many of the complications and limitations of the old methods have been solved by using enriched elements.
- In terms of the most destructive type of crack created in the slab, in order: flexural-shear crack,

flexural crack, shear crack (rarely happens in the structure)

- According to the load-displacement (capacity) diagram, the first flexural-shear crack at a force of 81000 newtons and a displacement of 6.5 mm, the first flexural crack at a force of 130000 newtons and a displacement of 8.1 mm, and the first shearing crack at a force of 160000 newtons and a displacement of 11.5 mm meters, so according to the results of the analysis, the probability of creating a flexural-shear crack in the slab is higher than other cracks.

References

[1] Sgambi, Luca, Konstantinos Gkoumas, and Franco Bontempi. "Genetic algorithm optimization of precast hollow core slabs." Computers and concrete 13.3 (2014): 389-409.

[2] Najm, Ibrahim N., Raid A. Daud, and Adel A. Al-Azzawi. "Behavior of reinforced concrete segmental hollow core slabs under monotonic and repeated loadings." Structural Monitoring and Maintenance 6.4 (2019): 269-289.

[3] [3] Reza Salehi, Abbas Akbarpour Nik Qalb Rashti. Numerical study of the behavior of prestressed one-way hollow slabs. International conference on civil engineering, architecture, and urban planning of contemporary Iran, 2016. P. 1-11

[4] [4] Behzad Shafi Rad, Amir Saedi Darian. Introducing a finite element modeling method for precast hollow core slabs by ABAQUS software and checking the friction coefficient changes on it. The first conference on civil engineering, new developments, and economic development, 2014. P. 1-9

[5] Genikomsou, Aikaterini S., and Maria Anna Polak. "Finite element analysis of punching shear of concrete slabs using damaged plasticity model in ABAQUS." Engineering structures 98 (2015): 38-48.

[6] Silva, Ricardo José Carvalho, et al. "Punching shear strength of waffle flat slabs." Revista IBRACON de Estruturas e Materiais 14 (2021): e14106.

[7] Hasan, Haider H. Shear Behavior of One-Way Reinforced Concrete Hollow Slabs Voided with PET Void Formers. Diss. 2023.

[8] Al-Azzawi, Adel A., and Sadeq Aziz Abed. "Numerical analysis of reinforced concrete hollow-core slabs." ARPN Journal of Engineering and Applied Sciences 11.5 (2006): 9284.

[9] Somasekhar, Anjaly, and Preetha Prabhakaran. "Analysis of reinforced concrete Waffle Slabs with openings." International Journal of Emerging technology and Advanced engineering 5 (2015): 86-90.

[10] Sheikhnasiri, Alireza. "Comparative study of numerical methods used in prediction of post-crack behavior of waffle slabs." Journal of Civil Engineering Researchers 4.4 (2022): 12-19.

Journal of Civil Engineering Researchers

Journal homepage: www.journals-researchers.com

Enhancing Concrete Strength with Polymer-Based Additives in the Cement Matrix: A Comprehensive Review

Sasan Kermani,[a,*] Soheil khalatbari[b]

[a] *Department of Civil Engineering, Nour Branch, Islamic Azad University (IAU), Nour, Iran*

[b] *Department of Civil Engineering, Ramsar Branch, Islamic Azad University (IAU), Ramsar, Iran*

ABSTRACT

The modern types of concrete consist of a mixture of aggregates, cement, water, and optional additives and admixtures. Polymer additives, such as superplasticizers, latexes, redispersible powders, polymer fibers, and recycled polymers, have shown promise in significantly altering the properties of concrete and mortar. These polymeric materials are widely used in the construction industry to enhance resistance to cracking and improve overall performance. This paper provides an overview of popular polymeric additives and their impact on concrete properties, as well as the relationship between the chemical structure of additives and the behavior of the resulting concrete.

ARTICLE INFO

Received: January 1, 2024
Accepted: March 8, 2024

Keywords:
Cement, additives
Superplasticizers
Polymer
Concrete additives
Redispersible powders

© 2024 Journals-Researchers. All rights reserved.

DOI: 10.61186/JCER.6.1.48
DOR: 20.1001.1.22516530.1399.11.4.1.1

1. Introduction

The cement industry, a major producer in terms of volume, supplies building materials for the construction industry. Cement is a key ingredient in concrete, the most widely used building material with diverse applications and primarily used for structural elements. The widespread use of concrete is due to factors such as abundant resources, low cost, and high compressive strength [1]. Concrete is a mixture of various substances serving different purposes, typically containing aggregates like gravel, sand, and/or stones, along with an adhesive usually made of cement and water (10–15% vol.). Different types of concrete exist, including high-performance concrete developed in the 1990s characterized by low water content due to the introduction of plasticizers and secondary binders. This type of concrete exhibits significantly increased compressive strength compared to standard-strength concrete [2]. The development of very tall buildings and large structures has led to increased requirements for concrete with features like high compressive strength and exceptional durability. To address these needs, lightweight concrete (LWC) was developed with a density ranging from about 1400 to 2000 kg/m3 due to inner voids in its

* Corresponding author. Tel.: +989123355282; e-mail: s_68_kermani@yahoo.com.

structure [4]. Additionally, ternary and quaternary binder systems have been introduced using different cementitious materials to achieve early strength, rapid setting, and better shrinkage compensation than standard OPC-based materials [6]. Furthermore, research has focused on improving concrete mechanical properties through the addition of polymers to the cementitious matrix. Polymer-modified concrete (PMC) or polymer-modified mortar (PMM) involves various forms of polymers such as latexes, liquid resins, water-soluble polymers and copolymers, fibers, and re-dispersible powders that can enhance properties like flowability, setting time, freezing–thawing resistance, mechanical properties, anti-penetrability, microstructure change, shrinkage reduction effect [10-18]. Fibers have also been examined as additives incorporated into the cementitious matrix to improve tensile and flexural performance while reducing shrinkage cracking [20-28]. Synthetic fibers can be replaced with recycled polymer material as a sustainable solution for utilizing polymer waste as filler or modifier in concrete production [29-31]. This paper provides an overview of recent developments and research on polymer additives used in concrete-based composites. It focuses on how various polymer additives impact the parameters of mortar and concrete.

The review is specifically focused on superplasticizers, latexes, redispersible powders, admixtures for improved crack resistance, fibers, and recycled polymers as potential additives in concrete-based composites. It emphasizes the connection between the chemical composition of these additives and the overall behavior of concrete

2. Plasticizers and Superplasticizers

The concrete industry experienced rapid development in the 1990s with the introduction of a new type of chemical admixture known as plasticizers. The initial generation was based on lignosulphonate compounds, which reduced the water/cement ratio by approximately 5–10% [32]. It is widely recognized that reducing the water content in mortar leads to a decrease in the overall porosity of concrete [16]. Consequently, decreasing the water amount in mortar has benefits for durability and workability, and also contributes to shrinkage reduction [33]. Fresh cement paste can generally be seen as a suspension dispersion with chemical reactivity. Upon exposure to water, the cement grains immediately begin to dissolve and hydrate, resulting in the accumulation of both positive and negative charges on the cement surface. As a result, electrostatic interactions between opposite charges on the surfaces of the grains lead to the flocculation of cement grains and subsequent water entrapment [34]. Water present in the mixture can be chemically bonded in hydrates, physically adsorbed on cement grain surfaces, entrapped in flocculated structures, or remain non-bonded as free water, serving as a dispersion medium. It is well established that macroscopic properties of liquid–solid dispersion, such as viscosity and flowability, are dependent on microstructure, which is closely linked to liquid–solid interface properties [35]. The addition of plasticizers or superplasticizers to the cementitious matrix brings about significant changes in solid–liquid interface properties (Figure 2) [36,37].

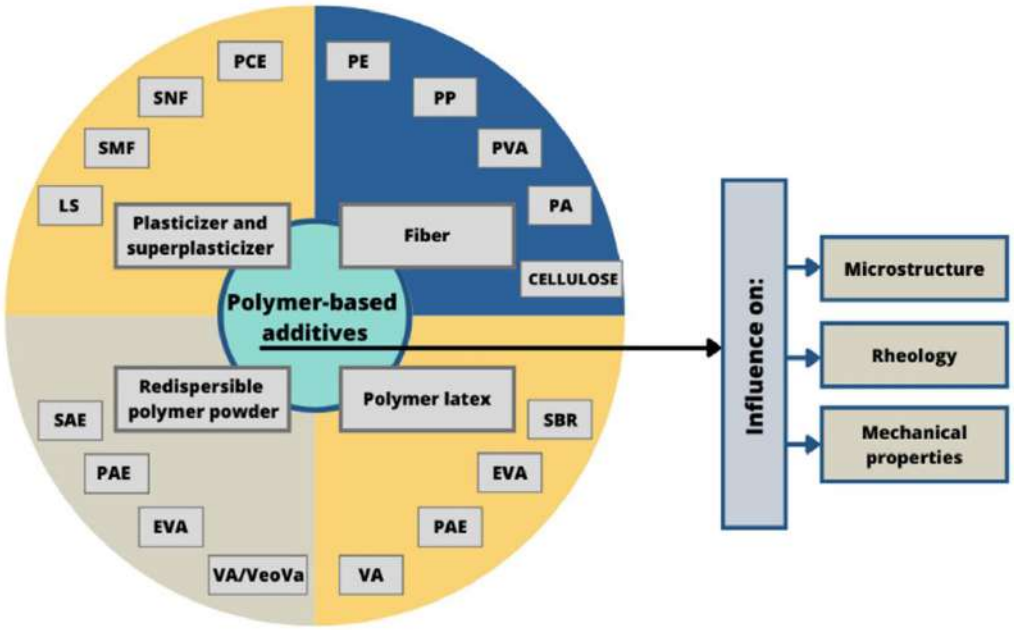

Figure 1. illustrates the types of additives and their impact on concrete-based composites.

A category of compounds that can reduce the water/cement ratio by approximately 25% is known as superplasticizers [38,39,40]. The introduction of these compounds has proven to be a convenient and practical method for enhancing the properties of concrete. However, the high fluidity they induce can lead to adverse effects such as bleeding and phase separation. To address these drawbacks of superplasticizers, the addition of viscosity-enhancing compounds was developed [41,42]. Superplasticizers come in various types with differing chemical structures and can be categorized into groups such as lignosulphonates, sulfonates, naphthenates, melamine sulfonates, and polycarboxylates [43]. Unlike plasticizers, superplasticizers operate through a different mechanism and consequently have varying effectiveness in reducing water mixing. The specifics of this mechanism are discussed later in this review. Different types of reactive groups present in the molecules of superplasticizers bond with Ca2+ cations at different strengths. According to published data, the strength of these bonds decreases in the following order: phosphate > carboxylate > sulfonate > sulfate > alkoxide and water [44]. Therefore, polycarboxylate containing -COO− groups demonstrates improved effectiveness in dispersing cement particles compared to plasticizers containing -SO3− groups, for example. Furthermore, research efforts have been made to investigate the efficiency of polymer admixtures containing the most effective groups for chelating calcium ions, such as phosphonates and phosphate groups [36,45,46].

J. Stecher and J. Plank synthesized a phosphated comb polymer superplasticizer, testing its dispersing performance in cement through slump tests in cement paste [45]. They found that polyphosphate superplasticizers exhibited improved dispersing performance compared to PCEs superplasticizers, with less retarding effect on cement. The authors emphasized that the high calcium complexing capacity of the phosphate group contributed to these results. Both plasticizers and superplasticizers are essential admixtures in concrete, listed in the European standard PN-EN 206 as a possible solution for achieving the right consistency by reducing water content, modifying consistency without changing water and cement amounts, or reducing cement content [52]. Superplasticizers, also known as high-range water reducers, are often used in concrete formulations to reduce water volume and achieve higher solid content while maintaining proper consistency. Scientists and engineers have identified basic properties of superplasticizers, confirming their ability to improve the workability of fresh concrete [53], chloride binding [54], and durability of cementitious materials [16]. However, using such compounds has introduced new challenges due to poor compatibility with the multi-component system of concrete, including cement, fine aggregate, and additional materials. Significant problems include bleeding, segregation, low initial slump, flash set, and set retardation [55]. Consequently, scientists have begun thorough investigations into the interactions between superplasticizers and particles in the cementitious matrix. N. Roussel et al. indicated that rheological properties of fresh concrete are determined by interactions among particles in the cementitious matrix. As the cement hydration process progresses, new rigid phases are created such as anhydrous phase at an early stage, ettringite, calcium silicate hydrate (CSH), and gypsum. This leads to increased yield stress, thixotropy, and hardening of the cementitious material significantly reducing workability [36,55]. The application of superplasticizer serves to keep distance among particles through distribution of polymer molecules adsorbed onto particle surfaces, decreasing interaction strength. Improved workability results from releasing a large quantity of water during deflocculation process [34,55]. Numerous studies have shown that fluidity of fresh cement paste depends on the amount of superplasticizer adsorbed by a square meter of solid particles [57-59]. The adsorption of superplasticizer on solid surface depends on polymer's chemical structure at solid interface and pore solution containing different dissolved ions [36]. It is important to note that processes of superplasticizer adsorption and cement hydration occur at a certain point during concrete formation [60]. At early stages during first period of cement hydration new phases develop leading to morphology changes in the cementitious matrix. Superplasticizers display different adsorption affinity toward surface of various hydration products and mineral phases affecting hydration process including ettringite formation. Therefore, hydration rate mortar morphology surface properties of hydration products their size and amount greatly influence concrete workability [61-63]. In case of Portland cement hydration main composition of solid surfaces is result of hydration calcium silicate aluminate phases among them certain interfaces can be specified separating ettringite gypsum CSH anhydrous phases. According to previous studies ettringite shows highest adsorption capacity for superplasticizers CSH phase adsorbs superplasticizers at least 3–10 times less than ettringite consequently ettringite is considered crucial phase for understanding fresh concrete rheology [36]. Marchon indicated that ettringite surface is entirely covered by polycarboxylate superplasticizer (PCE). Liu et al provided elucidatory description interaction between polycarboxylate polymer molecules and hydration products OPC surface coverage cement hydration products by PCE together with size distribution cement particles affects workability obtained material Polycarboxylate superplasticizer strongly adsorbs onto positively charged cement particles however adsorption process could be weakened through screening

effect counterions The other recently analyzed super plasticizer is Welan gum In work by Khayat it was established that Welan gum at low shear rates is able increase yield stress enhance rebuilt-up kinetics rest increase viscosity cement paste It is noteworthy that Portland cement not only type used practice there also other types have different mineral composition H Tian investigated effects polycarboxylate superplasticizers sulfoaluminate SAC systems SAC contains calcium sulfoaluminate fraction various calcium sulphates such CaSO4 CaSO4·2H2O CaSO4·0 5H2O responsible faster hydration SAC compared OPC article H Tian effects polycarboxylate superplasticizers obtained via radical copolymerization acrylic acid AA a-methallyl-x-hydroxy poly(ethylene glycol) monomer ratio 4 ordinary Portland investigated SAC system study confirms differences compatibility selected superplasticizer used The adsorption superplasticizer solid surface depends chemical structure polymer added superplasticizer adsorbed onto surface consequence electrostatic specific interaction interface Figure 3.

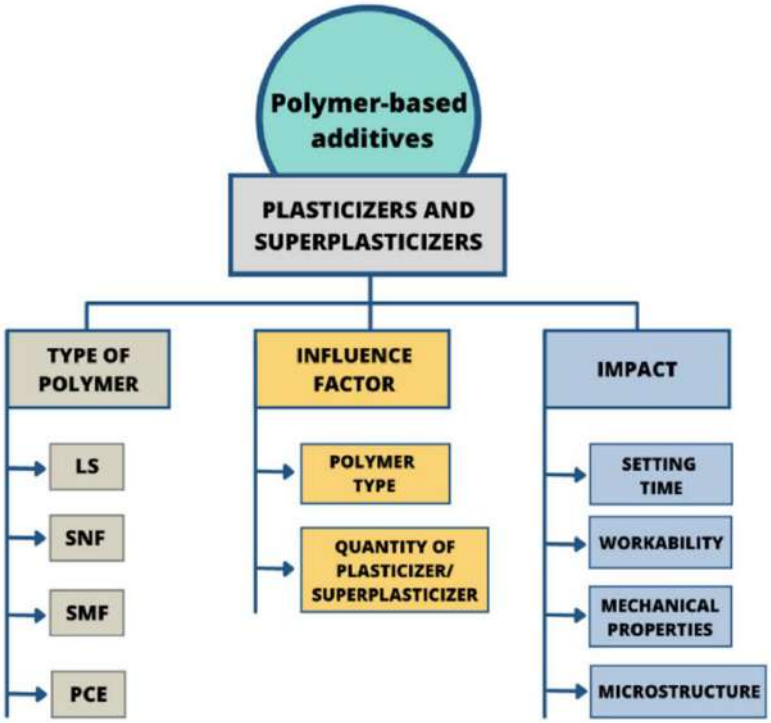

Figure 2. Diagram illustrating the different types of plasticizers and superplasticizers, factors that influence them, and the resulting changes in concrete-based composites.

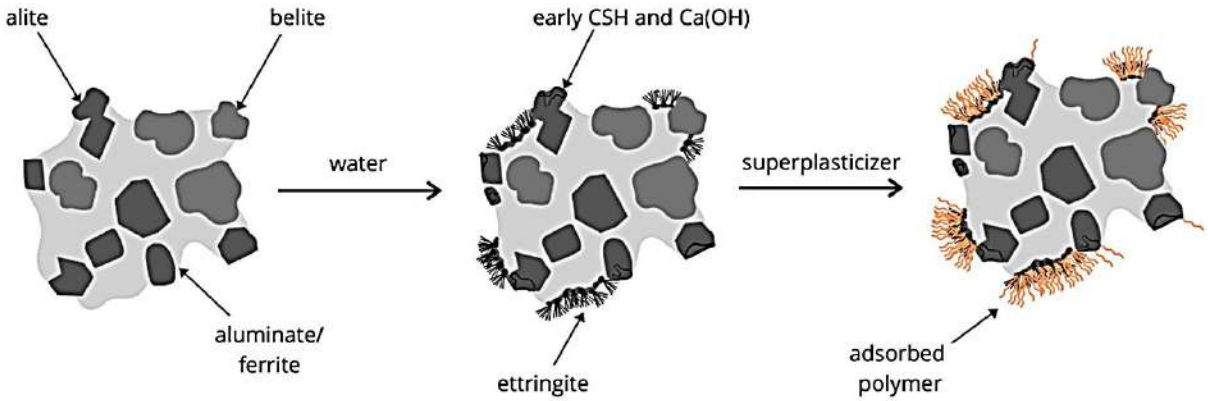

Figure 3. The diagram of a hydrating cement particle with non-uniform distribution of superplasticizer polymer on its surface (adapted from [67]).

It is widely acknowledged that the functional group of a superplasticizer has varying adsorption affinity towards a given surface. This was discussed by J. Stecher and J. Plank [45], who synthesized phosphate comb superplasticizers based on methacrylate ester and compared their properties with their carboxylate counterparts. They found that polyphosphate comb polymers outperform the polycarboxylate ones in terms of their dispersing capacity in cement paste, attach more readily to the cement surface, and impede cement hydration to a lesser degree [45]. In addition to the type of functional group of superplasticizers, other parameters of polymers significantly influence the adsorption process. These parameters include the number and density of the adsorbing groups, the length of the side-chain, as well as its grafting density [55,68]. Numerous studies indicate that the dispersing efficiency of PCE superplasticizer depends on either the dosage and quantity of PCE adsorbed on the surface of cement particles or the charge density and activity of the long side chain [69,70,71]. Furthermore, it has been noted that superplasticizers impact the setting time of fresh concrete and its mechanical properties. Polycarboxylate superplasticizers slow down ettringite formation but increase its total surface area [62]. It was found that PCE superplasticizers facilitate the formation of nano-sized ettringite, which is a primary source of incompatibility between cement and additives [61]. Moreover, PCE adsorbs onto reactive sites of 3CaO·SiO2 (C3S), inhibiting its dissolution and delaying the hydration process [64]. Shen et al. indicated that adding PCE to SAC could delay the setting time of cement-based substances [72]. Additionally, a superplasticizer can positively affect concrete's mechanical properties by improving microstructure, especially due to reducing water/cement ratio. Several studies have investigated how superplasticizers influence mechanical and rheological properties of mortar and concrete. Researchers have established that the effect of superplasticizers on hardened concrete performance depends on the type and dosage used as well as the binder [43,68,73]. M. Benaicha et al. presented a correlation between rheology and strength in self-compacting concrete (SCC), where compressive strength decreased with an increase in superplasticizer amount [70]. Superplasticizers act as dispersants in colloidal particle suspensions to prevent undesired agglomeration and reduce overall viscosity. To allow cement paste flow, it must exceed yield stress associated with rigid particle networks. The yield stress depends on colloidal and contact interactions among particles and nature of solid particles and their volume fraction [55]. Superplasticizers may interact with cement particles through different mechanisms directly related to their chemical structure. Generally, two mechanisms are distinguished: electrochemical forces and steric hindrance forces [74,75]. Figure 4 presents two different mechanisms of action for superplasticizers in the cementitious matrix.

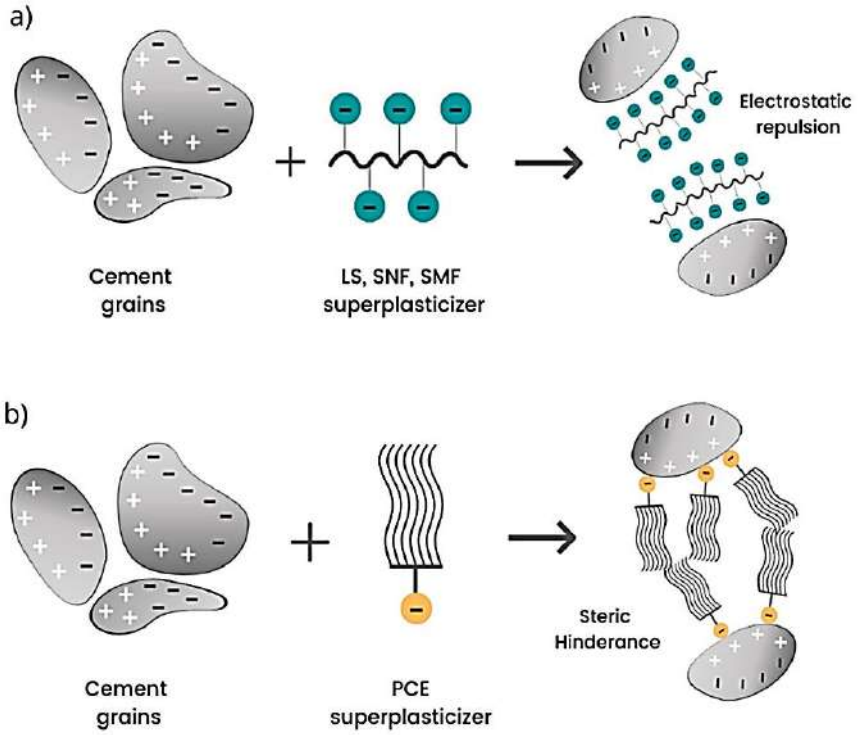

Figure 4. Diagram: (a) the impact of electrostatic repulsion on cement; (b) steric hindrance mechanism, adapted from [51].

The mechanism based on electrochemical forces was initially developed to explain the properties of plasticizers like lignosulphonate. Lignosulphonate compounds have a bipolar structure and exhibit typical polyelectrolyte properties. Their interaction mechanism is based on the physical repulsion of negatively charged cement particles, causing the disintegration of cement lumps into smaller particles, which reduces surface tension on the grains wetted by mixing water. Consequently, fine cement grains move more freely [47]. The electrostatic repulsion leads to an increase in the zeta potential, which depends on the presence of negative charges in the cementitious matrix [76,77]. Both naphthalene and melamine operate similarly to lignosulphonate plasticizers, providing an electrical dispersing effect [74]. In contrast to linear polycondensates that disperse cement particles through electrostatic repulsion, PCE molecules with comb-shaped structures achieve dispersion mainly through steric hindrance [46,65]. Generally, polycarboxylate-based superplasticizers, including polyacrylates, acrylic esters, and sulfonated polystyrene, consist of negatively charged backbone carboxylic groups and lateral grafted chains composed of ethylene oxide units (EOUs) [78]. The steric hindrance effect results from oriented adsorption of superplasticizer molecules on positively charged cement surfaces, weakening the attraction between cement particles. The negatively charged carboxylate anions at the polymer backbone adsorb onto positively charged surfaces of cement particles. Simultaneously, grafted side chains hinder aggregation of cement particles, introducing steric repulsion and a fluidizing effect. Upon adsorption of polycarboxylate superplasticizer, the particles' zeta potential changes from positive to negative or zero [75]. As a result of attaching superplasticizers to cement particles, they cannot approach each other and the attraction forces among them are weakened. Several studies have shown that mortar fluidity depends on the amount of superplasticizer adsorbed on particle surfaces [57,58]. A different perspective on superplasticizers and their interactions with cement has been presented in works by Flatt and Hust [79] and Flatt et al. [80]. According to their theory, introduced superplasticizer is divided into three parts. They have established that the first part is utilized during chemical reactions. The second part is adsorbed onto the cement surface while the last part constitutes the superplasticizer forming a saturated system after introduction of an adequate volume of additive. Moreover, according to Qian et al., it should be emphasized that an increase in PCE superplasticizer concentration leads to an increase in both the adsorbed part and remaining part of the additive.

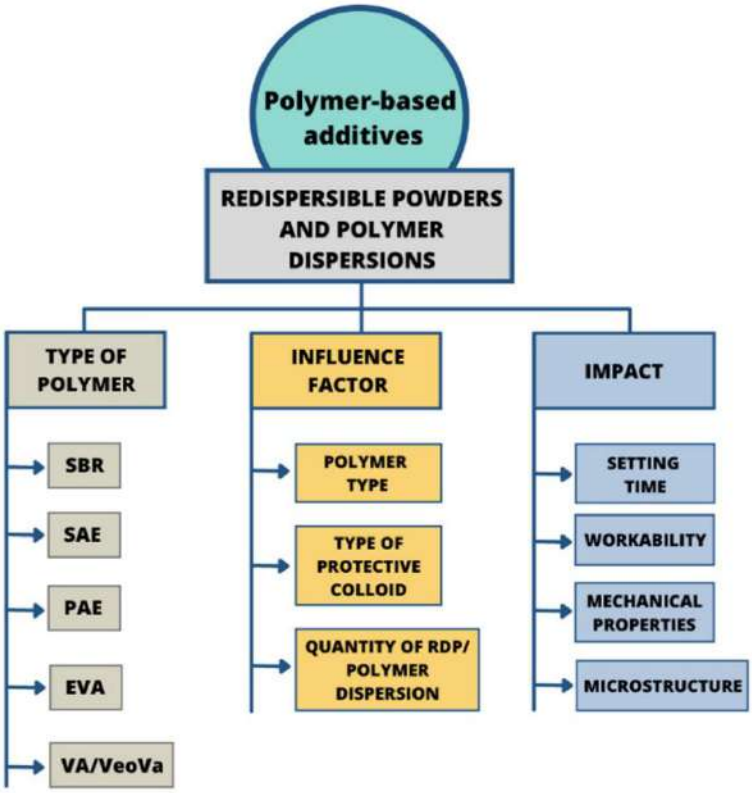

Figure 5. Diagram illustrating the impact factors and alterations induced in concrete-based composite by redispersible powders and polymer dispersion type.

3. Redispersible Powders and Polymer Dispersions

The rapid growth of the construction industry has led to efforts to enhance the fundamental properties of concrete and address its limitations, such as brittleness, low durability, and insufficient strain capacity, by modifying the microstructure of hydrated cement. In recent years, advancements in building construction have significantly progressed, and research on high-performance cement-based materials has been advanced to meet industry requirements. One way to improve concrete performance, including strength and durability, is by incorporating polymers into the cement matrix. Cement-polymer composites are formed by replacing all or part of the cement hydrate binder with polymers. Polymer-modified concrete was initially introduced in the 1990s and has since become a common construction material [10]. Today, various types and forms of polymers are used as chemical admixtures (Figure 5). Among these widely used additives are polymers with different chemical structures, such as lignosulfonates, polyvinyl acetate, ethylene-vinyl acetate, styrene-butadiene copolymers, styrene-acrylic, and polyacrylic ester [81,82]. Numerous studies have been conducted on these materials [12,83,84,85,86]. Currently, polymers are incorporated into cement in various forms, including latexes, liquid resins, redispersible powders, and water-soluble homo- or copolymers [81]. Given that the type of polymer used in the manufacturing process impacts the properties of the resulting composite, the selection of a polymer type and form depends on the intended use of concrete and is associated with desired properties such as strength, chemical resistance, and durability [87].

Initially, polymer-modified mortar and concrete were created by adding a polymer dispersion in latex or emulsion form to the plain cement-based mixture during the mixing process. The primary advantages of polymer latexes include their capacity to form flexible polymer films upon dehydration, as well as their ability to provide proper adhesion and cohesion in cementitious materials [12]. As previously mentioned, water-based polymer systems are utilized to enhance the properties of regular concrete, contributing to increased mechanical strength [10], improved workability [10,86], enhanced durability [13], reduced water absorption [88], and a decrease in overall porosity [89]. However, one limitation of these polymers is their potential for re-emulsification in humid alkaline conditions [10]. Due to their exceptional properties, cement-polymer composites are employed in various applications such as repair mortars, waterproofing membranes, self-leveling compounds, and tile adhesives.

Redispersible polymer powders (RDP) are a modern type of substances produced by spray-drying polymer dispersions and often used for the same purpose as polymer latexes. They are spray-dried to receive polymer powders [81]. It is important to emphasize that spray-drying auxiliaries strongly influence the properties of the RDP-modified mortar. It was observed that polyvinyl alcohol (PVA), which is an example of a colloidal stabilizer in the production of carboxylated styrene-butadiene latex, tends to screen the negative charges of polymeric carboxylate groups, which are to react with calcium ions. As a result, the process of forming a polymer film does not occur properly and the conversion from stage II to stage III is accelerated, as shown in Figure 3 and described in Section 3.1 [90,91].

The properties of cement–polymer concrete and mortars obtained using RDP powders are comparable to those formed in the process of polymer dispersion [93]. The major difference between these two types of concrete is the presence of the spray-dried auxiliaries in the first of the mentioned concrete types, which affects the composite properties. The spray-drying compounds adsorbed on the polymer surface need to dissolve or disperse from the polymer surface to allow coalescence and film formation. This requirement makes the polymer latexes less viable. Consequently, in many cases, they are replaced by an admixture of redispersible polymer powders because of their more straightforward application in concrete production.

3.1. The process of how the polymer film is formed within a cement-based matrix

The introduction of polymer into the cementitious matrix alters the microstructure of concrete [94]. The influence of adding polymer on the cement hydration process has been extensively studied in recent years. The nature of the relationship between polymer and cement particles is a topic of ongoing discussion among researchers. Many studies describe the physical interactions between the binders and the polymeric film created within the cementitious matrix, and their impact on the properties of hardened mortar and concrete. Scientists have also documented both chemical and physical interactions between cement and polymers, proposing the development of new complex structures and alterations in the morphology of cementitious materials, including changes in the composition and quality of hydrated phases [14]. The formation of a polymer film involves multiple stages, with researchers identifying four distinct phases (Figure 6).

The initial stage involves dispersing the polymer particles in water (solvent). As the water evaporates, the polymer particles agglomerate, leading to the formation of the second stage, which consists of a closely packed array with trapped water in the spaces between particles. The subsequent stage occurs as a result of water being expelled

from these spaces through hydration and evaporation processes, resulting in a dense array of hexagonal, distorted polymer particles. Some researchers suggest an additional intermediate stage (Stage III*) between stages III and IV, characterized by a randomly packed array of distorted particles surrounded by water-filled spaces. Finally, stage IV is formed when the polymer particles coalesce into a uniform polymer film. The transition from stage III to IV only occurs if the ambient temperature exceeds the glass transition temperature (Tg) of the polymer [95,96].

3.2. Physical Characteristics of Cement-Polymer Composites

Redispersible polymer powders, when mixed with water, create a uniform dispersion with properties similar to the original polymer dispersed in water. The formation of the polymer film occurs as individual latex particles coalesce after dehydration. These substances are designed for one-time dispersion, so if hardened concrete becomes wet again, they remain unchanged. The resulting films exhibit increased cohesion in the fresh state and adhesion in the hardened state [97]. Polymers can enhance various fundamental characteristics of concrete, including mechanical properties, fresh mortar flowability, resistance to permeability and freezing-thawing, as well as corrosion resistance. Studies have shown that the addition of polymers to the cementitious matrix significantly alters its microstructure and the strength of physical and chemical interactions within the cementitious phase [15]. Numerous studies have been conducted on the attributes of polymer-modified cement materials. According to some reports, styrene-butadiene rubber (SBR) latex enhances flexural and tensile strength, carbonation resistance, waterproofing properties, and anti-shrinkage of mortar. Ethylene-vinyl acetate copolymer latex, widely used in concrete technology, yields result similar to SBR while also increasing flexural and tensile bond strength and concrete durability. Styrene-acrylic ester (SAE) copolymer latex enhances durability but reduces the elastic modulus of cementitious materials [6,12,15,89,92,98]. Similar findings were observed in studies on the effects of using redispersible powders in cementitious materials. Many researchers have confirmed that the application of RDPs improves the mechanical strength of mortar and concrete, such as compressive strength and flexural strength, which gradually increases depending on the RDP content used. Furthermore, it is generally agreed that admixtures of polymer powders affect several properties of concrete, including freeze-thaw resistance, water permeability, elasticity modulus, and corrosion resistance [18,98,99].

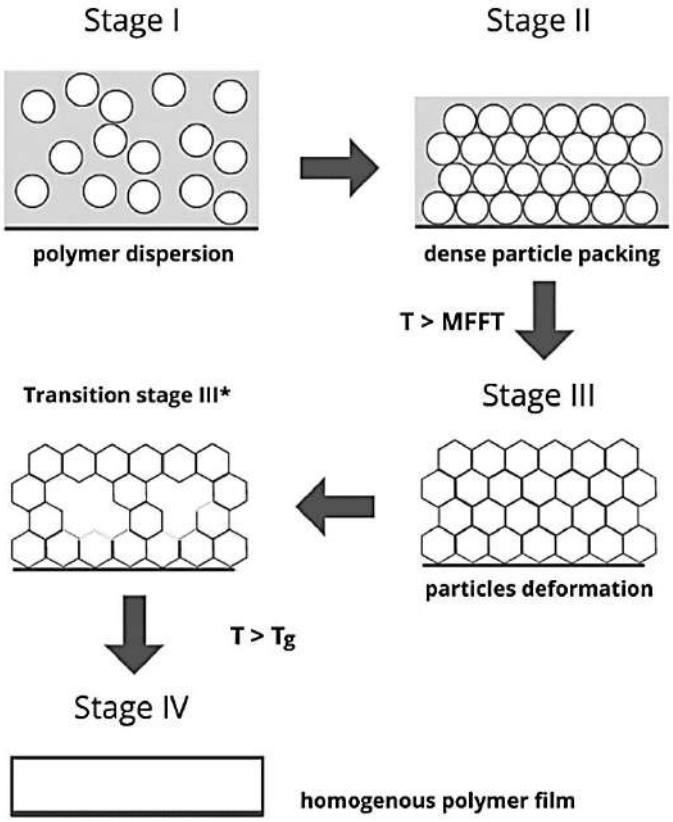

Figure 6. Diagram illustrating the formation of a polymer film from an aqueous dispersion, depicting stages I to IV (adapted from reference [95]).

Water permeability and curing conditions are critical factors that can impact the mechanical properties of concrete, ultimately affecting its service life. Young-Kug Jo [92] investigated the microstructure of polymer-modified concrete after curing in various conditions and the influence of these conditions on the tensile adhesion of concrete. The study examined three polymers—ethylene-vinyl acetate (EVA), styrene-butadiene rubber, and styrene-vinyl acrylic ester—in standard, dry, water, and high-temperature (70 °C) curing conditions. The adhesion in the tensile strength of polymer-modified concrete depends on both the type of polymer and the curing conditions. EVA achieved the highest adhesion in standard curing conditions, while dry curing provided adequate drying time for polymer film formation. However, in humid conditions, the polymer film was not uniformly dispersed in the cementitious matrix, resulting in lower adhesion after water curing [92]. In a separate study, S. Gwon et al. [18] investigated the impact of adding an acrylic redispersible polymer powder on the microstructure development and mechanical properties of ultra-rapid hardening concrete. The study focused on compressive strengths, rheology, hydration phase evolution, porosity, morphological transition, and setting time. Results indicated that adding a polymer delayed setting time but significantly strengthened the microstructure of ultra-rapid hardening cement systems. The optimal polymer-to-cement ratio was determined to be approximately 10% based on test results [18]. Medeiros et al. [14] confirmed that applying EVA or acrylate polymers to cement blends increased compressive tension and direct-shear bond strengths. Silva and Monteiro [100] examined the influence of EVA powder and cellulose ethers on the hydration of Portland cement phases, particularly C3S and C3A. Microscopic imagery revealed that EVA copolymer particles tended to agglomerate around C3S grains during hydration and acted as nucleation sites for the CSH phase. However, introducing EVA into the cementitious matrix hindered ettringite formation in the initial hours of cement hydration [100]. Studies involving vinyl acetate and versatate copolymer (VA/VeoVa) demonstrated improved resistance to alkaline hydrolysis compared to other copolymers containing vinyl acetate groups [101]. Additionally, VA/VeoVa powder exhibited water-reduction effects and retained water in cement mortar, significantly improving concrete toughness and reducing shrinkage rates. Furthermore, VA/VeoVa powder facilitated air entrapment, increasing total air content in fresh mortar. However, Wang et al.'s work showed that VA/VeoVa polymer powder reduced the compressive strength of concrete [15].

3.3. Effects of Aging on Cementitious Blends Modified with RDP

The presence of water leads to a partial prehydration of the cement surface and the polymer film formation. Polyvinyl alcohol (PVA) present on the redispersible polymer powder (RDP) particles' surface, which acts as a colloidal stabilizer in the spray-drying process, might dissolve in humid conditions, allowing the polymer powder to coalesce into a film, partially protecting the cement particles from aging. As a result, the mechanical properties, such as compressive and flexural concrete strengths, with RDP powder achieve higher values than concrete without RDPs after conditioning in humid air [19].

There is little information in the literature pertaining to the long-term performance and durability of cement–polymer concrete, especially with redispersible powder polymers. J. Schulze and O. Killermann [102] examined and described a long-term performance of three different RDPs admixtures, i.e., vinyl acetate-ethylene, styrene-acrylic and ethylene-vinyl chloride-vinyl laurate. They have established that the morphology of the polymers in the cementitious matrix does not change over the 10-year long storage, neither in dry nor humid conditions. The polymer particles were distributed in the matrix and formed secondary reinforcement in the pores and flaws of cementitious blends. Cement serves as an inorganic binder that contributes to compressive strength, while the redispersible powder, an organic binder, affects internal tensile strength and adhesion bond strength at interfaces. Both cement and redispersible powder work together to enhance the properties of mortar and concrete [19,102].

4. Fiber

The literature review uncovered numerous studies on the use of fibers in cement-based composites, known as fiber-reinforced concrete. Adding fibers to a cement blend enhances the mechanical properties, toughness, ductility, and resistance to cracking in mortar and concrete. Over the past few decades, various types of fibers have been investigated for use in cement-based materials. Steel fibers, glass fibers, natural fibers, and polymer fibers are the primary types used for concrete reinforcement. Steel fibers have been traditionally favored due to their ability to significantly improve the tensile and flexural strength of cementitious materials by absorbing energy and controlling cracks. Additionally, their high electrical and heat conductivity makes them suitable for special conditions. However, corrosion is a major drawback that can compromise the durability of structures made with steel fiber-reinforced concrete. Glass fibers and natural fibers such as wood, coconut, palm, and vegetable fibers also

provide good reinforcement but come with significant limitations. Glass fibers have poor alkali resistance, while natural fibers lack durability. The use of randomly distributed polymer-based fibers in the cement matrix has garnered considerable attention due to their effectiveness in enhancing the fundamental characteristics of concrete (Figure 7).

The application of polymer fibers has resulted in advantageous outcomes such as resistance to corrosion and alkaline reactions, salts, chlorine, and microorganisms. R.F. Zollo [103] has presented a schematic crack arrest mechanism for fiber-reinforced concrete (Figure 8). The diagram illustrates the ability of the fibers to absorb energy and control crack propagation. It depicts fiber rupture (1) and pull-out (2), tension bridging through the fiber (3), and debonding of the fiber from the matrix, effectively dissipating energy to prevent crack growth. The presence of fibers in the matrix (5) helps confine the cracking area, resulting in smaller cracks distributed in the adjacent space of the cementitious matrix, as shown in Figure 8. The reinforcing effect observed in concrete is not solely due to individual fibers but rather a cumulative effect of all fibers. In traditional concrete, micro-cracks are present even before loading due to drying shrinkage causing volume contraction. Some researchers have reported a decrease in drying and plastic shrinkage cracks due to fiber use [25,104]. Generally, micro-plastic fibers with lengths ranging from 5–30 mm and diameters from 5 to 100 µm can effectively reduce plastic shrinkage cracking. The prevention of crack propagation in concrete by micro and macro-fibers is depicted in Figure 9. Macro-plastic fibers ranging from 30 to 60 mm in length are utilized to control shrinkage, particularly drying shrinkage. The formation of plastic shrinkage cracks can be attributed to moisture loss after casting. If the rate of moisture evaporation exceeds 0.5 kg/m2 per hour, it can lead to internal strain induced by increasing negative capillary pressure within the matrix. Plastic shrinkage occurs at an early stage when the concrete strength has not yet developed [105]. Kim et al. [25] examined the impact of fiber geometry and volume fraction on moisture loss rate and plastic shrinkage cracking. They found that the volume of macro-plastic fibers and their geometry do not affect total moisture loss, while plastic shrinkage was reduced when the fiber fraction reached 0.25%.

According to the literature, the synthetic fibers most frequently utilized in concrete are polypropylene (PP) fibers, polyamide (PA) fibers, polyethylene (PE) fibers, and polyvinyl alcohol (PVA) fibers. All of these fibers are distinguished by their low density, resulting in a high volume of fiber content in the cementitious matrix relative to the mass of the fibers.

In recent years, researchers have examined how synthetic fibers affect the rheology and mechanical characteristics of cement-based materials. They have explored the impact of different types of fibers, which vary in chemical composition, volume within the cementitious matrix, size (macro- and micro-), and geometry [25,108]. Additionally, they have investigated the influence of individual and combined (various lengths and sizes) polymer fibers on concrete [27,110].

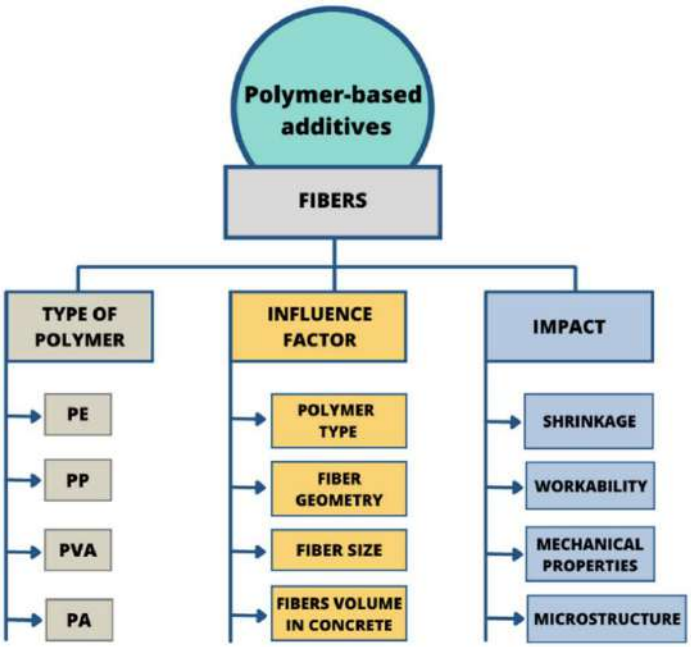

Figure 7. Impact of polymer fibers on the characteristics of concrete-based composites.

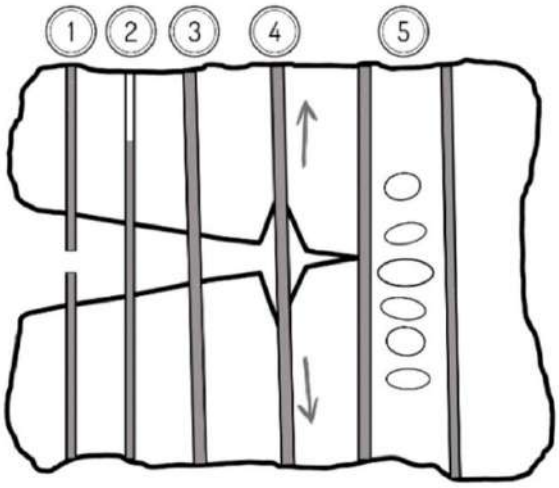

Figure 8. The diagram illustrating the absorption of energy between concrete and fibers (based on literature [103]). (1) Failure of the fiber; (2) pulling out of the fiber; (3) bridging by the fiber; (4) separation of the concrete matrix from the fiber; (5) cracking of the concrete matrix.

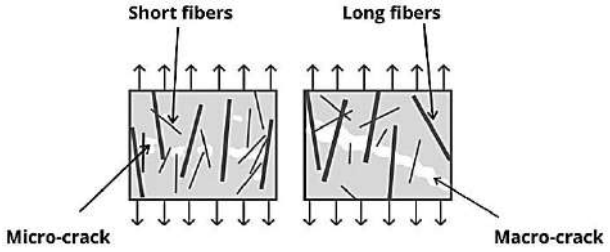

Figure 9. Prevention of crack spread in concrete reinforced with fibers [107].

4.1. The Rheological Characteristics and Mechanical Attributes of Cementitious Materials with Fibers

The inclusion of fibers in the cementitious matrix affects both the fresh and hardened states of concrete. It is widely recognized that polymer fibers decrease the workability of fresh mortar [106]. This occurs because a network structure forms within the concrete matrix, impeding the flow of the mixture. Additionally, a high volume and surface area of fibers can cause water adsorption, thereby increasing mortar viscosity [105,111]. However, Ramezanianpour et al. [28] proposed that the reduced workability of mortar with a higher fiber content in the cementitious matrix is due to trapped air in the inner pores. M. Tabatabaeian et al. [106] examined the rheological properties of fresh concrete reinforced by fibers and found that steel fibers cause a slight decrease in slump flow, while polypropylene fibers significantly reduce it. Yap et al. [112] demonstrated that mortar workability depends on micro-fiber geometry, with fibrillated polypropylene fibers having a lower effective surface area, resulting in better workability compared to multifilament fibers [113]. Hydrophobic polyolefin fibers such as polypropylene and polyethylene were observed to have similar effects on concrete properties, including fresh blend rheology. PE fibers were found to decrease slump flow to a similar extent as PP fibers [112,114,115]. The presence of PVA fibers leads to a reduction in workability proportional to an increase in fiber content. PVA fibers have a more significant effect on flow reduction than PE and PP fibers due to their hydrophilic nature [114]. As previously mentioned, the impact of fibers on concrete's mechanical strength depends on their size, chemical structure, and quantity within the cementitious matrix. Research by Yin et al. [105] suggests that macro-plastic fibers in cementitious materials have no significant impact on compressive strength, consistent with findings reported by Behfarnia and Beharvian [116]. However, Felekoğlu et al.'s study [117] showed that adding PP macro-fibers increased the compressive strength of foamed concrete.

Additionally, Gencel et al. [118] have verified the enhancement of compressive strength in self-compacting concrete resulting from the inclusion of PP macro-fibers. Ramezanianpour et al. [28] studied the impact of PP fibers on the mechanical properties of concrete for sleeper use and found that increasing the amount of PP fibers gradually decreased the compressive strength of concrete sleepers. M.Tabatabaeian et al. [106] examined the influence of PP fibers on the mechanical properties and durability of high-strength SCC compared to steel fibers, revealing a decrease in compressive strength with the incorporation of PP fibers. Furthermore, replacing steel fibers with PP fibers in hybrid mixes resulted in reduced compressive strength across all hybrid samples. Hybrid fibers have garnered attention due to their superior effects on composite performance compared to single fiber blends, as demonstrated by Chen and Liu's study [110] on high-strength lightweight concrete. Hsie et al. [119] investigated polypropylene hybrid fiber-reinforced concrete, finding that adding mixed PP macro- and micro-fibers to the cementitious matrix increased compressive and flexural strength compared to single fibers. Yun's research focused on PVA/ultra-high molecular weight PE hybrid fiber-reinforced concrete, showing that a higher amount of PVA fibers improved compressive performance compared to samples with more PE fibers [119]. Guler [108] explored the use of PA fibers in hybrid form in cement-based composites, finding that while the addition of both PA macro- and micro-fibers did not notably increase compressive strength, it did significantly enhance flexural strength. Cao et al. [109] developed a new multiscale hybrid fiber system comprising CaCO3 whiskers, PVA, and steel fibers, which significantly improved the mechanical properties of cementitious materials, enhancing flexural strength, energy absorption capacity, and reducing plastic shrinkage in concrete based on previous tests.

4.2. The Microstructural Composition of Cement-Based Materials Reinforced with Synthetic Fibers

The analysis of microstructure is a suitable approach for understanding the physical and mechanical properties of fiber-reinforced cementitious materials, and as a result, researchers have placed significant emphasis on the microstructural characterization of concrete. The literature review has identified numerous articles focused on studying the microstructures present in fiber-reinforced concrete using various techniques, including scanning electron microscopy (SEM) [28,120,121,122], energy dispersive spectroscopy (EDS) [123], X-ray diffraction analysis (XRD) [26,120,121,124,125], infrared absorption spectroscopy (IR) [123], Fourier transform infrared spectroscopy (FTIR) [120,123], and thermogravimetry analyses (TGA) [124]. Generally, the hydrophobic nature of polymer plastic fibers results in poor bonding in hydrophilic cementitious materials. SEM analysis reveals the presence of trapped air voids around polyolefin fibers (Figure 10). To address this issue, some researchers have modified the surface of fibers using chemical solutions [126,127,128] and plasma treatment [129]. Lopez-Buendia et al. [128] discussed the surface modification of polypropylene fibers through alkaline treatment (Figure 11), which led to cement crystal growth on the modified fibers' surface and improved fiber-cement adhesion. The literature review indicates that surface treatment enhances the mechanical properties of hardened concrete, such as flexural strength [127,129], crack strength [126], and toughness [126,129].

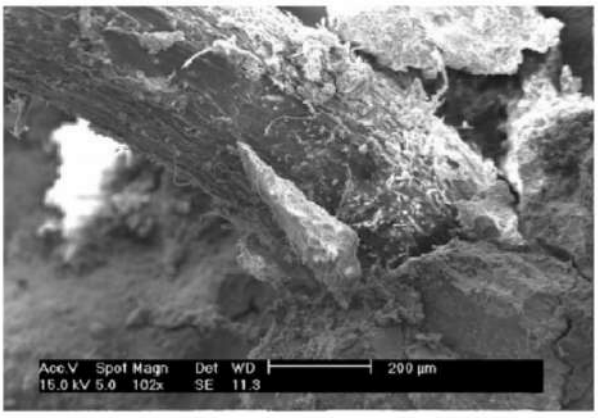

Figure 10. Inadequate adhesion and air voids trapped around a PE fiber within the concrete matrix [131].

Another method of surface modification for fibers that has been experimentally tested is thin layer coating. Hernandez-Cruz et al. [129] examined the chemical interactions between PP fibers coated with ethylene acrylic acid copolymer (EAA) and the cementitious matrix. They discovered that in the cement paste containing the EAA-coated fibers, bonding is enhanced due to the hydrophilic carboxyl groups present in EAA, which interact with the Ca2+ and Na+ cations from the cement paste. This improved bonding enhances the post-cracking behavior of concrete reinforced with the modified fiber compared to concrete reinforced with non-modified PP fiber. C. Signorini et al. [130] studied the impact of silica-coated PP fibers on the mechanical properties of fiber-reinforced concrete. Polypropylene fibers were coated with silica nanoparticles using the sol-gel technique. They found that nano-silica coating is an effective method for improving bond strength in the fiber-cementitious matrix. The SEM analysis (Figure 12) reveals that the surface of the fiber in a control sample appears scratched, with mortar adhering to its surface only in some places, whereas on the surface of modified fibers, attached mortar grains are visible.

4.3. Characteristics of Concrete Reinforced with Recycled Polymer Fibers

Recently, the potential use of recycled plastic waste fibers in concrete has garnered attention from researchers. A number of experimental studies have been conducted to investigate reinforcing concrete with recycled plastic fibers [131,132,133,134,135]. The focus has primarily been on plastics found in waste in significant quantities, such as PET fibers, rubber aggregates, and polystyrene wastes. These plastics are being tested as a partial replacement for sand in concrete, with an exchange ratio of 10% by volume potentially saving 820 million tons of sand per year [134].

B.S. Al-Tulaian et al. [133] examined the effects of recycled PET waste fibers on the mechanical properties of Portland cement mortar, including flexural strength, flexural toughness, and shrinkage cracking. They found that adding fibers reinforced concrete and led to increased flexural toughness and strength. Moreover, increasing the fiber volume fraction significantly improved the reduction of plastic shrinkage cracking. Different types of tested fibers varied in length and volume fractions but all resulted in a decrease in total crack areas and widths.

Ochi et al. [134] studied the bond behavior of concrete reinforced with recycled PET fibers from waste bottles. Samples with fiber content above 1% exhibited higher bending strength than reference samples. A similar effect was observed by Kim et al. [25], who studied the performance of concrete with different types of shredded, recycled PET. Embossed fibers showed superior mechanical bond strength followed by crimped and straight fibers. Additionally, samples with the highest bond strength also demonstrated the best resistance to plastic shrinkage cracking.

The influence of recycled PET fibers on early-age performance and mechanical characteristics of reinforced concrete has also been investigated. Borg et al. [31] used fibers shredded from waste plastic bottles of different sizes

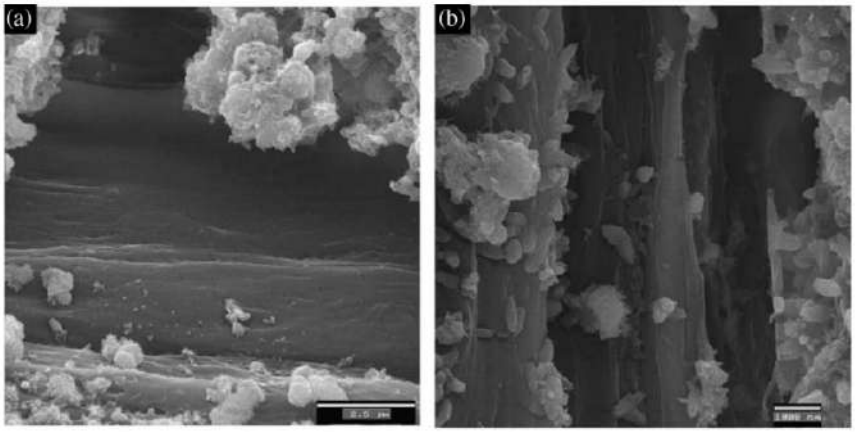

Figure 11. The exterior of polypropylene fibers: prior to alkaline treatment (a) and following alkaline treatment (b) [128].

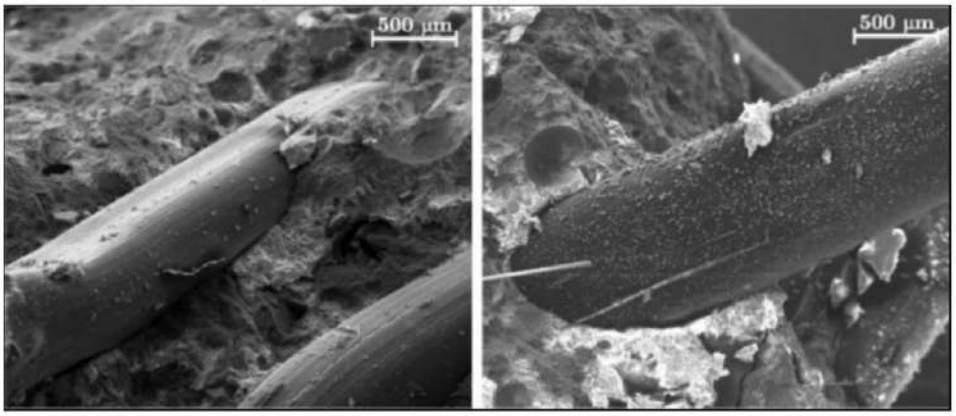

Figure 12. The appearance of the samples after the bending test: unmodified PP fibers (on the left) and PP fibers coated with silica (on the right) [130].

and geometries and found that their addition reduced compressive strength but restrained crack development induced by an environmental chamber.

M. Horgnies et al. [136] studied the effect of PA wastes on the microstructure of lightweight mortars and found that compressive strength decreased proportionately with an increase in polymer waste content while total porosity increased.

These studies demonstrate the potential benefits and challenges associated with using recycled plastic waste fibers in concrete applications [131,132,133,134,135].

5. Conclusions

In summary, research has been conducted on enhancing concrete by incorporating polymer-based additives into the cement matrix. The effects of adding superplasticizers, latexes, redispersible powders, admixtures, fibers, and recycled polymers to concrete have been explored. Reviewing the literature has led to several conclusions. The addition of a plasticizer or superplasticizer can achieve the desired consistency by reducing water or cement content. Key factors influencing the properties of resulting concrete composites include the type, number, and density of adsorbing groups, side-chain length, and grafting density. Additionally, the dosage and quantity of superplasticizer used significantly impact its efficiency in adhering to cement particles. Redispersible powders and polymer dispersions influence the cement hydration process and can form flexible polymer films after dehydration, providing proper adhesion and cohesion in cementitious materials. Polymeric fibers are known for their elasticity, chemical resistance, high strength, and excellent wear resistance. Consequently, cement-based materials containing fibers exhibit improved mechanical properties, toughness, ductility, and post-cracking resistance. Furthermore, the low melting temperature of polymeric fibers results in reduced spalling in concrete composites at higher temperatures. The literature review demonstrates that polymer-based additives are valuable components that can overcome limitations in concrete. Future studies are likely to focus on self-repairing concrete composites. Technological advances have been made to produce concrete without reinforcement using self-compacting technology with high aesthetic values and quality while being lighter, safer, more flexible, durable, and environmentally friendly. Additionally, future concrete may have the potential to utilize solar and wind energy and capture/consume CO2 and NOx.

References

[1] Iyer, N.R. An Overview of Cementitious Construction Materials; Elsevier Inc.: Amsterdam, The Netherlands, 2020.

[2] Cwirzen, A.; Penttala, V.; Vornanen, C. Reactive powder based concretes: Mechanical properties, durability and hybrid use with OPC. Cem. Concr. Res. 2008, 38, 1217–1226.

[3] Braunauer, S.; Yudenfreund, M.; Odler, I.; Skalny, J. Hardened Portland cement pastes of low porosity VI. Mechanism of the hydration process. Cem. Concr. Res. 1973, 3, 129–147.

[4] Wang, J.Y.; Chia, K.S.; Liew, J.Y.R.; Zhang, M.H. Flexural performance of fiber-reinforced ultra lightweight cement composites with low fiber content. Cem. Concr. Compos. 2013, 43, 39–47.

[5] Bremner, T.W. Lightweight Concrete; Woodhead Publishing Limited: Sawston, UK, 2008; ISBN 9781845692636.

[6] Zhang, X.; Li, G.; Song, Z. Influence of styrene-acrylic copolymer latex on the mechanical properties and microstructure of Portland cement/Calcium aluminate cement/Gypsum cementitious mortar. Constr. Build. Mater. 2019, 227, 116666.

[7] Zajac, M.; Skocek, J.; Adu-Amankwah, S.; Black, L.; Ben Haha, M. Impact of microstructure on the performance of composite cements: Why higher total porosity can result in higher strength. Cem. Concr. Compos. 2018, 90, 178–192.

[8] Lothenbach, B.; Scrivener, K.; Hooton, R.D. Supplementary cementitious materials. Cem. Concr. Res. 2011, 41, 1244–1256.

[9] Pott, U.; Jakob, C.; Jansen, D.; Neubauer, J.; Stephan, D. Investigation of the incompatibilities of cement and superplasticizers and their influence on the rheological behavior. Materials 2020, 13, 977.

[10] Aggarwal, L.K.; Thapliyal, P.C.; Karade, S.R. Properties of polymer-modified mortars using epoxy and acrylic emulsions. Constr. Build. Mater. 2007, 21, 379–383.

[11] Sarwar, W.; Ghafor, K.; Mohammed, A. Regression analysis and Vipulanandan model to quantify the effect of polymers on the plastic and hardened properties with the tensile bonding strength of the cement mortar. Results Mater. 2019, 1, 100011.

[12] Li, L.; Wang, R.; Lu, Q. Influence of polymer latex on the setting time, mechanical properties and durability of calcium sulfoaluminate cement mortar. Constr. Build. Mater. 2018, 169, 911–922

[13] Moodi, F.; Kashi, A.; Ramezanianpour, A.A.; Pourebrahimi, M. Investigation on mechanical and durability properties of polymer and latex-modified concretes. Constr. Build. Mater. 2018, 191, 145–154.

[14] Medeiros, M.H.F.; Helene, P.; Selmo, S. Influence of EVA and acrylate polymers on some mechanical properties of cementitious repair mortars. Constr. Build. Mater. 2009, 23, 2527–2533.

[15] Wang, R.; Wang, P.M. Action of redispersible vinyl acetate and versatate copolymer powder in cement mortar. Constr. Build. Mater. 2011, 25, 4210–4214.

[16] Grzeszczyk, S.; Matuszek-Chmurowska, A. Microstructure of reactive powder concrete. Cem. Wapno Beton 2018, 1, 1–15

[17] Zuo, W.; Feng, P.; Zhong, P.; Tian, Q.; Liu, J.; She, W. Effects of a novel polymer-type shrinkage-reducing admixture on early age microstructure evolution and transport properties of cement pastes. Cem. Concr. Compos. 2019, 95, 33–41.

[18] Gwon, S.; Jang, S.Y.; Shin, M. Microstructure evolution and strength development of ultra rapid hardening cement modified with redispersible polymer powder. Constr. Build. Mater. 2018, 192, 715–730

[19] Pique, T.M.; Baueregger, S.; Plank, J. Influence of temperature and moisture on the shelf-life of cement admixed with redispersible polymer powder. Constr. Build. Mater. 2016, 115, 336–344.

[20] Fallah, S.; Nematzadeh, M. Mechanical properties and durability of high-strength concrete containing macro-polymeric and polypropylene fibers with nano-silica and silica fume. Constr. Build. Mater. 2017, 132, 170–187.

[21] Afroughsabet, V.; Ozbakkaloglu, T. Mechanical and durability properties of high-strength concrete containing steel and polypropylene fibers. Constr. Build. Mater. 2015, 94, 73–82

[22] Shehab El-Din, H.K.; Eisa, A.S.; Abdel Aziz, B.H.; Ibrahim, A. Mechanical performance of high strength concrete made from high volume of Metakaolin and hybrid fibers. Constr. Build. Mater. 2017, 140, 203–209.

[23] Sun, Z.; Xu, Q. Microscopic, physical and mechanical analysis of polypropylene fiber reinforced concrete. Mater. Sci. Eng. A 2009, 527, 198–204

[24] Sivakumar, A.; Santhanam, M. Mechanical properties of high strength concrete reinforced with metallic and non-metallic fibres. Cem. Concr. Compos. 2007, 29, 603–608.

[25] Kim, J.H.J.; Park, C.G.; Lee, S.W.; Lee, S.W.; Won, J.P. Effects of the geometry of recycled PET fiber reinforcement on shrinkage cracking of cement-based composites. Compos. Part B Eng. 2008, 39, 442–450.

[26] Topçu, I.B.; Canbaz, M. Effect of different fibers on the mechanical properties of concrete containing fly ash. Constr. Build. Mater. 2007, 21, 1486–1491.

[27] Koniki, S.; Prasad, D.R. A study on mechanical properties and stress-strain response of high strength. Cem. Wapno Beton 2018, 1, 67–77.

[28] Ramezanianpour, A.A.; Esmaeili, M.; Ghahari, S.A.; Najafi, M.H. Laboratory study on the effect of polypropylene fiber on durability, and physical and mechanical characteristic of concrete for application in sleepers. Constr. Build. Mater. 2013, 44, 411–418.

[29] Raffoul, S.; Garcia, R.; Escolano-Margarit, D.; Guadagnini, M.; Hajirasouliha, I.; Pilakoutas, K. Behaviour of unconfined and FRP-confined rubberised concrete in axial compression. Constr. Build. Mater. 2017, 147, 388–397.

[30] Siddika, A.; Al Mamun, M.A.; Alyousef, R.; Amran, Y.H.M.; Aslani, F.; Alabduljabbar, H. Properties and utilizations of waste tire rubber in concrete: A review. Constr. Build. Mater. 2019, 224, 711–731.

[31] Borg, R.P.; Baldacchino, O.; Ferrara, L. Early age performance and mechanical characteristics of recycled PET fibre reinforced concrete. Constr. Build. Mater. 2016, 108, 29–47.

[32] Collepardi, M. Admixtures used to enhance placing characteristics of concrete. Cem. Concr. Compos. 1998, 20, 103–112.

[33] Bravo, M.; de Brito, J.; Evangelista, L.; Pacheco, J. Durability and shrinkage of concrete with CDW as recycled aggregates: Benefits from superplasticizer's incorporation and influence of CDW composition. Constr. Build. Mater. 2018, 168, 818–830.

[34] Qian, Y.; Lesage, K.; El Cheikh, K.; De Schutter, G. Effect of polycarboxylate ether superplasticizer (PCE) on dynamic yield stress, thixotropy and flocculation state of fresh cement pastes in consideration of the Critical Micelle Concentration (CMC). Cem. Concr. Res. 2018, 107, 75–84.

[35] Zhu, W.; Feng, Q.; Luo, Q.; Bai, X.; Lin, X.; Zhang, Z. Effects of -PCE on the dispersion of cement particles and initial hydration. Materials 2021, 14, 3195.

[36] Dalas, F.; Nonat, A.; Pourchet, S.; Mosquet, M.; Rinaldi, D.; Sabio, S. Tailoring the anionic function and the side chains of comb-like superplasticizers to improve their adsorption. Cem. Concr. Res. 2015, 67, 21–30.

[37] Zhang, Y.; Luo, X.; Kong, X.; Wang, F.; Gao, L. Rheological properties and microstructure of fresh cement pastes with varied dispersion media and superplasticizers. Powder Technol. 2018, 330, 219–227.

[38] Mangane, M.B.C.; Argane, R.; Trauchessec, R.; Lecomte, A.; Benzaazoua, M. Influence of superplasticizers on mechanical

properties and workability of cemented paste backfill. Miner. Eng. 2018, 116, 3–14.
[39] Jiao, D.; De Schryver, R.; Shi, C.; De Schutter, G. Thixotropic structural build-up of cement-based materials: A state-of-the-art review. Cem. Concr. Compos. 2021, 122, 104152.
[40] Jiao, D.; Shi, C.; Yuan, Q.; An, X.; Liu, Y.; Li, H. Effect of constituents on rheological properties of fresh concrete-A review. Cem. Concr. Compos. 2017, 83, 146–159.
[41] Ma, B.; Peng, Y.; Tan, H.; Jian, S.; Zhi, Z.; Guo, Y.; Qi, H.; Zhang, T.; He, X. Effect of hydroxypropyl-methyl cellulose ether on rheology of cement paste plasticized by polycarboxylate superplasticizer. Constr. Build. Mater. 2018, 160, 341–350.
[42] Wu, Y.; Li, Q.; Li, G.; Tang, S.; Niu, M.; Wu, Y. Effect of naphthalene-based superplasticizer and polycarboxylic acid superplasticizer on the properties of sulfoaluminate cement. Materials 2021, 14, 662.
[43] Yang, L.; Yilmaz, E.; Li, J.; Liu, H.; Jiang, H. Effect of superplasticizer type and dosage on fluidity and strength behavior of cemented tailings backfill with different solid contents. Constr. Build. Mater. 2018, 187, 290–298.
[44] Zhao, H.; Yang, Y.; Shu, X.; Wang, Y.; Wu, S.; Ran, Q.; Liu, J. The binding of calcium ion with different groups of superplasticizers studied by three DFT methods, B3LYP, M06-2X and M06. Comput. Mater. Sci. 2018, 152, 43–50.
[45] Stecher, J.; Plank, J. Novel concrete superplasticizers based on phosphate esters. Cem. Concr. Res. 2019, 119, 36–43.
[46] Stecher, J.; Plank, J. Adsorbed layer thickness of polycarboxylate and polyphosphate superplasticizers on polystyrene nanoparticles measured via dynamic light scattering. J. Colloid Interface Sci. 2020, 562, 204–212.
[47] Sebök, T.; Stráňel, O. Relationships between the properties of ligninsulphonates and parameters of modified samples with cement binders. Cem. Concr. Res. 2000, 30, 511–515.
[48] Topçu, İ.B.; Ateşin, Ö. Effect of high dosage lignosulphonate and naphthalene sulphonate based plasticizer usage on micro concrete properties. Constr. Build. Mater. 2016, 120, 189–197.
[49] El-Didamony, H.; Heikal, M.; Khalil, K.A.; Al-Masry, S. Effect of delaying addition time of SMF superplasticizer on the physico-mechanical properties and durability of cement pastes. Constr. Build. Mater. 2012, 35, 261–269.
[50] Collepardi, M. Chemical Admixtures Today. In Proceedings of the Second International Symposium on Concrete Tecnology for Sustainable February—Development with Emphasis on Infrastructure, Hyderabad, India, 27 February–3 March 2005; pp. 527–541.
[51] Al-Neshawy, F.; Ojala, T.; Punkki, J. Stability of Air Content in Fresh Concretes with PCE-Based Superplasticizers. Nord. Concr. Res. 2019, 60, 145–158.
[52] Górażdże-Heidelberg Cement Group Beton wg Normy PN-EN 206:2014. 2014. Available online: https://www.nexto.pl/upload/sklep/pwn/ebook/beton_i_jego_technologie-zygmunt_jamrozy-pwn/public/beton_i_jego_technologie-pwn-demo.pdf (accessed on 7 October 2021).
[53] Gołaszewski, J.; Szwabowski, J. Influence of superplasticizers on rheological behaviour of fresh cement mortars. Cem. Concr. Res. 2004, 34, 235–248.
[54] Feng, W.; Xu, J.; Chen, P.; Jiang, L.; Song, Y.; Cao, Y. Influence of polycarboxylate superplasticizer on chloride binding in cement paste. Constr. Build. Mater. 2018, 158, 847–854.
[55] Liu, J.; Yu, C.; Shu, X.; Ran, Q.; Yang, Y. Recent advance of chemical admixtures in concrete. Cem. Concr. Res. 2019, 124, 105834.
[56] Roussel, N.; Lemaître, A.; Flatt, R.J.; Coussot, P. Steady state flow of cement suspensions: A micromechanical state of the art. Cem. Concr. Res. 2010, 40, 77–84.
[57] Pourchet, S.; Liautaud, S.; Rinaldi, D.; Pochard, I. Effect of the repartition of the PEG side chains on the adsorption and dispersion behaviors of PCP in presence of sulfate. Cem. Concr. Res. 2012, 42, 431–439.
[58] Hanehara, S.; Yamada, K. Rheology and early age properties of cement systems. Cem. Concr. Res. 2008, 38, 175–195.
[59] Hot, J.; Bessaies-Bey, H.; Brumaud, C.; Duc, M.; Castella, C.; Roussel, N. Adsorbing polymers and viscosity of cement pastes. Cem. Concr. Res. 2014, 63, 12–19.
[60] Lin, X.; Pang, H.; Wei, D.; Lu, M.; Liao, B. Effect of superplasticizers with different anchor groups on the properties of cementitious systems. Colloids Surfaces A Physicochem. Eng. Asp. 2021, 630, 127207.
[61] Sobolev, K.; Shah, S.P. Nanotechnology in Construction 3; Springer: Berlin/Heidelberg, Germany, 2009; ISBN 9783319170879.
[62] Dalas, F.; Pourchet, S.; Rinaldi, D.; Nonat, A.; Sabio, S.; Mosquet, M. Modification of the rate of formation and surface area of ettringite by polycarboxylate ether superplasticizers during early C3A-CaSO4 hydration. Cem. Concr. Res. 2015, 69, 105–113.
[63] Meier, M.R.; Rinkenburger, A.; Plank, J. Impact of different types of polycarboxylate superplasticisers on spontaneous crystallisation of ettringite. Adv. Cem. Res. 2016, 28, 310–319.
[64] Marchon, D.; Juilland, P.; Gallucci, E.; Frunz, L.; Flatt, R.J. Molecular and submolecular scale effects of comb-copolymers on tri-calcium silicate reactivity: Toward molecular design. J. Am. Ceram. Soc. 2017, 100, 817–841.
[65] Khayat, K.H.; Meng, W.; Vallurupalli, K.; Teng, L. Rheological properties of ultra-high-performance concrete—An overview. Cem. Concr. Res. 2019, 124, 105828.
[66] Tian, H.; Kong, X.; Cui, Y.; Wang, Q.; Wang, D. Effects of polycarboxylate superplasticizers on fluidity and early hydration in sulfoaluminate cement system. Constr. Build. Mater. 2019, 228, 116711.
[67] Plank, J.; Hirsch, C. Impact of zeta potential of early cement hydration phases on superplasticizer adsorption. Cem. Concr. Res. 2007, 37, 537–542.
[68] Sha, S.; Wang, M.; Shi, C.; Xiao, Y. Influence of the structures of polycarboxylate superplasticizer on its performance in cement-based materials-A review. Constr. Build. Mater. 2020, 233, 117257.
[69] Alonso, M.M.; Palacios, M.; Puertas, F. Compatibility between polycarboxylate-based admixtures and blended-cement pastes. Cem. Concr. Compos. 2013, 35, 151–162.
[70] Benaicha, M.; Hafidi Alaoui, A.; Jalbaud, O.; Burtschell, Y. Dosage effect of superplasticizer on self-compacting concrete: Correlation between rheology and strength. J. Mater. Res. Technol. 2019, 8, 2063–2069.
[71] Erzengin, S.G.; Kaya, K.; Perçin Özkorucuklu, S.; Özdemir, V.; Yıldırım, G. The properties of cement systems superplasticized with methacrylic ester-based polycarboxylates. Constr. Build. Mater. 2018, 166, 96–109.
[72] Ma, B.; Ma, M.; Shen, X.; Li, X.; Wu, X. Compatibility between a polycarboxylate superplasticizer and the belite-rich sulfoaluminate cement: Setting time and the hydration properties. Constr. Build. Mater. 2014, 51, 47–54.
[73] Mardani-Aghabaglou, A.; Tuyan, M.; Yilmaz, G.; Ariöz, Ö.; Ramyar, K. Effect of different types of superplasticizer on fresh, rheological and strength properties of self-consolidating concrete. Constr. Build. Mater. 2013, 47, 1020–1025.
[74] Burgos-Montes, O.; Palacios, M.; Rivilla, P.; Puertas, F. Compatibility between superplasticizer admixtures and cements with mineral additions. Constr. Build. Mater. 2012, 31, 300–309.

[75] Ferrari, L.; Kaufmann, J.; Winnefeld, F.; Plank, J. Interaction of cement model systems with superplasticizers investigated by atomic force microscopy, zeta potential, and adsorption measurements. J. Colloid Interface Sci. 2010, 347, 15–24
[76] Qian, Y.; De Schutter, G. Different effects of NSF and PCE superplasticizer on adsorption, dynamic yield stress and thixotropy of cement pastes. Materials 2018, 11, 695.
[77] Uchikawa, H.; Hanehara, S.; Sawaki, D. The role of steric repulsive force in the dispersion of cement particles in fresh paste prepared with organic admixture. Cem. Concr. Res. 1997, 27, 37–50.
[78] Keller, H.; Plank, J. Mineralisation of CaCO3 in the presence of polycarboxylate comb polymers. Cem. Concr. Res. 2013, 54, 1–11.
[79] Flatt, R.J.; Houst, Y.F. A simplified view on chemical effects perturbing the action of superplasticizers. Cem. Concr. Res. 2001, 31, 1169–1176.
[80] Flatt, R.J.; Houst, Y.F.; Bowen, P.; Hofmann, H. Electrostatic repulsion induced by superplasticizers between cement particles—An Overlooked Mechanism? In Proceedings of the 6th CANMET/ACI International Conference on Superplasticizers and Other Chemical Admixtures in Concrete; Malhotra, V.M., Ed.; American Concrete Institute: Farmigton Hills, MI, USA, 2000; pp. 29–42
[81] Ohama, Y. Polymer-based admixtures. Cem. Concr. Compos. 1998, 20, 189–212.
[82] Breilly, D.; Fadlallah, S.; Froidevaux, V.; Colas, A.; Allais, F. Origin and industrial applications of lignosulfonates with a focus on their use as superplasticizers in concrete. Constr. Build. Mater. 2021, 301, 124065.
[83] Silva, D.A.; Roman, H.R.; Gleize, P.J.P. Evidences of chemical interaction between EVA and hydrating Portland cement. Cem. Concr. Res. 2002, 32, 1383–1390
[84] Betioli, A.M.; Hoppe Filho, J.; Cincotto, M.A.; Gleize, P.J.P.; Pileggi, R.G. Chemical interaction between EVA and Portland cement hydration at early-age. Constr. Build. Mater. 2009, 23, 3332–3336.
[85] Göbel, L.; Osburg, A.; Pichler, B. The mechanical performance of polymer-modified cement pastes at early ages: Ultra-short non-aging compression tests and multiscale homogenization. Constr. Build. Mater. 2018, 173, 495–507.
[86] Sun, K.; Wang, S.; Zeng, L.; Peng, X. Effect of styrene-butadiene rubber latex on the rheological behavior and pore structure of cement paste. Compos. Part B Eng. 2019, 163, 282–289.
[87] Buczyński, P.; Iwański, M.; Mazurek, G.; Krasowski, J.; Krasowski, M. Effects of portland cement and polymer powder on the properties of cement-bound road base mixtures. Materials 2020, 13, 4253.
[88] Dołan, M.; Bideci, A. Effect of Styrene Butadiene Copolymer (SBR) admixture on high strength concrete. Constr. Build. Mater. 2016, 112, 378–385.
[89] Barluenga, G.; Hernández-Olivares, F. SBR latex modified mortar rheology and mechanical behaviour. Cem. Concr. Res. 2004, 34, 527–535.
[90] Baueregger, S.; Perello, M.; Plank, J. Role of PVOH and kaolin on colloidal stability of liquid and powder EVA and SB latexes in cement pore solution. Colloids Surfaces A Physicochem. Eng. Asp. 2013, 434, 145–153.
[91] Pavlitschek, T.; Jin, Y.; Plank, J. Film formation of a non-ionic ethylene-vinyl acetate latex dispersion in cement pore solution. Adv. Mater. Res. 2013, 687, 316–321.
[92] Jo, Y.K. Adhesion in tension of polymer cement mortar by curing conditions using polymer dispersions as cement modifier. Constr. Build. Mater. 2020, 242, 118134.
[93] Ohama, Y. Recent progress in concrete-polymer composites. Adv. Cem. Based Mater. 1997, 5, 31–40.
[94] Zalegowski, K.; Piotrowski, T.; Garbacz, A. Influence of polymer modification on the microstructure of shielding concrete. Materials 2020, 13, 498.
[95] Gretz, M.; Plank, J. An ESEM investigation of latex film formation in cement pore solution. Cem. Concr. Res. 2011, 41, 184–190.
[96] Keddie, J.L.; Meredith, P.; Jones, R.A.L.; Donald, A.M. Kinetics of Film Formation in Acrylic Latices Studied with Multiple-Angle-of-Incidence Ellipsometry and Environmental SEM. Macromolecules 1995, 28, 2673–2682.
[97] Van Gemert, D.; Czarnecki, L.; Maultzsch, M.; Schorn, H.; Beeldens, A.; Łukowski, P.; Knapen, E. Cement concrete and concrete-polymer composites: Two merging worlds: A report from 11th ICPIC Congress in Berlin, 2004. Cem. Concr. Compos. 2005, 27, 926–933.
[98] Ma, C.; Chen, B. Properties of magnesium phosphate cement containing redispersible polymer powder. Constr. Build. Mater. 2016, 113, 255–263.
[99] Dong, X.; Wang, S.; Gong, C.; Lu, L. Effects of aggregate gradation and polymer modifiers on properties of cement-EPS/vitrified microsphere mortar. Constr. Build. Mater. 2014, 73, 255–260.
[100] Silva, D.A.; Monteiro, P.J.M. The influence of polymers on the hydration of portland cement phases analyzed by soft X-ray transmission microscopy. Cem. Concr. Res. 2006, 36, 1501–1507.
[101] Gomes, C.E.M.; Ferreira, O.P.; Fernandes, M.R. Influence of vinyl acetate-versatic vinyl ester copolymer on the microstructure characteristics of cement pastes. Mater. Res. 2005, 8, 2–7.
[102] Schulze, J.; Killermann, O. Long-term performance of redispersible powders in mortars. Cem. Concr. Res. 2001, 31, 357–362.
[103] Zollo, R.F. Fiber-reinforced Concrete: An Overview after 30 Years of Development. Cem. Concr. Compos. 1997, 19, 107–122.
[104] Mardani-aghabaglou, A.; Metin, İ.; Özen, S. The effect of shrinkage reducing admixture and polypropylene fi bers on drying shrinkage behaviour of concrete. Cem. Wapno Beton 2019, 3, 227–237.
[105] Yin, S.; Tuladhar, R.; Shi, F.; Combe, M.; Collister, T.; Sivakugan, N. Use of macro plastic fibres in concrete: A review. Constr. Build. Mater. 2015, 93, 180–188.
[106] Tabatabaeian, M.; Khaloo, A.; Joshaghani, A.; Hajibandeh, E. Experimental investigation on effects of hybrid fibers on rheological, mechanical, and durability properties of high-strength SCC. Constr. Build. Mater. 2017, 147, 497–509.
[107] Pakravan, H.R.; Latifi, M.; Jamshidi, M. Hybrid short fiber reinforcement system in concrete: A review. Constr. Build. Mater. 2017, 142, 280–294.
[108] Guler, S. The effect of polyamide fibers on the strength and toughness properties of structural lightweight aggregate concrete. Constr. Build. Mater. 2018, 173, 394–402.
[109] Cao, M.; Xie, C.; Guan, J. Fracture behavior of cement mortar reinforced by hybrid composite fiber consisting of CaCO3 whiskers and PVA-steel hybrid fibers. Compos. Part A Appl. Sci. Manuf. 2019, 120, 172–187.
[110] Chen, B.; Liu, J. Contribution of hybrid fibers on the properties of the high-strength lightweight concrete having good workability. Cem. Concr. Res. 2005, 35, 913–917.
[111] Wang, W.; Shen, A.; Lyu, Z.; He, Z.; Nguyen, K.T.Q. Fresh and rheological characteristics of fiber reinforced concrete—A review American Society of Testing Materials. Constr. Build. Mater. 2021, 296, 123734.
[112] Yap, S.P.; Alengaram, U.J.; Jumaat, M.Z. Enhancement of mechanical properties in polypropylene- and nylon-fibre reinforced oil palm shell concrete. Mater. Des. 2013, 49, 1034–1041.
[113] Jang, J.G.; Kim, H.K.; Kim, T.S.; Min, B.J.; Lee, H.K. Improved flexural fatigue resistance of PVA fiber-reinforced concrete subjected to freezing and thawing cycles. Constr. Build. Mater. 2014, 59, 129–135.

[114] Said, S.H.; Abdul, H. The effect of synthetic polyethylene fi ber on the strain hardening behavior of engineered cementitious composite (ECC). JMADE 2015, 86, 447–457.
[115] Blazy, J. Case Studies in Construction Materials Polypropylene fiber reinforced concrete and its application in creating architectural forms of public spaces. Case Stud. Constr. Mater. 2021, 14, e00549.
[116] Behfarnia, K.; Behravan, A. Application of high performance polypropylene fibers in concrete lining of water tunnels. Mater. Des. 2014, 55, 274–279.
[117] Feleko, B.; Tosun, K.; Baradan, B. Effects of fibre type and matrix structure on the mechanical performance of self-compacting micro-concrete composites. Cem. Concr. Res. 2009, 39, 1023–1032.
[118] Gencel, O.; Ozel, C.; Brostow, W. Mechanical properties of self-compacting concrete reinforced with polypropylene fibres. Mater. Res. Innov. 2011, 15, 216–225.
[119] Hsie, M.; Tu, C.; Song, P.S. Mechanical properties of polypropylene hybrid fiber-reinforced concrete. Mater. Sci. Eng. A 2008, 494, 153–157.
[120] Yun, H. Effect of accelerated freeze-thaw cycling on mechanical properties of hybrid PVA and PE fiber-reinforced strain-hardening cement-based composites (SHCCs). Compos. Part B 2013, 52, 11–20.
[121] Verdolotti, L.; Iucolano, F.; Capasso, I.; Lavorgna, M.; Iannace, S.; Liguori, B. Recycling and Recovery of PE-PP-PET-based Fiber Polymeric Wastes as Aggregate Replacement in Lightweight Mortar: Evaluation of Environmental Friendly Application. Environ. Prog. Sustain. Energy 2014, 33, 1445–1451.
[122] Xu, W.; Li, Q.; Zhang, Y. Influence of temperature on compressive strength, microstructure properties and failure pattern of fiber-reinforced cemented tailings backfill. Constr. Build. Mater. 2019, 222, 776–785.
[123] Cao, S.; Yilmaz, E.; Song, W. Fiber type effect on strength, toughness and microstructure of early age cemented tailings backfill. Constr. Build. Mater. 2019, 223, 44–54.
[124] Pi, Z.; Xiao, H.; Du, J.; Liu, M.; Li, H. Interfacial microstructure and bond strength of nano-SiO2-coated steel fibers in cement matrix. Cem. Concr. Compos. 2019, 103, 1–10.
[125] dos Santos, V.; Tonoli, G.H.D.; Mármol, G.; Savastano, H. Fiber-cement composites hydrated with carbonated water: Effect on physical-mechanical properties. Cem. Concr. Res. 2019, 124, 105812.
[126] Wang, C.; Li, K.; Li, H.; Jiao, G.; Lu, J.; Hou, D. Effect of carbon fiber dispersion on the mechanical properties of carbon fiber-reinforced cement-based composites. Mater. Sci. Eng. A 2008, 487, 52–57.
[127] Payrow, P.; Nokken, M.R.; Banu, D. Effect of surface treatment on the post-peak residual strength and toughness of polypropylene / polyethylene-blended fiber-reinforced concrete. J. Compos. Mater. 2011, 45, 2047–2054.
[128] López-Buendía, A.M.; Romero-Sánchez, M.D.; Climent, V.; Guillem, C. Surface treated polypropylene (PP) fi bres for reinforced concrete. Cem. Concr. Res. 2013, 54, 29–35.
[129] Hernández-Cruz, D.; Hargis, C.W.; Bae, S.; Itty, P.A.; Meral, C.; Dominowski, J.; Radler, M.J.; Kilcoyne, D.A.; Monteiro, P.J.M. Cement & Concrete Composites Multiscale characterization of chemical—Mechanical interactions between polymer fibers and cementitious matrix. Cem. Concr. Compos. 2014, 48, 9–18.
[130] Signorini, C.; Sola, A.; Malchiodi, B.; Nobili, A.; Gatto, A. Failure mechanism of silica coated polypropylene fibres for Fibre Reinforced Concrete (FRC). Constr. Build. Mater. 2020, 236, 117549.
[131] Pešic, N.; Zivanowic, S.; Garcia, R.; Papastergious, P. Mechanical properties of concrete reinforced with recycled HDPE plastic fibres. Constr. Build. Mater. 2016, 115, 362–370.
[132] Thorneycroft, J.; Orr, J.; Savoikar, P.; Ball, R.J. Performance of structural concrete with recycled plastic waste as a partial replacement for sand. Constr. Build. Mater. 2018, 161, 63–69.
[133] Al-Tulaian, B.S.; Al-Shannag, M.J.; Al-Hozaimy, A.R. Recycled plastic waste fibers for reinforcing Portland cement mortar. Constr. Build. Mater. 2016, 127, 102–110.
[134] Ochi, T.; Okubo, S.; Fukui, K. Development of recycled PET fiber and its application as concrete-reinforcing fiber. Cem. Concr. Compos. 2007, 29, 448–455.
[135] Martínez-García, R.; Jagadesh, P.; Fraile-Fernández, F.J.; Del Pozo, J.M.M.; Juan-Valdés, A. Influence of design parameters on fresh properties of self-compacting concrete with recycled aggregate—A review. Materials 2020, 13, 5749.
[136] Horgnies, M.; Gutiérrez-González, S.; Rodríguez, A.; Calderón, V. Effects of the use of polyamide powder wastes on the microstructure and macroscopic properties of masonry mortars. Cem. Concr. Compos. 2014, 52, 64–72.

Author Guidelines EditEdit Author Guidelines

GENERAL GUIDELINES FOR AUTHORS

Journal of civil engineering researches invites unsolicited contributions of several forms: articles, reviews and discussion articles, translations, and fora. Contributions should fall within the broad scope of the journal, as outlined in the statement of scope and focus. Contributors should present their material in a form that is accessible to a general anthropological readership. We especially invite contributions that engage with debates from previously published articles in the journal.

Submissions are double-blind peer-reviewed in accordance with our policy. Submissions will be immediately acknowledged but due to the review process, acceptance may take up to three months. Submissions should be submitted via our website submission form (see links above for registration and login). Once you login, make sure your user profile has "author" selected, then click "new submission" and follow the instructions carefully to submit your article. If problems arise, first check the FAQ and Troubleshooting guide posted below. If you are still experiencing difficulty, articles can be submitted to the editors as email attachments.

Each article should be accompanied by a title page that includes: all authors' names, institutional affiliations, address, telephone numbers and e-mail address. Papers should be no longer than 10,000 words (inclusive of abstract 100-150 words, footnotes, bibliography and notes on contributors), unless permission for a longer submission has been granted in advance by the Editors. Each article must include a 100 words "note on contributor(s)" together will full institutional address details, including email address. We request that you submit this material (title page and notes on the contributors) as "supplementary files" rather than in the article itself, which will need to be blinded for peer-review.

We are unable to pay for permissions to publish pieces whose copyright is not held by the author. Authors should secure rights before submitting translations, illustrations or long quotes. The views expressed in all articles are those of the authors and not necessarily those of the journal or its editors. After acceptance, authors and Special Issue guest editors whose institutions have an Open Access library fund must commit to apply to assist in article production costs. Proof of application will be requested. Though publication is not usually contingent on the availability of funding, the Journal is generally under no obligation to publish a work if funding which can be destined to support open access is not made available.

Word template and guidelines

Our tailored Word template and guidelines will help you format and structure your article, with useful general advice and Word tips.

(La)TeX template and guidelines

We welcome submissions of (La)TeX files. If you have used any .bib files when creating your article, please include these with your submission so that we can generate the reference list and citations in the journal-specific style

Artwork guidelines

Illustrations, pictures and graphs, should be supplied with the highest quality and in an electronic format that helps us to publish your article in the best way possible. Please follow the guidelines below to enable us to prepare your artwork for the printed issue as well as the online version.

Format: TIFF, JPEG: Common format for pictures (containing no text or graphs).

EPS: Preferred format for graphs and line art (retains quality when enlarging/zooming in).

Placement: Figures/charts and tables created in MS Word should be included in the main text rather than at the end of the document.

Figures and other files created outside Word (i.e. Excel, PowerPoint, JPG, TIFF, EPS, and PDF) should be submitted separately. Please add a placeholder note in the running text (i.e. “[insert Figure 1.]")

Resolution: Rasterized based files (i.e. with .tiff or .jpeg extension) require a resolution of at least 300 dpi (dots per inch). Line art should be supplied with a minimum resolution of 800 dpi.

Colour: Please note that images supplied in colour will be published in colour online and black and white in print (unless otherwise arranged). Therefore, it is important that you supply images that are comprehensible in black and white as well (i.e. by using colour with a distinctive pattern or dotted lines). The captions should reflect this by not using words indicating colour.

Dimension: Check that the artworks supplied match or exceed the dimensions of the journal. Images cannot be scaled up after origination

Fonts: The lettering used in the artwork should not vary too much in size and type (usually sans serif font as a default).

Authors services:

For reformatting your manuscript to fit the requirement of the Journal of Civil Engineering Researchers and/or English language editing please send an email to the following address:

researchers.services@gmail.com

Noted: There is a fixed charge for these mentioned services that is a function of the manuscript length. The amount of this charge will be notified through a reply email.

FAQ AND TROUBLESHOOTING FOR AUTHORS

I cannot log in to the system. How do I acquire a new user name and password?

If you cannot remember your username, please write an email to (journals.researchers@gmail.com), who will locate your username and notify you. If you know your username, but cannot remember your password, please click the "Login" link on the left-hand menu at homepage. Below the fields for entering your username and password, you will notice a link that asks "Forgot your password?"; click that link and then enter your email adddress to reset your password. You will be sent an automated message with a temporary password and instructions for how to create a new password. TIP: If you do not receive the automated email in your inbox, please check your SPAM or Junk Mail folder. For any other issues, please contact our Managing Editor,Kamyar Bagherinejad (admin@journals-researchers.com).

How do I locate the online submission form and fill it out?

First you need to register or login (see above). Once you are logged in, make sure the "roles" section of your profile has "Author" selected. Once you assign yourself the role of "Author," save your profile and then click the "New Submission" link on your user home page.

Once you arrive at the submission form page, please read the instructions carefully filling out all necessary information. Unless specified otherwise by the editors, the journal section to be selected for your submission should be "Artlcles." Proceed to the remaining sections, checking all boxes of the submission preparation checklist, and checking the box in the copyright notice section (thus agreeing to journals-researchers's copyright terms). Once the first page is completed, click "Save and Continue." The next page allows you to upload your submission. Use the form to choose your file from your computer. Make sure you click "Upload." The page will refresh and you may then click "Save and Continue." You will then proceed to a page for entering the metadata for your article. Please fill out all required fields and any further information you can provide. Click "Save and Continue." The next page allows you to upload supplementary files (images, audiovisual materials, etc.). These are not required, but if you wish to provide supplementary materials, please upload them here (do no forget to click "Upload." Then click "Save and Continue." This brings you to the final page of the submission form. Please click "Finish Submission" in order to close the

submission process. You wil then be notified by email that your article has been successfully submitted. TIP: If you do not receive the automated email in your inbox, please check your SPAM or Junk Mail folder. For any other issues, please contact our Managing Editor, Kamyar Bagherinejad (admin@journals-researchers.com).

Why am I not receiving any email notifications from HAU?

Unfortunately, some automated messages from Open Journal Systems arrive in users' Spam (or Junk Mail) folders. First, check those folders to see if the message was filtered into there. You may also change the settings of your email by editing your preferences to accept all mail from [jcer] and related journals-researchers.com email accounts.

I am trying to upload a revised article following an initial round of peer-review, but I cannot locate where to upload the article. Where do I submit a revised article?

Follow the login process outlined above and when you successfully login you will see on your user home page a link next to "Author" for "active" articles in our system (usually it is only one article, but if you have mulitple submissions currently in our system, the number could be higher. Click the "Active" link and you will be led to a page that lists your authored articles currently in our system. Click the link under the column labeled "Status" and this will take you to a page showing the current review status of your article. At the very bottom of the screen, you will see an upload form under the heading "Editor decision." Here you may upload your revised article. An automated email will be sent to the editors and you may also notify them directly via email. You may then logout.

I successfully submitted an article; how long will it take for the editors to respond to me with a decision.

For all articles that are recommended for peer-review, the editors of JCER strive to notify authors of a decision within 4-6 weeks. You may contact JCER's Managing Editor, Kamyar Bagherinejad (admin@journals-researchers.com). if you have any questions relating to the review process and its duration.

For all other inquiries, please contact: Kamyar Bagherinejad (Managing Editor)

Privacy Statement

The names and email addresses entered in this journal site will be used exclusively for the stated purposes of this journal and will not be made available for any other purpose or to any other party.

Articles

Section default policy

Make a new submission to the Articles section.

Copyright Notice EditEdit Copyright Notice

Journal of Civil Engineering Researchers follows the regulations of the International Committee on Publication Ethics (COPE) and the ethical principles of publishing articles in this journal are set based on the rules of this committee, and in case of problems, it will be treated according to these rules.

This work is licensed under a Creative Commons Attribution 4.0 International License (CC BY 4.0).

In short, copyright for articles published in this journal is retained by the authors, with first publication rights granted to the journal. By virtue of their appearance in this open access journal, articles are free to use, with proper attribution and link to the licensing, in educational, commercial, and non-commercial settings

Privacy Statement EditEdit Privacy Statement

The names and email addresses entered in this journal site will be used exclusively for the stated purposes of this journal and will not be made available for any other purpose or to any other party.

Scholars Pavilion

Scholars Pavilion or **Scholars Chartagi** is a monument donated by the Islamic Republic of Iran to the United Nations Office at Vienna. The monument architecture is claimed by the Islamic Republic News Agency of Iran to be a combination of Islamic and Achaemenid architecture, although the latter clearly predominates in the decorative features, with Persian columns and other features from Persepolis and other remains from the Achaemenid dynasty. The Chahartaq pavilion form runs through the architecture of Persia from pre-Islamic times to the present.

Statues of four famous Persian medieval scholars, Omar Khayyam, Al-Biruni, Muhammad ibn Zakariya al-Razi and Ibn-Sina are inside the pavilion. This monument donated in June 2009 in occasion of Iran's peaceful developments in science.

J-Researchers